Optimal co-design of microgrids and electric vehicles: synergies, simplifications and the effects of uncertainty

by

John W. Whitefoot

A dissertation submitted in partial fulfillment
of the requirements for the degree of
Doctor of Philosophy
(Mechanical Engineering)
in The University of Michigan
2012

Doctoral Committee:
Professor Panos Y. Papalambros, Chair
Professor Ian A. Hiskens
Professor Huei Peng
Professor Anna G. Stefanopoulou

© John W. Whitefoot
2012

Acknowledgements

I would like to firstly acknowledge the funding sources that allowed me to return to the University of Michigan to complete my doctoral degree. This work was supported through a non-traditional student fellowship from Rackham Graduate School, a fellowship from the Department of Mechanical Engineering, and the Dwight D. Eisenhower Transportation Fellowship. Additionally, this research was funded through the Automotive Research Center, a US Army Center of Excellence in Modeling and Simulation of Ground Vehicles, headquartered at the University of Michigan. This support is gratefully acknowledged.

I would like to thank Professor Panos Papalambros, both for helping to cobble together this collection of funding and more importantly for agreeing to once again take me on as a student. His guidance in research has been greatly appreciated and I always gain from our conversations, which ranged from the esoteric to the practical to the personal. His perspective and advice were always welcome and seasoned with depth of experience.

I would like to thank my committee members. Their comments and critiques of this dissertation have made it a far stronger body of research. In addition, I have found their classes to be extremely challenging and their research ideas to be shrewd and helpful. Their collective experience is one that would be hard to replicate anywhere else.

I would like to thank my colleagues within the Optimal Design Laboratory for all the research and non-research discussions. Kukhyun Ahn taught me about the importance of getting results right, even if it means redoing them innumerable times, and he also taught me the proper way to eat bi bim bop. Diane Peters and Abigail Mechtenberg were valuable project collaborators during the formative stages of the microgrid phase of my research. Michael Kokkolaras was instrumental in helping me add design for uncertainty

to my research. Yi Ren provided mathematical expertise that would have taken me exponentially longer than it took him. Kendra Borchers was a valuable research assistant, running many important studies that were implemented in this work. I'd like to give special thanks to Michael Alexander, for without the use of his EV model I would never have graduated on time. Steven Hoffenson got me out of the lab and playing softball and eating lunch with other MechE graduates. Kwang-Jae Lee helped keep all our computational assets up and running and was always ready to challenge me to explain the nuanced meaning of various English words and phrases. Sou Montezari brought a new spark of enthusiasm and creativity to the lab, which was greatly appreciated.

I'd like to thank my family, both biological and not, for their love and support. Foremost, I'd like to thank my parents, who always quietly allowed me to exceed my own expectations, and both of whom are excellent engineers in their own rights. Special thanks to Anna Fodde-Reguer and Erin MacDonald for checking in on me and giving me motivation during the writing of my dissertation. Finally, infinite thanks to my partner, Katie, for her initial support in my return to school and her continuing support, both emotional and technical. Having a partner who knows me and my work so well is an immeasurable benefit, and for her time, patience, and love I am truly grateful.

TABLE OF CONTENTS

LIST OF TABLES

Table

LIST OF FIGURES

Figure

NOMENCLATURE

$\boldsymbol{x}$	Design variables (vector)
$\boldsymbol{u}(t)$	Dispatch variables (vector)
$\boldsymbol{p}$	System parameters (vector)
u_i^t	Dispatch of power generation resource *i* at time *t*
u_j^t	Dispatch of energy storage resource *j* at time *t*
i	Index of power generation resources
j	Index of energy storage resources
k	Index of electric vehicles
t	Current time increment (hour)
t_{horiz}	Time horizon length (hours)
T_{final}	Total time of optimal dispatch problem (hours)
p_{fuel}	Price of fuel ($/kWh)
$\boldsymbol{g}(\boldsymbol{x},\boldsymbol{u}(t))$	Inequality constraints of optimal dispatch problem (vector)
$\boldsymbol{h}(\boldsymbol{x},\boldsymbol{u}(t))$	Equality constraints of optimal dispatch problem (vector)
E_{fuel}^t	Fuel energy used in time increment *t* (kWh)
$\overline{E}_j$	Maximum capacity of energy storage resource *j* (kWh)
$\underline{E}_j$	Minimum capacity of energy storage resource *j* (kWh)
E_j^t	State of charge of energy storage resource *j* at time *t* (kWh)
$\overline{P}_j$	Maximum power available from energy storage resource *j* (kW)
P_{ls}^t	Transmission power losses at time *t* (kW)
P_{ld}^t	Total power load at time *t* (kW)
$\overline{P}_i$	Maximum (rated) power of generation resource *i* (kW)
N_i	Number of power generation resources
N_j	Number of energy storage resources
$f_{O\&M}(\boldsymbol{x},\boldsymbol{u}(t))$	Operation and maintenance cost of microgrid ($)
$\hat{\boldsymbol{u}}(\boldsymbol{T},\boldsymbol{x})$	Matrix of optimal dispatch factors
$\hat{\boldsymbol{g}}(\boldsymbol{T},\boldsymbol{x})$	Dispatch problem inequality constraints at optimum
$\hat{\boldsymbol{h}}(\boldsymbol{T},\boldsymbol{x})$	Dispatch problem equality constraints at optimum
$f_{cap}(\boldsymbol{x})$	Capital cost function ($)
h	Index of microgrid hubs

$P_{hub,h}$	Power balance of microgrid hub *h* (kW)
L_h	Power load at microgrid hub *h* (kW)
P_{gen1}	Power produced by Generator 1 (kW)
P_{gen2}	Power produced by Generator 2 (kW)
η_{PV}	Efficiency of PV array inverter
P_{PV}	Power produced by PV array (kW)
P_{batt}	Power produced/absorbed by storage battery (kW)
$P_{net,h}$	Power at microgrid hub *h* including transmission losses (kW)
a	Generator fuel use model fit parameter
$P_{reserve}$	Operating reserve of microgrid (kW)
L_{gen}	Load on generator (%)
L_d	Daily total power load (kW)
L_b	Average yearly power load (kW)
T_{av}	Average air temperature for a given day (°F)
T_g	Goal temperature (°F)
p	Maximum power of resource for cost calculation (kW)
C	Maximum capacity of resource for cost calculation (kWh)
c	Index of microgrid components
L_c	Lifetime of component *c* (years)
p_c	Unitized capital cost of component *c* ($/kW)
$\bar{P}_{gen1}$	Rated power of Generator 1 (kW)
$\bar{P}_{gen2}$	Rated power of Generator 2 (kW)
$\bar{E}_{batt}$	Energy capacity of storage battery (kWh)
$\bar{P}_{PV}$	Rated power of PV array (kW)
σ_L	Mean value of power load (kW)
μ_L	Standard deviation of power load (kW)
$P_{f,k}$	Allowable probability of failure of constraint *k*
ε	Error of reliability calculation using Monte Carlo Sampling (%)
p_{Tf}	True probability of failure
N_{MCS}	Number of Monte Carlo Samples
Pr_{inj}	Probability of injury due to IED blast
$Priority_v$	Charging priority of vehicle *k*
c_k	Connectivity variable for vehicle *k*

$\bar{E}_v$	Maximum allowed state of charge of vehicle battery pack (kWh)
$\underline{E_v}$	Minimum allowed state of charge of vehicle battery pack (kWh)
$E_{v,k}^t$	State of charge of battery pack for vehicle *k* at time *t* (kWh)
P_{veh}^t	Total charging station power command at time *t* (kW)
$P_{v,k}^t$	Power command to plugged-in vehicle *k* at time *t* (kW)
N_v	Number of vehicles
E_{vIC}^t	Fuel use of non-electrified vehicles at time *t* (kWh)
m_b	EV: baseline vehicle mass (kg)
m_{occ}	EV: occupant mass (kg)
m_T	EV: total vehicle mass (kg)
L	EV: wheelbase (m)
W_o	EV: overall vehicle width (m)
C_d	EV: drag coefficient
A_f	EV: frontal area (m^2)
ρ_a	EV: air density (m^3)
m_{us}	EV: unsprung mass (kg)
ζ	EV: damping ratio per wheel (N-s/m)
k_s	EV: suspension stiffness per wheel (N/m)
g_h	EV: geared hub ratio
r_{go}	EV: gearbox output gear radius (m)
$r_{go,i}$	EV: gearbox output idler gear radius (m)
$r_{gi,i}$	EV: gearbox input idler gear radius (m)
I_{yt}	EV: tire/wheel assembly spin inertia per axle (kg-m^2)
C_r	EV: tire rolling resistance
r_t	EV: tire radius (m)
r_v	EV: vehicle range (km)
P_{acc}	EV: accessory power load (W)
b_w	EV: battery pack width packaging limit (m)
b_l	EV: battery pack length packaging limit (m)
t_{0-50}	EV: acceleration time 0 – 50mph (s)
T_{frnt}	EV: torque of front motors (N-m)
T_{rear}	EV: torque of rear motors (N-m)
T_{max}	EV: torque limit – electric motors (N-m)
N_{frnt}	EV: operating speed of front motors (rad/s)
N_{rear}	EV: operating speed of rear motors (rad/s)
N_{max}	EV: speed limit – electric motors (rad/s)
P_{vbatt}	EV: power supplied by vehicle battery (W)
P_{max}	EV: power limit of vehicle battery (W)
E_{vbatt}	EV: energy capacity of vehicle battery (A-h)

D_s	EV: directional stability metric
E_{km}	EV: electrical energy use per kilometer (W-h/km)
B_I	Battery electrode insertion scale
B_W	Battery electrode width (cm)
B_L	Battery number of folds/windings
V_s	IM: RMS AC source voltage (V)
L_m	IM: mutual inductance
R_s	IM: winding resistance of stator
L_{ls}	IM: leakage of stator
L_{lr}	IM: leakage of rotor
s	IM: slip
R_r	IM: variable electric resistance through the rotor
V_{sm}	IM: maximum stator voltage (V)
p	IM: number of stator poles
q	IM: number of slots per phase per pole
m_1	IM: number of motor phases
σ_{Yr}	IM: rotor yield stress (MPa)
ν	IM: rotor Poisson ratio
SF	IM: rotor safety factor
ω_{inv}	IM: maximum inverter frequency (rad/s)
ρ_{fe}	IM: iron density (kg/m^3)
C_{m1}	IM: 1st *cm* parameter
C_{m2}	IM: 2nd *cm* parameter
C_{m3}	IM: 3rd *cm* parameter
C_{m4}	IM: 4th *cm* parameter
n_a	IM: slot volume ratio
n_p	IM: wire packaging ratio
t_s	IM: stator radius proportionality factor
k_e	IM: end effect ratio
ρ_{cu}	IM: copper resistivity (Ω-m)
C_{I1}	IM: constant I_{sm} parameter
C_{I2}	IM: linear I_{sm} parameter
C_{I3}	IM: quadratic I_{sm} parameter

Chapter 1: Introduction

In the early-21st century, humanity is faced with multiple converging trends that threaten the environment, our health, and our quality of life. Worldwide energy use is projected to increase by 53% from 2008 to 2035, with most of the growth (~85%) in non-OECD countries [Energy Information Administration 2011]. Additionally, the United Nations projects that world will increase by more than two billion people by 2050 [United Nations 2010]. Concurrently, economic expansion in high-population countries has blossomed car ownership, e.g., China's per capita vehicle ownership grew by 15% in 2007 and 2008 [World Bank 2011] and the total passenger car fleet is expected to double to 1.7 billion vehicles by 2035 [International Energy Agency 2011]. The continuation of these trends and the finite limit of fossil fuel resources requires dramatic shifts in how we use energy and from where we derive that energy.

Until recently, transportation energy and electrical power generation were treated as separate entities, mainly because transportation energy is typically petroleum-sourced, whereas electrical power comes from a variety of fossil and non-fossil sources, but is rarely petroleum-sourced. The burgeoning electrification of vehicles is causing these two energy systems to overlap, and future predictions of vehicle electrification, e.g., Pike Research's projection of 5.2 million plug-in vehicles by 2017 [Pike 2010], will only serve to increase that overlap.

This oncoming convergence of transportation and electrical energy systems, coupled with the need to reduce fossil fuel use and greenhouse gas emissions, requires us to consider both systems simultaneously in order to develop a combined system perspective that serves our needs best while minimizing deleterious effects. Though each system is designed by separate industries, it is necessary to study the interface of the two systems to understand the effects of one system on the other and look for synergies that

can provide a more efficient super-system design and serve more people with a smaller carbon footprint.

There is much research studying the effects of plug-in vehicles on existing regional electrical power systems (i.e., the "macrogrid"). However, the design of the macrogrid will not change (or will change very slowly) in reaction to the addition of plug-in electrified vehicles (PEVs). Localized micropower systems, including local "microgrids," are more likely to adapt their designs in response to PEVs and are also more likely to reap benefits from the inclusion of PEVs in the system, such as buffering power spikes and renewable energy variability or voltage and frequency regulation.

1.1 Microgrids and vehicles

The design of localized, distributed energy generation systems is a particularly important research issue, especially as the deployment of renewable energy sources increases [Jiayi et al. 2008]. The control of energy flows and electrical power quality from a large number of resources is inherently different than the highly-centralized electrical distribution system in the U.S. and other industrialized countries [Meliopoulos et al. 2002, Colson et al. 2009]. In addition, with the installation of small, renewable energy sources there exists the potential to increase energy security at the local level by networking a system of Distributed Energy Resources (DERs) into a so-called "microgrid." One definition of a microgrid is:

> "A set of dispatchable (turbines, reciprocating engines, fuel cells) and/or non-dispatchable generators (wind turbines, PV), electrical and thermal energy storage, a grid connection for import and/or export of electricity, heat and power distribution infrastructure and an energy management system." [Lasseter et al. 2003]

These microgrids are of particular interest to areas or entities where energy independence and/or energy security are especially important, such as military bases, medical complexes, remote cities, and island communities [Shaffer et al. 2006, Ashok et al. 2007, Gupta et al. 2010].

Various levels of microgrid designs exist, some simple with just one DER element and a passive control system, others complex enough to be able to separate from the external macrogrid during times of grid instability or grid failure and supply all of their own power, thus increasing the energy security of the local microgrid region [Friedman et al. 2005]. As microgrid systems increase in complexity, their design and control must be carefully coordinated, both to minimize the capital and operating costs as well as to ensure the microgrid's stability and reliability. Furthermore, rather than existing in a load-following state, where electricity production is ramped up to meet demand, microgrids can have the capability of controlling the loads as well, through smart switches and circuit breakers that are centrally-controlled. These "smart grid" technologies offer the potential of reducing power demand during peak times and further increasing the independence and reliability of the microgrid.

Previous research has shown that plug-in vehicles can be a complementary technology to microgrids [Gage et al. 2003, Tomić et al. 2007, Galus et al. 2008]. Both plug-in hybrid electric vehicles (PHEVs) and battery electric vehicles (BEVs) can be linked with a microgrid in order to store off-peak renewable energy and either use it for vehicle propulsion or return some of that stored energy to the microgrid during times of peak energy use. This can maximize the utilization of renewable energy sources, reduce fossil energy use and reduce the greenhouse gas footprint of the microgrid area. This is doubly advantageous in that this vehicle/microgrid system addresses both transportation energy use as well as electrical energy use. However, other research questions the economic viability of vehicle-to-grid (V2G) power flow, as it can cause increased degradation of the vehicle batteries [Peterson et al. 2010b], requires additional control and communication equipment [Hiskens and Callaway 2009], and may reduce the utility of the vehicle for its owner [Momber et al. 2010].

Additionally, plug-in vehicles can be a high-load strain on a local microgrid, especially given the random nature of when drivers will want to charge their vehicles. Therefore, additional design and control considerations must be made to ensure reliable operation of both the microgrid and the vehicles. This necessitates formulating a coordinated, system-level design and control problem that considers the microgrid and its

individual DER elements and control strategy as well as the design and control of the electrified vehicles that connect to the microgrid.

1.2 Motivation of this work

Microgrids and electric vehicles are separately-designed, but interacting, systems. Such separation is natural as different organizations undertake the design of a microgrid and the design of a vehicle. It is also easier to address each problem separately, rather than looking at combining them into a potentially complex and difficult to solve integrated problem. A system designer, however, will recognize that systems that significantly interact have the potential to mutually benefit if they are designed concurrently, or "co-designed" [Fathy et al. 2001, Reyer et al. 2002, Peters et al. 2009]. Given the caveat above, research is necessary to quantify the range and magnitude of the potential benefits of co-design to understand the system interactions better and develop tools, insights, and heuristics for the designers of these systems and their interfaces.

Ad-hoc design of a microgrid is often based upon the expected peak load on the system, but this is a conservative approach that has the potential to oversize components, especially if the dispatch (operation and scheduling) of the components is not considered simultaneously to the system design. Additionally, if the actual power load deviates significantly from the expected power load, the system may suffer from loss-of-load and have poor reliability. This necessitates a coordinated, system-level design and dispatch problem that considers the sizing of individual DER elements and their dispatch control strategy, including consideration of system uncertainties. The complexity of solving the microgrid design problem is due to having to evaluate each design by determining the operation of the microgrid at discrete time steps over some time period. Additionally, the special case of a DER being an EV or HEV adds significantly more complexity when combined design and control of the vehicle must be combined with the design and control problem of the microgrid.

This dissertation will focus on optimizing efficiency of the system by analyzing the power of the microgrid on long time scales (hours to years). This dissertation will not

consider the regulation and power quality of the microgrid, which requires simulation on short time scales (milliseconds to seconds).

1.3 Dissertation overview and contributions

This dissertation seeks to develop methods for and quantify the potential benefits of co-design of microgrids and electric vehicles. The dissertation will explore formal methods for designing each system, focusing on model-based, numerical design optimization methods, and will develop new methods and heuristics for co-design of both systems. The major contributions of this work are:

(1) Investigation and strategies to exploit the benefits of simultaneously designing an electrical microgrid and connected electric vehicles, as well as potential limitations.
(2) Methods to optimally design a distributed energy system and connected electric vehicles with uncertain parametric inputs.
(3) Categorization of different types of optimal microgrid-level power dispatch problems and assessment of appropriate methods to solve each type.

The rest of this dissertation is organized as follows. Chapter 2 will explain the optimal dispatch problem, its purpose, formulation, complications, and various methods for simplification. The end of the chapter will summarize various classes of optimal dispatch problems and discuss how each should be formulated (Contribution #3). Chapter 3 discusses design optimization of microgrids, the formulation of optimal microgrid design problems with nested optimal dispatch problems, and solve a simple example optimization of a military microgrid. Chapter 4 will introduce microgrid design under parametric uncertainty, focusing on power load uncertainty and renewable energy uncertainty in the form of solar power. The uncertainty distributions will be modeled and incorporated into an efficient method to optimize the design in order to maintain microgrid reliability. Examples will be solved to show how this method optimizes the design of the military microgrid discussed in Chapter 3, but this time including

parametric uncertainty. Chapter 5 will introduce the concept of co-design of electric vehicles and microgrids. An overview of vehicle powertrain optimization will be followed by a description of how to formulate the co-design optimization problem including uncertainty (Contribution #2). A case study will follow, demonstrating co-design of a military microgrid and its attached electric vehicles (Contribution #1). The results will be used to develop design insights into these two systems and their interactions, resulting in the development of additional heuristics for designers. Finally, Chapter 6 will summarize the dissertation and suggest future work.

Chapter 2: Microgrid dispatch optimization

The core of any microgrid design problem is evaluating how a particular design will operate. The operation of some microgrid components, e.g., generators, microturbines, fuel cells, storage batteries, are directly controlled, e.g., by dedicated controllers. These devices are known as "dispatchable" components. Other "passive" components are not directly controlled, such as renewable power sources. These are known as "non-dispatchable" components. To understand the operation of the entire microgrid, it is necessary to simulate the expected operation of the non-dispatchable components and simultaneously simulate how the microgrid controllers will operate the dispatchable components to supply the electric load and store energy. The dispatch problem that seeks to achieve some optimal objective, e.g., cost minimization or minimization of loss-of-load, is known as an optimal dispatch problem.

2.1 Description of dispatch problems and literature review

The operations research community has generated much research into optimal dispatching of microgrid components to minimize the operation cost while meeting the necessary electrical loads. This research for microgrid dispatching is an offshoot of approaches used for power distribution in regional electrical grids to dispatch power generation plants, which is known as the "unit commitment" problem [Hawkes et al. 2009]. The difficulty in the optimal dispatching problem is that it must make optimal decisions for many devices at each time step along some time horizon (finite or infinite), resulting in a high-dimensional optimization problem.

2.1.1 Linear methods

The most widely-used approach for solving the optimal dispatch problem is to linearize and solve it via linear programming (LP). The advantages of this approach are that large-scale systems can be efficiently solved over long periods of time and a globally-optimal solution is guaranteed. A typical goal for microgrids is to minimize the operating cost at discretized time increments (e.g., one hour) over a year to understand the performance of a given design, which requires solving for of thousands of dispatch decisions per dispatchable device. Microgrid design software that uses linear programming, such as those implemented in Lawrence Berkeley National Laboratories DER-CAM software, can solve the entire year's dispatch simultaneously [Stadler et al. 2009]. However, the solution of the entire time period simultaneously is not strictly necessary, and in fact may not be representative of how a microgrid will be operated in practice. Instead, a much smaller subset of time (the "decision horizon") can be solved using estimates of future microgrid operation. A disadvantage of solving the dispatch problem via LP is that the linearization may not represent underlying nonlinear functions sufficiently well, such as efficiency of generators as a function of load, battery internal resistance as a function of state-of-charge, or electrical resistance losses as a function of current.

Solution of microgrid dispatching via LP is the most common method used in the literature, so only a subset of implementations that also address microgrid design, stochasticity, or other topics relevant to this dissertation are listed here. For example, the DER-CAM microgrid design and optimization software developed by Lawrence Berkeley National Laboratories uses LP to solve its dispatch problems [Stadler et al. 2009, Momber et al. 2010]. LP is also used by del Real et al. with their microgrid problems, which included nonlinear energy storage models and cost functions, which they linearized and solved hourly over a 24-hour period [del Real et al. 2009]. Gupta et al. evaluated microgrid designs for a remote community by solving a mixed-integer linear program for the optimal dispatch [Gupta et al. 2010].

Hawkes and Leach extended the optimal dispatching problem to include the stochastic nature of wind energy, as well as to address the issue of optimal dispatching

during both microgrid "islanding" (isolated from an external electrical grid) and during grid-connection [Hawkes et al. 2009]. They incorporated wind-energy uncertainty by drawing Monte Carlo samples from a Weibull distribution of wind speeds and solving the full-year dispatch problem for each draw.

2.1.2 Nonlinear methods

Some researchers have used nonlinear programming to solve the dispatch problem, using either quadratic programming (quadratic cost function and linear constraints) or generalized nonlinear programming. These methods typically do not solve an entire year simultaneously, as the large number of variables make the problems computationally intractable for nonlinear programming methods.

Asano and Bando solved the optimal dispatch of a microgrid by separating the year into six representative days and then solving each day as a separate problem [Asano et al. 2007]. Their approach does not consider the boundaries of the solved days by linking the time before and after the representative days. Thus, their approach provides an approximation of the microgrid performance, but may differ from how the microgrid will be controlled and operated in practice.

Almassalkhi and Hiskens solved a multi-period, mixed-integer quadratic programming problem for a 24-hour day with 1-hour time increments [Almassalkhi et al. 2010]. The integer variables result from the formulation of energy storage charging and discharging, where they implement a binary variable to denote one or the other state, which eliminates a discontinuity in the charging/discharging efficiencies. They do not implement their dispatch solution over longer time periods, though this could be accomplished by solving a sequence of these one-day problems.

Geidl and Andersson developed a generalizeable hub-based microgrid model with an emphasis on multiple energy carriers (e.g., electrical, heat, gas). They formulate a quadratic programming dispatch problem for each hub and then they formulate a non-convex nonlinear programming problem to solve the optimal power flow between hubs [Geidl et al. 2007]. This second problem is solved by sequential quadratic programming (SQP).

Whitefoot et al. [2011] formulated a nonlinear dispatch problem over a moving 24-hour time horizon, and solved a sequence of these problems using sequential quadratic programming (SQP). This preserves the nonlinearities of the problem while providing a computationally-tractable way of solving the dispatch for longer periods of time, e.g., an entire year. In addition, use of a moving time horizon emulates other, practical control methods, such as model-predictive control (MPC), which could be implemented on an actual microgrid to centrally-control the dispatch of the components. Thus, this approach may come closer to representing how an actual microgrid would operate. Their implementation used the optimization problem structure and many of the simplifications that will be described in this dissertation.

2.1.3 Other solution methods

Of all of the previous publications, only HOMER Energy used a rule-based (heuristic) strategy to solve for the dispatch [Lambert et al. 2006]. Their strategy minimizes operating cost in a single time increment and uses heuristics for charging and discharging energy storage without explicitly planning energy storage for future time periods. This method has the advantage of operating very quickly because each time increment is solved sequentially. Thus, no optimization problem needs to be solved and a single design can be efficiently evaluated. However, this method is not an "optimal" dispatch strategy in that it is a fixed strategy that does not seek out operational improvements through an algorithmic search procedure.

Lu et al. [2011] solved for the operation of a hybrid energy system including energy storage, solar power, and wind power. Their system does not include any dispatchable power generation, so they only have to decide the dispatch of the energy storage at each time increment. Their dispatch objective is to minimize the probability of loss of load (LoL) given uncertainty in the renewable energy inputs. They solve the dispatch of energy storage for each design at one-hour increments using stochastic Markov chains to minimize the probability of LoL. They are able to use Markov chains because the dispatch solution to minimize LoL for a given time increment only requires information from the previous time increment. This is contrasted to economic dispatch,

which requires solving the dispatch of the energy storage over multiple time increments simultaneously (ideally, over the entire time period of interest).

Mohamed and Koivo used mesh-adaptive direct search (MADS), a derivative-free pattern search algorithm, to find the optimal dispatch solution for a fixed microgrid design to minimize cost while meeting customer electrical demands [Mohamed et al. 2009]. They compare the results from MADS to their results using SQP. For their problem MADS is shown to provide better solutions than SQP, though no reasons are given for this improvement.

Other research has used model-predictive control (MPC) to represent better actual microgrid operation to solve the multi-period dispatch problem with a finite time horizon using expectations of system inputs and future microgrid states. Arnold et al. [2009] formulated an MPC problem for a hub-based microgrid, similar to Geidl and Andersson [2007]. Peters et al. also used model-predictive control to solve the dispatch problem and used this method to investigate the effects of prediction error and time horizon length [Peters et al. 2011].

2.1.4 Summary of methods and issues

These various approaches for solving the optimal dispatch problem typically use historical data for power loads, renewable energy supply, and other inputs, and most assume perfect knowledge (no uncertainty) to solve for the dispatch strategy (with the exception of [Hawkes et al. 2009, Geidl et al. 2009, and Lu et al. 2011]). Some of the methods, such as linear programming or HOMER's rule-based dispatch strategy, seek efficiency at the risk of sub-optimality. Other methods seek to preserve problem nonlinearities, incurring increased computational cost and the likelihood of poor scalability to larger problems. The use of derivative-free methods in the literature is limited. These methods have the flexibility to handle mixed-integers, binary variables, or functional discontinuities, but they are slow to converge and thus may take significant computation time. Also, they can only handle a relatively small number of variables. Their use for microgrid design is therefore limited, since the dispatch problem must be solved for each design in order to compare their performances.

The question of which method is best may be most appropriately addressed by understanding the purpose for solving the optimal dispatch problem. While solving the entire year simultaneously seems to be ideal, it does not represent how a microgrid would operate in practice with an actual controller. A real-time controller, even one that used forward-looking predictions, would have to react to disturbances, prediction uncertainties, and other variations in the operating conditions that are not captured when solving an entire year's dispatch simultaneously. Thus, a microgrid design that is evaluated using LP may have good performance in an ideal situation, but degraded performance in a realistic implementation because the estimates of future operating states may not match reality. To predict the actual performance of a microgrid design, it is necessary to simulate its dispatch using controllers that would be actually implemented to control the system.

2.2 Energy storage dispatch vs. power generation dispatch

The optimal dispatch problem will take different forms and require different solution strategies depending on the goal of the optimal dispatch (e.g., economic dispatch or minimizing loss of load) the types and number of dispatchable power generation resources, and whether energy storage is present. Economic dispatch of only power generation resources is a common problem solved in the power generation industry as the unit commitment problem [Hawkes et al. 2009]. The costs of operating various components can often be placed in a hierarchy, operating the cheapest resources first and only operating more expensive components when necessary to meet the load. Thus, the optimal dispatch solution can be predetermined for any given load and the actual operation decision for each time period can be decided independently of the preceding or following time periods. Note, however, that this solution only considers the direct operation costs and assumes no ramping costs or other transient costs for starting/stopping a particular resource.

When only energy storage is present along with non-dispatchable power generation (e.g., renewable power resources), economic dispatch is not considered because there are typically no operation costs, only maintenance/degradation costs. This

type of system is typically seen in remote areas where fossil fuels and external grid connection are not available. An example can be seen in [Lu et al. 2011]. For these cases, the goal of optimal dispatch is often to minimize loss-of-load (LoL). The dispatch of the energy storage is typically rule-based: to charge when excess power is present (when the renewable sources are producing more than the power load) and to discharge when the renewable sources are not meeting the power load (to prevent LoL).

When minimizing LoL, the structure of the optimal dispatch problem will be different if the goal is to minimize the *total loss of load* or if the goal is to minimize the *total number of hours* when LoL occurs independent of the amount of LoL. For the former case, the total LoL can be minimized by making dispatch decisions for each time period independently of preceding or following periods. However, for the case where the goal is to minimize the total number of hours where LoL occurs, the optimal dispatch solution for energy storage will be improved by using a decision horizon. Then, the optimal dispatch strategy would use the finite energy storage resources during periods of small LoL. For example, if a microgrid was predicted to experience five periods of a 10 kW LoL and two periods of a 25 kW LoL, the energy storage could be expended during the five 10 kW LoL periods, thus maximizing system "up-time." This can be especially important for microgrids that cannot shed load if LoL occurs and where any LoL can threaten to cause failure of the entire microgrid.

When both dispatchable power (or external grid connection) and energy storage are present, the economic dispatch solution should consider a decision horizon to minimize operation cost [Whitefoot et al. 2011]. By doing so, the dispatch strategy can seek to use the energy storage when the marginal operation costs are highest.

2.3 Optimal dispatch problem formulation

The optimal dispatch formulation described and used in this dissertation is the economic dispatch over a time horizon, where dispatchable power generation and dispatchable energy storage are present in the system.

2.3.1 Generalized problem formulation

The generalized optimal dispatch problem is to minimize some cost function, over some time period by choosing the optimal operation of each component at every time step. The cost function, $f_{cost}(\boldsymbol{x},\boldsymbol{u}(t))$, is a function of the microgrid design parameters, $\boldsymbol{x}$, which are held fixed, and the dispatch variables, $\boldsymbol{u}(t)$, which determine the operation of each dispatchable component at every time t. The time range over which the optimal dispatch problem is solved (t_0 to t_{horiz}) is known as the time horizon. This minimization is subject to some inequality constraints, $\boldsymbol{g}(\boldsymbol{x},\boldsymbol{u}(t))$, which define the power and energy limits of each component and other practical system limitations. Additionally, there may be equality constraints, $\boldsymbol{h}(\boldsymbol{x},\boldsymbol{u}(t))$, to ensure system power balance. The generalized problem structure is shown in Eqs. (2.1).

$$\min_{\boldsymbol{u}(t)} \sum_{t=t_0}^{t_{horiz}} f_{cost}\big(\boldsymbol{x},\boldsymbol{u}(t)\big) \tag{2.1a}$$

subject to:

$$\boldsymbol{g}\big(\boldsymbol{x},\boldsymbol{u}(t)\big) \leq \boldsymbol{0} \tag{2.1b}$$

$$\boldsymbol{h}\big(\boldsymbol{x},\boldsymbol{u}(t)\big) = \boldsymbol{0} \tag{2.1c}$$

2.3.2 Problem-specific formulation

A typical problem formulation for a microgrid with some dispatchable power resources and energy storage is shown in Eqs. (2.2). This formulation will provide the framework of all the optimal dispatch problems solved in this dissertation. Note: the formulation below assumes time discretization in one-hour increments. This allows easy conversion between power in kW and energy in kWh, which simplifies the formulation.

$$\min_{\boldsymbol{u}(t)} \sum_{t=1}^{T_{horiz}} p_{fuel}\, E_{fuel}^{t} \qquad \text{fuel cost for time horizon} \tag{2.2a}$$

subject to:

$$\underline{E}_j \leq E_j^t \leq \overline{E}_j \qquad \text{storage energy capacity limits, } \forall j, \forall t \tag{2.2b}$$

$$E_j^{t+1} = E_j^t + u_j^t \overline{P}_j \quad \text{storage energy balance, } \forall j, \forall t \quad (2.2c)$$

$$\sum_i u_i^t \overline{P}_i + \sum_j u_j^t \overline{P}_j - P_{ls}^t \geq P_{ld}^t \quad \text{network power balance, } \forall t \quad (2.2d)$$

$$E_{fuel}^t = \sum_i f(u_i^t, \overline{P}_i) \quad \text{fuel use of resource } i \text{ at time } t, \forall i, \forall t \quad (2.2e)$$

$$0 \leq u_i^t \leq 1 \quad \text{resource power limits, } \forall i, \forall t \quad (2.2f)$$

$$-\overline{P}_j \leq u_j^t \leq \overline{P}_j \quad \text{storage power limits, } \forall j, \forall t \quad (2.2g)$$

$$\boldsymbol{u}(t) = \left[\boldsymbol{u}_i(t)\, \boldsymbol{u}_j(t)\right];\ t \in \{1,..,24\};\ i \in \{1,..,N_i\};\ j \in \left\{1,..,N_j\right\}$$

In the preceding formulation, the vector of dispatch factors, ***u(t)***, is comprised of the dispatch factors for all power generation resources, $\boldsymbol{u}_i(t)$, and all energy storage devices, $\boldsymbol{u}_j(t)$, at all time increments (where subscript *i* refers to power generation resources and subscript *j* refers to energy storage devices), *t*; p_{fuel} is the fuel price; E_{fuel}^t is the fuel energy used at time *t*; $\overline{E}_j$ and $\underline{E}_j$ are the maximum and minimum capacity of energy storage resource *j*, respectively, and E_j^t is the state of charge (SOC) of resource *j* at time *t*; u_j^t is the dispatch factor of energy storage *j* at time *t*; $\overline{P}_j$ is the maximum power available from energy storage *j*; u_i^t is the dispatch factor of power resource *i* at time *t*; $\overline{P}_i$ is the maximum power available from power resource *i*; P_{ls}^t is the power loss of the system due to transmission or other efficiencies at time *t*; P_{ld}^t is the electrical power load at time *t*; N_i is the number of power generation resources; and N_j is the number of energy storage resources.

The network power balance constraint, Equation (2.2d), is formulated as an inequality constraint. It ensures no loss-of-load (LoL), or insufficient power on the network, however it does not strictly enforce equality. This is necessary because the non-dispatchable renewable energy may produce more power than the system can absorb, and in these cases it is assumed the excess power is dissipated or sent to ground.

Renewable power sources can be added to this system as a "negative load" in the network power balance, Equation (2.2d). Equation (2.2e) is an intermediate equation to relate the dispatch of the power resources to the fuel use of the system in the objective. As such, it does not need to be presented in the optimization formulation, as it can be

substituted into the objective function and eliminated. However, it is presented here for completeness.

2.3.3 Optimization algorithm and numerical issues

The optimal dispatch problem presented here is a nonlinear problem with continuous variables. Therefore, a general-purpose nonlinear programming algorithm, Sequential Quadratic Programming (SQP), was chosen to solve it. Matlab's *fmincon* implementation of SQP was used with finite differencing to estimate gradients and the following algorithm parameters:

Table 2.1 – SQP parameters used within Matlab's *fmincon* function

Parameter	Value
SQP strategy	'active-set'
Finite difference: maximum step	1.0
Finite difference: minimum step	1e-5
Convergence tolerance: objective function	5e-6
Convergence tolerance: constraints	1e-4

The algorithm was highly sensitive to these parameter values, both in efficiency and also in whether it could converge at all. A single starting point was chosen, as multiple start points (to investigate for local minima) would increase the simulation cost too significantly.

The problem often suffers from numerical issues which can affect convergence and efficiency. The main problem is that the Hessian can often be rank-deficient. The most common source of this is that the problem formulation has variables and constraints for every time increment within the time horizon. Thus, for a 24-hour time horizon, there will be 24 similar constraints, e.g., for network power balance. Under certain conditions, these constraints can be identical, resulting in degeneracy and a rank-deficient Hessian. There may exist other problem formulations that can eliminate this issue; in this case, it was necessary to choose an implementation of SQP that was robust enough to be able to recover from these instabilities.

As a final note on Matlab's *fmincon* function: the results in this dissertation were generated using version 2010a. It was noticed that the results can change when using older versions of Matlab, e.g., version 2009a. Users of Matlab are cautioned to note this anomaly.

2.4 Problem simplification

As mentioned at the beginning of the chapter, formulating an optimal dispatch problem with many dispatchable devices over a long time period can result in a large-dimensional optimization problem. For example, solving a ten-device problem hourly over an entire year results in (10 devices)(8760 hrs) = 87,600 variables. The problem can be linearized and solved as a linear programming (LP) problem, but this can result in loss of solution fidelity for highly nonlinear problems. It may be possible to solve the problem using piece-wise linearization, which can preserve the trends of the nonlinearities depending on their actual form.

If the problem is left in its original nonlinear form, it can be solved by nonlinear programming (NLP) methods if it is simplified and reduced in various ways, for example by reducing the amount of time over which the problem is solved, reducing the number of dispatch variables via lumped components, and problem decomposition. The methods evaluated in this dissertation include:

1) Solving the optimal dispatch over a moving time horizon
2) Minimizing the length of the time horizon
3) Increasing the step-size between sequential time horizons
4) Using variable reduction via lumping of similar elements
5) Separating the energy storage dispatch and power generation dispatch
6) Reducing the total time modeled by using representative days

Each of these methods aims to simplify and reduce the optimal dispatch problem computation and will be described in the following sections. Some of these methods are dependent on specific assumptions and may not be applicable to all problems.

2.4.1 Distribution of power amongst similar elements

Often, a microgrid will have numbers of similar elements, e.g., a series of diesel generators or a bank of storage batteries. When this occurs, it may be possible to combine the similar elements into a single lumped "device" and treat its dispatch as a single entity. This can reduce the complexity of the overall optimal dispatch problem.

2.4.1.1 Vehicle batteries

Multiple vehicles parked at a single charging station can be treated as a lumped storage device when solving the microgrid-level optimal dispatch problem, which reduces the dimension of the optimal dispatch problem and saves computation time. The lumped storage device would have the power and storage capacity of the sum of devices, and the division of power between each individual device can be handled by a subproblem algorithm or local controller. Much research exists on how to implement charge controllers for multiple plug-in vehicles, for example, [Galus et al. 2008, Hiskens et al. 2009, Peças Lopes et al. 2009, Markel et al. 2009, Li et al. 2011, Ahn et al. 2011a]. The choice of a particular charging algorithm or controller depends on the goals of the problem, e.g., state-of-charge equalization, minimizing battery degradation, or maximizing renewable energy potential. Throughout this dissertation, a charge controller developed by Peters et al. is chosen with the goal of equalizing battery state of charge (SOC) between all plugged-in vehicles [Peters et al. 2011]. It will be described in detail in Chapter 5.

2.4.1.2 Multiple generators

Similar to the case for multiple plugged-in vehicles, multiple co-located power generation devices can be lumped and treated as a single device when solving the microgrid-level dispatch problem. This is viable under the assumption that all power from these co-located devices is supplied to the microgrid through a common connection, and thus will have the same transmission losses regardless of which generation device is operating. Often, as described in Section 2.2, the dispatch strategy for these co-located

generation devices can be determined *a priori* as a function of the power required, which saves computation time when calculating the microgrid-level dispatch problem.

This procedure can be shown by the example of two generators of different sizes, each available to supply a given power load. The first generator, Gen1, has a rated power of 70 kW, and the second generator, Gen2, has a rated power of 40 kW. Their respective fuel-use vs. power output curves are shown in Fig. 2.1. These curves are the output from a surrogate model generated using published data sheets for diesel generators [Cummins 2011]. The surrogate model is explained in detail in Section 3.4.1.2.

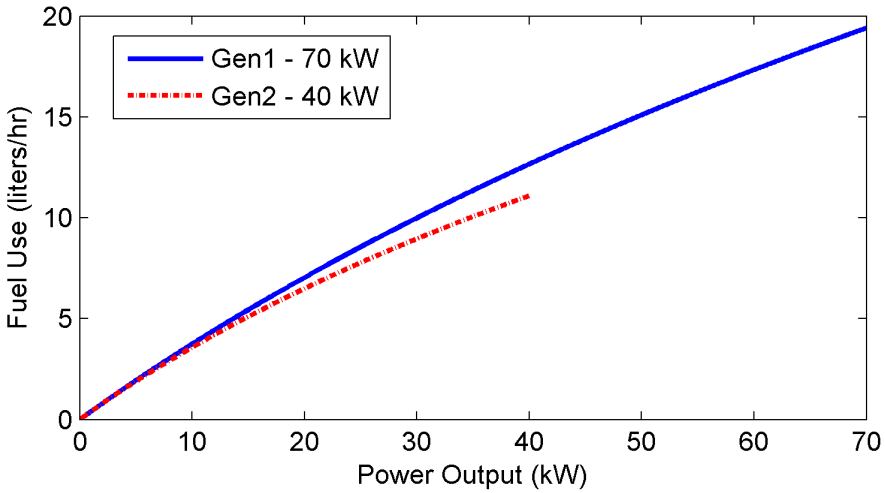

Figure 2.1 – Fuel use vs. power output for two generators, 40 kW and 70 kW

The figure shows that the smaller generator, Gen2, uses less fuel for any output power up to its rated power. Therefore, the optimal economic dispatch strategy for power outputs from zero to 40 kW can be determined: run Gen2 only. Once the required output power is greater than what Gen2 can supply, the optimal dispatch strategy becomes more complicated. However, if the two generators have different fueling curves a globally-optimal dispatch strategy can be determined for totaloutput power up to the maximum output from both generators (110 kW)(Note: if two or more generators have identical fueling curves, there will be multiple, equivalent solutions to this problem).

The fueling curves are smooth and monotonic, so the optimal dispatch strategy to minimize total fuel use from the generators can easily be solved at small increments of total output power. An example solution for the two generator case is shown in Fig. 2.2.

The figure shows that the optimal dispatch strategy increases the load on Gen2 until its maximum output (40 kW), then begins increasing the load on Gen1. At a load of 52 kW, Gen2 is shut off and the entire load is shifted to Gen1. Once the load is above the maximum output of Gen1 (70 kW), Gen2 is again switched on to produce the remaining power. Note: this solution assumes no idling of generators and no startup fuel penalty, which is reasonable when studying dispatch strategy changes at long time increments, e.g., 1 hour.

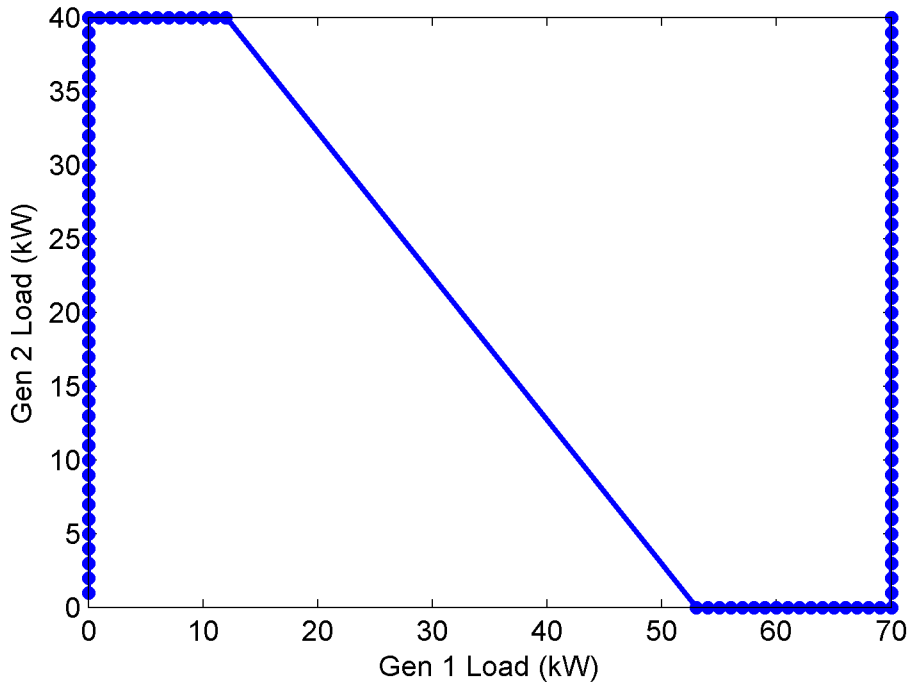

Figure 2.2 – Optimal dispatch strategy for two generators, 70 kW and 40 kW

The shutting down of Gen2 at total output of 52 kW may not be intuitive initially, but can easily be understood by looking at the fueling curves in Fig. 2.3. As seen in the figure, the fuel used by Gen1 only is less than using Gen1 and Gen2 simultaneously for power loads from 52 – 70 kW.

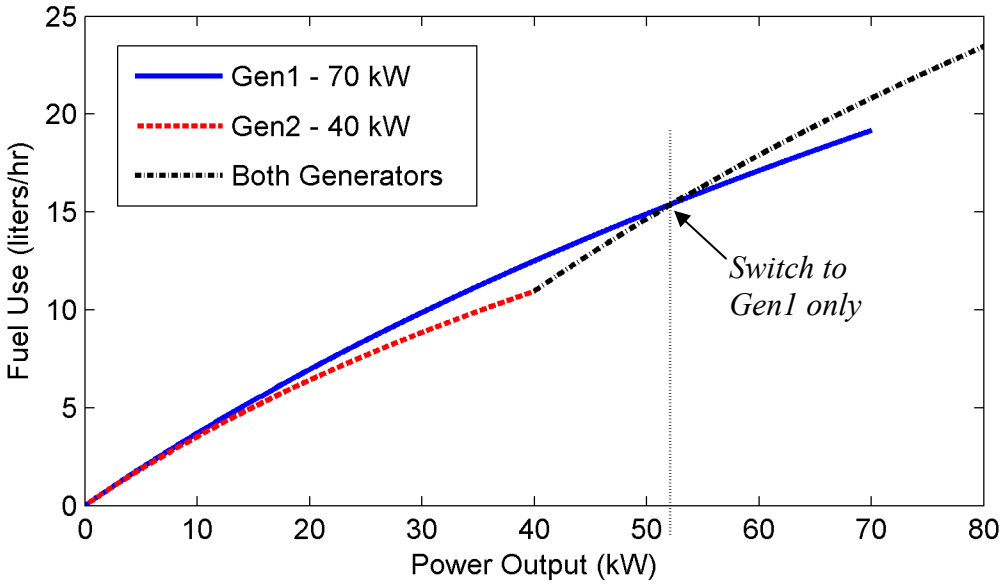

Figure 2.3 – Fuel use for one generator (70 kW) vs. two generators (40 kW and 70 kW)

By deciding this subproblem dispatch strategy beforehand, multiple generators can be lumped into one device if they are co-located or if their transmission losses are equivalent. This reduces the dimensionality of the system-level optimal dispatch problem, allowing for reduced computation time and greater scalability to allow for larger systems to be solved.

2.4.2 Separation of power generation dispatch problem

As mentioned in Section 2.2, when there is no energy storage the optimal economic dispatch of the power generation devices in a microgrid can be predetermined for any given load and the actual operation decision for each time period can be decided independently of the preceding or following time periods. Again, this solution only considers the direct operation costs and assumes no ramping costs or other transient costs for starting/stopping a particular resource. An example of this was shown for two generators in the previous section.

A similar process can be applied for the case where energy storage dispatch is included as well. We previously solved the power generation dispatch as a function of the

required load, as shown in Figure 2.2. For the case with energy storage included we must solve the power generation dispatch as a function of the power load *and* all possible energy storage dispatch scenarios. For a single energy storage element, the result is a 2-dimensional matrix of power generation dispatch solutions as a function of energy storage dispatch and power load.

Ren solved the optimal dispatch of two generators with a single energy storage element and showed that the generator dispatch strategy can be solved for the ranges of possible energy storage dispatch and power loads [Ren 2011]. The derivation can be found in the working paper and the resulting 2-dimensional plots of the optimal dispatch strategies for the generators are shown in Fig. 2.4.

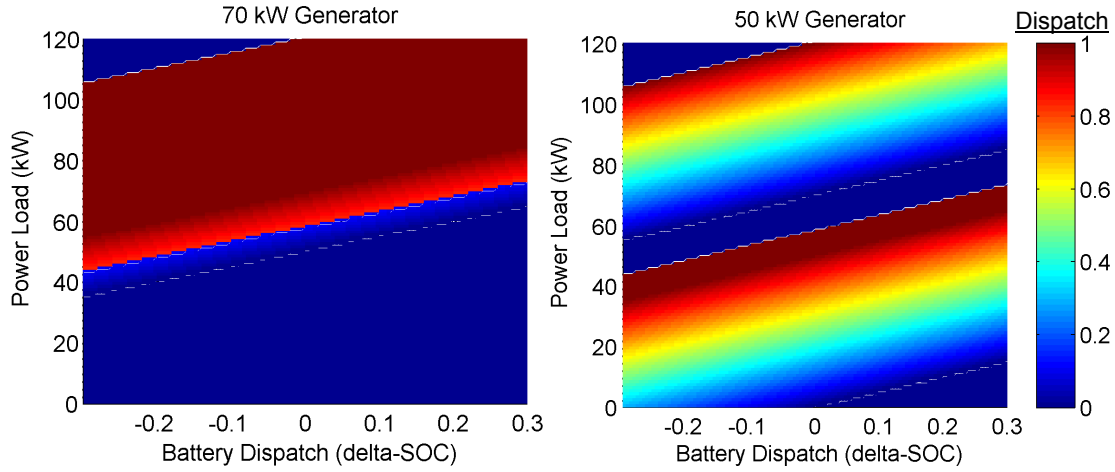

Figure 2.4 – Optimal dispatch for two generators (50 and 70 kW) as a function of battery dispatch and power load

We can compare these results to the case with no energy storage by choosing vertical slices through the graphs where the battery dispatch is zero. Looking only at these slices, we can again see that the optimal dispatch strategy is to initially use the smaller generator up to its maximum output, then increasing the load on the larger generator. At some point the load switches entirely to the larger generator, until its maximum output is reached. Then the load on the smaller generator is increased until the maximum total output is reached.

The effect of adding the battery storage on the optimal dispatch strategy for the generators is to increase the total load on the generators (when charging the storage) or

decrease the total load when discharging. This has the effect of shifting the dispatch strategies as a function of power load, as seen by the sloped transitions in Fig. 2.4. However, pre-solving for these matrices allows us to know the optimal generator dispatch for any energy storage dispatch. Thus, solving for the dispatch problem over a time horizon can be reduced to only solving for the energy storage dispatch, with the optimal generator dispatch chosen from the matrices as a function of the energy storage dispatch and power load.

Note that these optimal dispatch matrices would increase in dimension for each additional energy storage element, thus the benefits of separation may decrease rapidly as too much pre-processing would be involved. Also, as mentioned in Section 2.2., this *a priori* solution of power generation dispatch is only valid if transmission losses are constant for any dispatch strategy, e.g., the power generation devices are co-located or the power loads are co-located load with similar transmission losses for all power generation components.

2.4.3 Reduction of time considered

The optimal dispatch problem is often solved over some long time period, e.g., one year, in order to estimate the operating costs of the microgrid over the various seasons of the year. This is necessary because the power loads will change as heating, cooling, and lighting needs change, and renewable energy supply is often seasonal as well. Solving the optimal dispatch simultaneously over the entire year is possible using linear programming, but is intractable for nonlinear programming and also not representative of how the microgrid will actually operate. The computation time to solve the optimal dispatch problem can be reduced by breaking the whole-year problem into smaller time segments and additionally by solving for a subset of the entire year and using those results to estimate the operation over the entire year. The following four sub-sections describe various methods implemented to achieve these goals.

2.4.3.1 Implementing a moving time horizon

Optimizing the dispatch over a forward-looking time horizon is necessary to determine the optimal energy storage strategy, which requires decision making over multiple time increments. Ideally the entire time period from T_1 to T_{final} would be solved simultaneously, but it is necessary to decompose the time period into a series of overlapping time windows (the time horizon) because solving the optimal dispatch for all time increments simultaneously is computationally infeasible for nonlinear programming.

The problem structure is shown in Fig 2.5. For clarity, we refer to the entire time period by the uppercase variable T and the current time horizon, which is a subset of T, by the lowercase variable t. For a microgrid design, $\boldsymbol{x}$, the optimal dispatch problem is solved over the finite time horizon ($t=1$ to t_{horiz}) and then stepped forward one hour in time and re-solved, until the entire time period of interest (T_1 to T_{final}) is completed. For each time horizon, only the vector of optimal dispatch for the first time step, $t=1$, is saved as part of the overall optimal dispatch matrix, $\hat{\boldsymbol{u}}(\boldsymbol{T},\boldsymbol{x})$. At the end of the series of optimal dispatch problems, the optimal dispatch matrix is returned along with the total operation and maintenance (O&M) cost, $f_{O\&M}(\boldsymbol{x},\hat{\boldsymbol{u}})$, and the feasibility information of the optimal dispatch problem, $\hat{\boldsymbol{g}}$ and $\hat{\boldsymbol{h}}$. This optimal dispatch problem structure will be nested in an optimal design problem in Chapter 3.

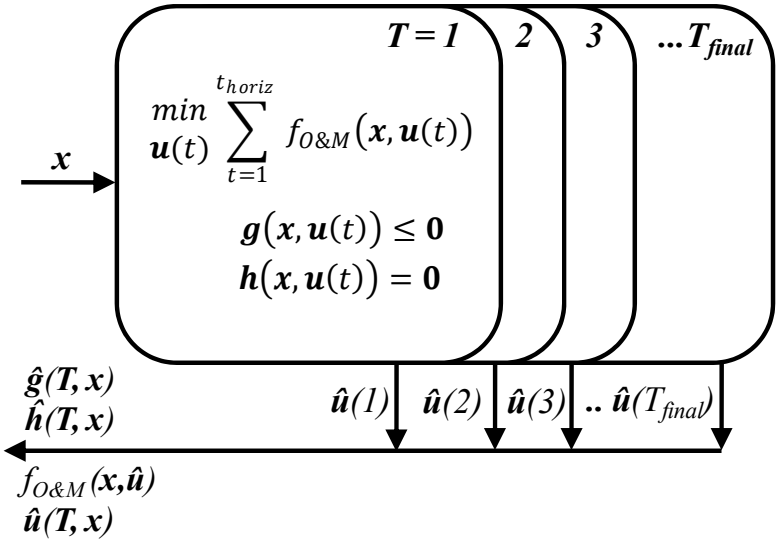

Figure 2.5 – Structure of solving a sequence of forward-looking optimal dispatch problems

The choice of time horizon length is an issue under research. Longer time horizons will theoretically provide better planning of energy storage, but at the cost of increased computation time. In addition, some research has shown that increased time horizons offer no benefits when uncertainty is included, as the error in future predictions will compound as the prediction horizon increases [Peters et al. 2011]. A heuristic choice for time horizon would be 24 hours because the solar supply and power loads also follow a 24-hour cycle. This issue will be explained further in the following section.

2.4.3.2 Time horizon length

Time horizon length affects the optimal dispatch solution and its computation time. Heuristically, a time horizon length of 24 hours would capture the diurnal nature of power load and solar energy supplies, so it is a natural choice. A study was performed on a fixed-design microgrid to analyze the effect of time horizon length on the optimal dispatch strategy and predicted fuel use, with the results in Table 2.2. This is similar to a study performed in [Peters et al. 2011]. Time horizon lengths were chosen from 4 - 24 hours, with comparisons made to the 24-hour time horizon.

Table 2.2 – Effect of time horizon length on dispatch solution

Time Horizon (hrs)	Step Size (hr)	Objective variation	Calculation time reduction
24	1	-	-
22	1	0.10%	13%
20	1	0.04%	27%
18	1	0.08%	39%
16	1	0.12%	47%
14	1	0.16%	57%
12	1	0.13%	65%
10	1	0.18%	72%
8	1	0.27%	77%
6	1	0.42%	84%
4	1	---- FAIL ----	

The results show that the variation in the objective is 0.1% or less for time horizons from 18 – 24 hours. The objective increased for shorter time horizons, up to 0.42% for the 6-hour horizon. To balance computation time reduction with accuracy, the time horizon was set at 18 hours for studies performed within this dissertation.

2.4.3.3 Step size between time horizons

To save additional computation time, the variation in step sizes between time horizons was studied. Theoretically, the minimum step size possible is one time period and the maximum step size would be the length of the time horizon (zero overlap). Various step sizes were studied for a single microgrid example with a 24-hour time horizon and 1-hour minimum step size, with the deviation in the objective function and calculation time reduction shown in Table 2.3. The results show that steps up to 12 hours do not degrade the solution significantly (< 0.16%); however, a step size of 18 hours degrades the solution over 2%, showing that some overlap of the time horizons is necessary.

Table 2.3 – Effect of step size between time horizons on optimal dispatch solution

Time Horizon (hrs)	Step Size (hr)	Objective variation	Calculation time reduction
24	1	-	-
24	2	0.03%	43%
24	3	0.04%	59%
24	4	0.16%	69%
24	6	0.06%	79%
24	8	0.08%	83%
24	12	0.02%	84%
24	18	2.03%	90%

When combined with the 18-hour time horizon chosen in Section 2.4.3.2, a step size of 4 hours between time horizons provided an objective function accuracy within 0.1% while saving 80% of the computation time compared to the 24-hour time horizon, 1-hour step size case.

2.4.3.4 Partial-year solution

Solving the optimal dispatch for a single design over an entire year is computationally intensive, taking 2–3 hours on a 2.8GHz, quad-core i7 processor PC with 8GB of RAM. Therefore, steps were taken to estimate the operating costs based on the optimal dispatch for representative days of the year. This approach is a modified version of Asano and Bando's [Asano et al. 2007], though their strategy only solved the optimal dispatch over single, independent days without considering the connection to preceding and following days.

A study was performed by Kendra Borchers to identify the minimum number of days necessary to accurately predict the yearly fuel use [Borchers 2011]. The study calculated the optimal dispatch for various numbers of consecutive days (2, 7, and 14 days) run during various numbers of months distributed equally throughout the year (3, 4, 6, and 12 months). The predicted yearly fuel use was compared to the actual yearly fuel use calculated when running the optimal dispatch for the entire year. The error between each case studied and the actual fuel use is shown in Table 2.4.

Table 2.4 – Error in fuel use prediction for partial-year solutions

	3 months	**4 months**	**6 months**	**12 months**
2 Day Trials	49.2%	47.8%	47.7%	48.1%
7 Day Trials	13.3%	10.5%	10.5%	10.9%
14 Day Trials	7.4%	3.0%	3.4%	3.4%

The results show that running 14-day trials for four or more months of the year can result in fuel use predictions within 3% of actual while providing significant reduction in computation time. For this dissertation, 14-day trials were chosen for three months of the year, which results in increased prediction error but saves additional computation time. If increased prediction accuracy is sought, it is recommended to run 14-day trials for at least four months of the year. Also, these results were generated using deterministic, known input parameters (e.g., power load and solar irradiance). It is unknown whether the accuracy will hold when considering stochastic input parameters, as will be done in Chapter 4.

2.5 Effects of transmission losses within the microgrid

The optimal dispatch strategy of a microgrid will be affected by transmission losses between components of the system, especially if the losses are significantly different for various power sources to supply a particular load. In some cases, transmission losses may dictate that the optimal dispatch strategy is to use a power source with lower inherent efficiency simply because it is closer to the load and the combined efficiency losses plus transmission losses are lower than a more efficient power source that is further away.

A simple example can demonstrate this effect. Consider two diesel generators on a microgrid, G_1 and G_2, both rated at 100 kW peak power. For simplicity, assume the efficiency of G_1 is a constant 30% ($\eta_{G1} = 0.30$) and the efficiency of G_2 is a constant 28% ($\eta_{G2} = 0.28$), where efficiency is defined as the electrical energy out divided by the fuel energy consumed. In addition, there are two electrical loads on the microgrid, L_1 = 50 kW and L_2 = 30 kW. A schematic of this example is shown in Fig. 2.6.

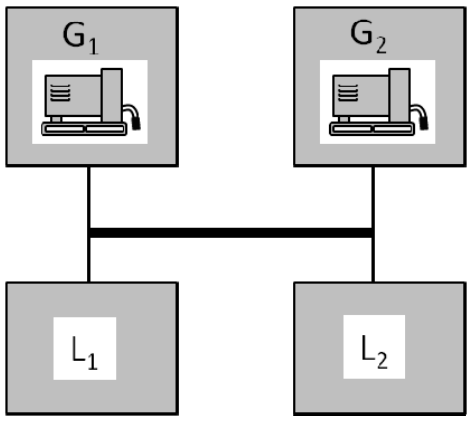

Figure 2.6 - An example microgrid with two generators, G_1 and G_2, and two loads, L_1 and L_2.

If we assume no transmission losses, the fuel power consumed by G_1 to supply the entire load is 80 kW / 0.30 = 266.7 kW, whereas if we operated G_2 instead, it would consume fuel at a rate of 285.7 kW. Thus, the optimal dispatch strategy is for G_1 to operate at 80 kW output to supply the two loads, with G_2 off. If we assume constant transmission losses between each generator and each load, for example 5% losses (η_{TL} = 95%), the overall efficiency of G_1 to supply any load is now $\eta_{G1}\,\eta_{TL} = (0.3)(0.95) =$

0.285. Similarly, we can calculate the overall efficiency of G_2 to supply any load as η_{G2} η_{TL} = (0.28)(0.95) = 0.266. It is clear that the dispatch strategy will be the same as the no-loss scenario: operating G_1 until its maximum power is exceeded, with G_2 taking the remaining load. Thus, we can say for this simple example with constant or zero transmission losses that the efficiency of G_2 is always dominated by G_1.

In this case, the dispatch strategy can be pre-determined for any case simply by knowing the total electrical load required. This leads to the ability to separate power generation dispatch from the optimal dispatch problem, as it can be deterministically solved for any state of the system. This simplification reduces the dimension of the optimal dispatch problem and therefore also reduces the computation time required to solve the problem.

However, if we assume variable transmission losses between each generator and each load, the optimal dispatch strategy is less clear. This is especially true if the losses are nonlinear, e.g., a function of the voltage and current of the power flow and the resistance of the electrical lines. To show this, we modify the previous example as shown in Fig. 2.7. Now, if G_1 supplies power to L_2 or G_2 supplies power to L_1 there is an additional transmission loss η_{TL} = 0.90. For our original example where L_1 = 50 kW and L_2 = 30 kW, the optimal dispatch solution changes to operating G_1 at 52.6 kW and G_2 at 31.6 kW. We can see that as the transmission losses increase the optimal dispatch strategy will favor localized power generation.

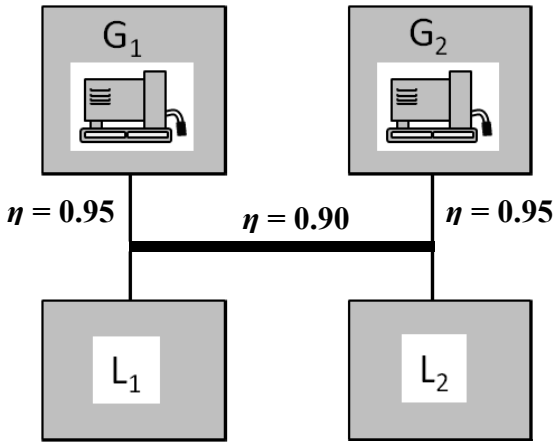

Figure 2.7 - An example microgrid with variable transmission losses between components.

For systems with realistic, nonlinear transmission losses, the dispatch strategy cannot be pre-determined, but must be determined for every specific state of the system. In this case, the power generation dispatch cannot be separated from the optimal dispatch problem. However, in some cases where power generation is co-located and where the transmission losses from each generating unit are the same, e.g., multiple generators in a single location, the total power generation can be lumped and that lumped power can be used in solving the optimal dispatch problem. The dispatch of each generator in that lumped system can then be solved as a separate subproblem.

2.6 Possibility of multiple equivalent solutions

The optimal dispatch problem is not guaranteed to have a unique solution. This can lead to numerical instability of the optimization algorithm, e.g., by causing a rank-deficient Hessian matrix for quasi-Newton methods. Specific problem formulations that can lead to multiple equivalent solutions include:

(1) Multiple identical elements, e.g., similar electric vehicles at a charging station.
(2) Negligible loss of energy storage over time, e.g., zero battery self-discharge over one hour.

In Case (1), if two vehicles are parked at a charging station and they have identical battery packs and charging efficiencies, then the optimal dispatch cannot discern between charging one vehicle or the other. A similar situation occurs if there are multiple identical diesel generators available to supply power. This problem can be remediated by lumping the identical elements into a single device for the purposes of solving the optimal economic dispatch. The actual dispatch strategy for the lumped elements can then be solved as a subproblem, perhaps with a different objective, e.g., state-of-charge equalization between electric vehicles or minimizing diesel generator on/off cycling.

In Case (2), it is valid to assume that the charge lost from a battery in a single hour is negligible. Thus, charging or discharging the battery some fixed amount at time t or at time $t+1$ may have the same effect on the optimal dispatch objective function and

constraints. These two dispatch solutions are then equivalent. Simply including self-discharge may not solve this problem, as the amount of self-discharge may be so small that the optimization algorithm has difficulty numerically discerning between the dispatch strategies. A method to address this issue is unknown to the author. Instead, it is important to choose an optimization code that is robust to dealing with rank-deficient Hessians and other numerical instabilities.

2.7 Summary of economic dispatch optimization methods for different scenarios

Based on all of the optimal dispatch studies performed for this dissertation, the various problem-specific scenarios can be classified into four generic cases. Each case has characteristics that make different problem formulations appropriate and allow for various simplifications. By identifying the case that best matches a given problem, the optimal dispatch can be solved more efficiently, which is a critical component for optimal design of a microgrid where the optimal dispatch problem is nested within. The four cases are described as follows, in order of increasing solution complexity.

Case 1: No energy storage, *n* dispatchable power generation resources

- Perform economic dispatch during individual time increments without consideration of other time increments;
- Solve to minimize power costs (external grid + internal dispatch - renewable generation);
- For multiple dispatchable resources, it can pre-decide deterministic hierarchical ordering of least cost resources ("unit commitment problem");
- It can include loss-of-load (LoL) probability, if islanded.

Case 2: Have energy storage but no dispatchable power generation

- Must be islanded—no external grid connection (if grid connected, it becomes Case 3);
- Solve dispatch for loss-of-load only;

- Energy storage strategy is to charge when power is available, discharge when there is a LoL (deterministic heuristic);
- Solve single time increments—no advantage to use a time horizon unless seeking to minimize number of hours where loss of load occurs, rather than total loss of load.

Case 3: Energy storage with dispatchable power generation

- Dispatchable power generation may include external grid connection;
- For optimality, should solve energy storage dispatch over a time horizon;
- If cost of dispatched energy is constant, e.g., for residential grid electricity with single-tiered pricing, this case collapses to Case 2;
- If cost of dispatched energy varies (e.g., multi-tiered electricity pricing or variable generator efficiency), it can solve the unit commitment problem separately (similar to Case 1) for each level of load and energy storage dispatch to generate a matrix of solutions;
- Once optimal power generation is determined, problem becomes deciding optimal energy storage dispatch over time horizon;
- Optimal power generation dispatch of multiple components can be treated as a subproblem to solve only if transmission losses are constant for any dispatch strategy, e.g., co-located power generation devices or co-located load with similar transmission losses for all components;
- Optimal dispatch of multiple energy storage devices can be treated as a subproblem to solve if storage devices are co-located (e.g., electric vehicles), or if transmission losses are similar/negligible for all devices.

Case 4: Energy storage with multiple dispatchable power generation components and varying transmission losses (not co-located)

- Must solve multi-period dispatch for all resources simultaneously;
- Cannot predetermine power generation dispatch;
- Cannot solve lumped energy storage/power generation dispatch problem;

- Can still solve dispatch of co-located resources as a lumped problem/subproblem.

It is important to make some additional notes on transmission losses**.** Constant transmission efficiencies will not change the dispatch strategy as load changes location or level (hierarchical economic dispatch strategy). However, nonlinear or varying transmission efficiencies may change the dispatch strategy as the load changes location or level (non-hierarchical economic dispatch strategy).

2.8 Summary

This chapter has proposed an approach to solve a sequential series of nonlinear optimal dispatch problems with a finite time horizon. Problem simplifications were proposed to reduce the computation time. Additionally, optimal dispatch problems were grouped into four scenarios to understand the types of problem formulation and applicable simplifications. For the rest of this dissertation, we will implement the time reduction procedures but not the simplifications that assume constant transmission losses (e.g., we cannot decompose the solution of energy storage dispatch and power generation dispatch), which means we are assuming Case 4 as defined in the previous section. The optimal dispatch approach will be nested within an optimal microgrid design problem in Chapter 3.

Chapter 3: Microgrid design optimization

Ad-hoc design of a microgrid would be to size components to meet the expected peak load on the system. This is a conservative approach that has the potential to oversize components because the actual system dispatch is not considered. Instead, each microgrid design should be evaluated by solving the optimal dispatch problem of Chapter 2. This leads to coordinated optimal design and optimal dispatch problems that consider the sizing of individual microgrid elements simultaneously with their dispatch strategy.

3.1 Literature review

As described in Chapter 2, much research has been devoted to solving the optimal dispatch problem. A subset of this research also seeks to design the microgrid in addition to solving its dispatch problem. This research can be separated into four categories.

1. Non-optimal design approaches that use design of experiments or other methods to compare different design choices without performing design optimization;
2. Optimal design methods that do not solve for the optimal dispatch but instead use rule-based or fixed-controller methods to decide the microgrid operation;
3. Formulations that solve the optimal design and optimal dispatch problems as a combined All-in-One (AiO) problem;
4. Formulations that decompose the optimal design and optimal dispatch problems into separate, coordinated subproblems.

Non-optimal design approaches

HOMER Energy solves the optimal design problem using a full-factorial design of experiments on number and size of components, using a rule-based dispatch strategy to evaluate the microgrid operation. The HOMER approach solves the dispatch strategy for

minimum cost in a single time increment without explicitly planning energy storage for future time increments [Lambert et al. 2006]. The approach is not formally an "optimal" design problem as the full-factorial DOE chooses component sizes at a limited number of fixed intervals.

Zoka et al. compared the performance of four specific microgrid designs by solving the optimal dispatch problem for each, but they do not provide for more general design optimization capability [Zoka et al. 2007].

Optimal design without optimal dispatch

Vallem and Mitra used the simulated annealing algorithm to solve a mixed-integer, nonlinear sizing and siting (topology) of a microgrid to minimize system cost while maintaining system reliability [Vallem et al. 2005]. Their formulation uses generic "distributed power" of constant cost per unit power and does not directly consider an optimal dispatch problem. They do include a subproblem for power flow to minimize loss-of-load.

Pelet et al. used genetic algorithms to solve the nonlinear sizing problem incorporating detailed, physics-based models of the microgrid components [Pelet et al. 2005]. Their objective is to minimize capital and operational costs, with a tradeoff objective (Pareto objective) of minimizing CO_2 emissions. They use a rule-based control strategy to solve for the energy use of each component rather than an optimal dispatch problem.

Research by del Real et al. studied both optimal dispatch [del Real et al. 2009a] and the optimal sizing of a microgrid [del Real et al. 2009b], though not concurrently. In the optimal sizing case, they formulate a sizing problem with renewable energy (wind) and hydrogen storage. Instead of solving for an optimal dispatch problem they use "estimated operating conditions" to ensure that the design can meet the necessary load under various wind resource scenarios. Their objective function is formulated as a convex sum of equipment capital costs with no operating or maintenance costs, and the constraints are all linear functions. Therefore, they are able to solve a mixed-integer quadratic program.

Lu et al. solved a nonlinear microgrid design problem by decomposing it using MDO techniques to solve each time increment individually while coupled to other time increments through battery storage linking variables [Lu et al. 2010]. However, their approach does not calculate a multi-component optimal dispatch; instead, they use non-dispatchable components (wind and solar) to determine when battery storage should charge or discharge. In addition, they solve the problem using one-day time increments, which does not consider the hourly dynamics of renewable energy supply and energy storage.

Lu et al. extended their research to find the optimal design (sizing) of a hybrid energy system including energy storage, solar power, and wind power, with the objective of minimizing the capital cost of the system while also minimizing loss of load (LoL) given uncertainty in the renewable energy inputs [Lu et al. 2011]. As mentioned in Chapter 2, they solve the dispatch of energy storage for each design at one-hour increments using stochastic Markov chains to minimize the probability of LoL.

AiO approaches

Stadler et al. posed the design and dispatch problem as an All-in-One (AiO) problem for the entire year by linearization and solution using linear programming [Stadler et al. 2009], thus increasing solution efficiency but with the limitation of linearizing submodels, such as diesel generator efficiency as a function of load, or battery internal resistance as a function of state-of-charge.

Asano et al. solved a mixed-integer, nonlinear design (optimal sizing and component selection) and dispatch problem by separating the year into six representative days, then solving each day as a fixed AiO problem [Asano et al. 2007]. However, their approach does not consider the boundaries of the solved days by linking the time before and after the representative days. As such, the approach provides an approximation of the microgrid performance, but may differ from how the microgrid will be controlled and operated in practice.

Geidl's dissertation includes a section discussing optimal sizing and layout of microgrid components [Geidl et al. 2007b]. Though Geidl has also addressed the optimal

dispatching problem, he does not consider how to solve the optimal dispatch and optimal design problems concurrently.

Decomposed approaches

A decomposed method of microgrid sizing followed by controller design is proposed by del Real et al. but not implemented. In addition, their proposed framework does single-pass optimization, where an optimal controller is designed for an optimal design. This type of single-pass optimization has been shown to often result in a suboptimal design [Fathy et al. 2001].

The method presented in this chapter is a decomposition-based approach. The optimal dispatch problem is nested within the optimal design problem, as described further in Section 3.2.1 and first explained in [Whitefoot et al. 2011]. This type of nested optimization can result in a globally-optimal solution if the problem is shown to be convex, though non-convex functions are often present. This nested strategy is commonly used in combined optimal design and optimal control problems [Fathy et al. 2001, Peters et al. 2009], but has not been used previously for optimal design and optimal dispatch problems.

3.2 Problem formulation

The problem formulation of the optimal microgrid design problem varies depending on the variables chosen. The most basic microgrid design problem is to find the optimal size of components, where the number and type of components are held fixed, as is the microgrid topology.

3.2.1 Nested solution of optimal dispatch problem

The design and dispatch problems cannot be solved simultaneously (all-in-one) because, as mentioned in Chapter 2, the optimal dispatch problem is decomposed into a series of optimization problems solved over a moving time window. Therefore, the overall problem is separated into an outer loop design problem with a nested optimal dispatch problem, as shown in Figure 3.1. The optimal design problem (outer loop)

passes a vector of design variables, $\boldsymbol{x}$, to the optimal dispatch problem (inner loop). These design variables are treated as parameters (held fixed) by the optimal dispatch problem. The optimal dispatch problem is solved over its time horizon ($t=1$ to t_{horiz}) and then stepped forward one hour in time and re-solved, until the entire time period of interest (T_1 to T_{final}) is completed. For each time horizon, only the vector of optimal dispatch for the first time increment, t_0, is saved as part of the overall optimal dispatch matrix, $\hat{\boldsymbol{u}}(\boldsymbol{T},\boldsymbol{x})$. At the end of the series of optimal dispatch problems (inner loop), the optimal dispatch matrix is returned to the optimal design problem along with the total operation and maintenance (O&M) cost over the time period from T_1 to T_{final}, $f_{O\&M}(\boldsymbol{x},\hat{\boldsymbol{u}})$, and the feasibility information of the optimal dispatch problem, $\hat{\boldsymbol{g}}$ and $\hat{\boldsymbol{h}}$. The optimal design problem collects this information to evaluate each design's total objective function, annualized capital cost, $f_{cap}(\boldsymbol{x})$, combined with the annual O&M cost, $f_{O\&M}(\boldsymbol{x},\hat{\boldsymbol{u}})$, from the optimal dispatch problem. The outer optimal design problem is subject to the constraint that the optimal dispatch problem is feasible.

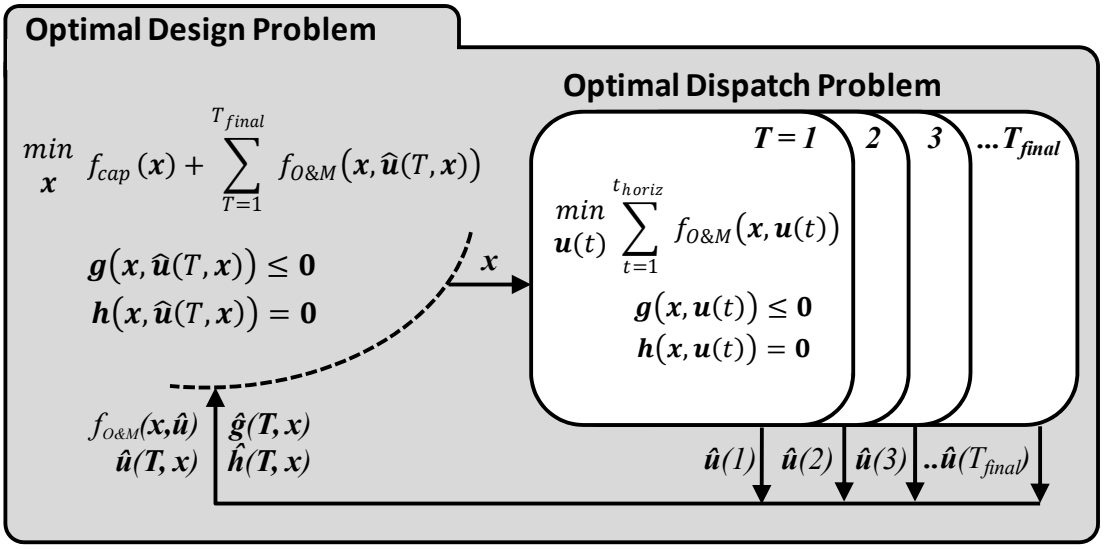

Figure 3.1 – Optimal design problem structure with nested optimal dispatch problem

If the optimal dispatch problem was known to be convex, this nested problem structure could be proven to provide the global optimum [Fathy et al. 2001]. However,

the microgrid problems in this dissertation contain non-convex functions, e.g., the generator fuel use as a function of load, thus there is the possibility for multiple optima and no claims can be made about global optimality or combined optimality.

3.2.2 Optimal design problem formulation

The goal of the optimal design problem is to minimize the combined capital cost, $f_{cap}(\boldsymbol{x})$, and operation and maintenance (O&M) costs, $f_{O\&M}(\boldsymbol{x}, \boldsymbol{u}(\boldsymbol{t}))$, of the microgrid by changing the size and number of microgrid components. Defining the objective this way balances the marginal benefit of investing in additional capital to reduce O&M costs. The O&M costs are defined over some specific time period, $T \in \{1, .., T_{final}\}$, so net present value calculations should be used to define the portion of capital cost that is depreciated during that same time period. The O&M costs are calculated from solving the optimal dispatch problem over the entire time period, so the optimal design problem is also a function of the optimal dispatch variables, denoted as $\widehat{\boldsymbol{u}}(T, \boldsymbol{x})$. The optimal design problem is only feasible if the nested optimal dispatch problem is feasible. Therefore, it is subject to the inequality and equality constraints, $\boldsymbol{g(x, \widehat{u}(T,x))}$ and $\boldsymbol{h(x, \widehat{u}(T,x))}$, which are passed from the optimal dispatch problem. The generalized optimization statement for the optimal microgrid design problem is shown in Eqs. (3.1). A problem-specific formulation will be shown in the example at the end of the chapter.

$$\min_{\boldsymbol{x}} \quad f_{cap}(\boldsymbol{x}) + \sum_{T=1}^{T_{final}} f_{O\&M}\big(\boldsymbol{x}, \widehat{\boldsymbol{u}}(\boldsymbol{T}, \boldsymbol{x})\big) \tag{3.1a}$$

subject to:

$$\boldsymbol{g}\big(\boldsymbol{x}, \widehat{\boldsymbol{u}}(\boldsymbol{T}, \boldsymbol{x})\big) \leq \boldsymbol{0} \tag{3.1b}$$

$$\boldsymbol{h}\big(\boldsymbol{x}, \widehat{\boldsymbol{u}}(\boldsymbol{T}, \boldsymbol{x})\big) = \boldsymbol{0} \tag{3.1c}$$

3.3 Choice of optimization algorithm

Solving the series of SQP problems for the optimal dispatch results in a numerically noisy function for operating cost because small changes in algorithm

convergence propagate through the series of SQP problems. Therefore, a non-gradient-based algorithm is selected to solve the optimal design problem. Additionally, in some formulations there are integer variables, such as to select the number of components (vehicles). Thus, the chosen algorithm must be able to handle mixed-integer problems as well.

The algorithm chosen for the studies in this dissertation is the DIRECT derivative-free algorithm, which can handle noisy objective functions and mixed integer and continuous variables [Jones 2001]. DIRECT is a robust, deterministic, global-search algorithm that can handle high levels of noise and discontinuity in the objective function. It works by dividing the design space into three hyper-rectangles along one variable dimension at a time. Upon evaluation of the center-points of the hyper-rectangles, it decides which rectangles to further subdivide. During each iteration of the algorithm, it will balance global and local searching by selecting high-performing rectangles of various sizes. Example iterations of DIRECT on a two-variable problem are shown in Fig. 3.2, where the rectangles selected for further subdivision in each iteration are greyed-out. For additional explanation of DIRECT, refer to the abbreviated description in [Whitehead 2001] or the full algorithm description in [Jones 2001].

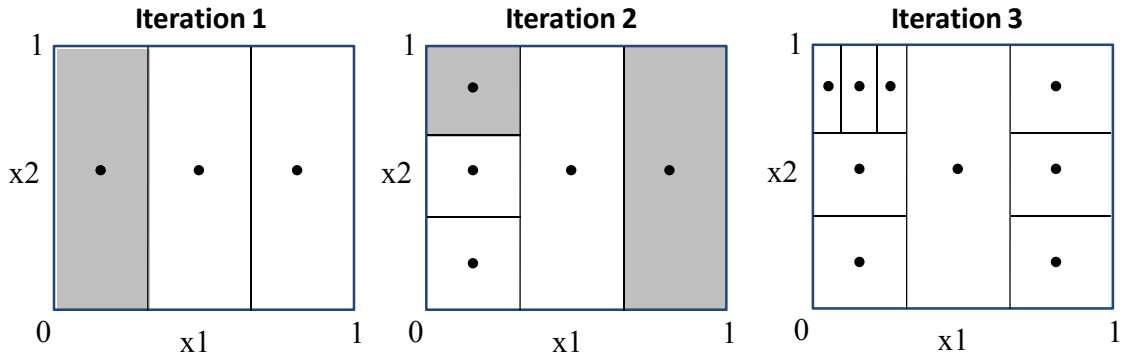

Figure 3.2 – Example iterations of the DIRECT algorithm

DIRECT's major drawback is that its performance suffers as problem dimensionality increases. Typically, it is not used for problems with more than 10 – 12 design variables, unless the computation of function calls is particularly inexpensive (~1 second or less). Furthermore, the DIRECT algorithm has no formal convergence criteria;

it runs for the number of design evaluations specified by the user. This disadvantage is remediated somewhat because the algorithm is deterministic and can be re-started from where it left off, if additional function evaluations are desired.

3.4 Example: Optimization of a military microgrid

The optimal microgrid design approach with nested optimal dispatch strategy was applied to the case of a small, islanded military microgrid. The microgrid is an example of a small Forward Operating Base (FOB) near Kabul, Afghanistan with approximately 50 soldiers. The goal of the optimization is to solve for the sizing of two diesel generators, a solar panel, and storage battery to meet the expected load of the base over a year. The operation cost for this base is solely from the fuel consumed by the diesel generators; maintenance costs were neglected for this analysis.

3.4.1 System modeling

The system topology is represented as four separate energy hubs, each with its own share of the power load and some of the hubs with power resources and/or storage devices. Hub 1 contains Generator 1, the PV array, and the storage battery. Hubs 2 and 3 are solely power loads and Hub 4 contains Generator 2. This layout is shown in Figure 3.3.

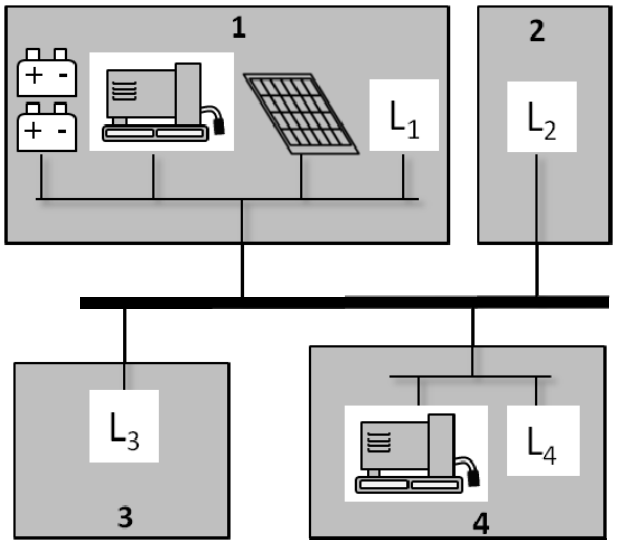

Figure 3.3 – Layout of hubs in military microgrid example

3.4.1.1 Microgrid network

It is assumed that there are no transmission losses within a single hub, which gives efficiency precedence to producing power locally to supply the load within a given hub. Power transfer is assumed to go through a common bus, with transmission losses modeled equivalently between any two hubs. The losses are assumed to scale quadratically with current, in keeping with I^2R resistance losses. Because of the high power flows (up to 80 kW), the bus voltage was assumed to be 400V and the conductors were assumed to be AWG 000 wire (0.4" Dia, 200 Amp capacity, 0.2 milliohm/meter) with a distance of 150m between any two hubs. This results in voltage and power losses of less than 4% at maximum current, which is within typical electrical specifications.

Before the network power balance is calculated, the power required by each hub is calculated by subtracting produced power from the power load within each hub, as shown in Eqs. (3.2). If the sum is positive the hub is importing power from other hubs, and vice versa. Transmission losses are then accounted for by applying Eq. (3.3) to each hubs' internal power balance, where *h* is the index of each hub. The effect of this equation is to require higher power when importing power and reduce the power available when exporting power.

Hub 1 $$P_{hub1} = L_1 - P_{gen1} - \eta_{PV}P_{PV} - \eta_{batt}P_{batt} \quad (3.2a)$$

Hub 2 $$P_{hub2} = L_2 \quad (3.2b)$$

Hub 3 $$P_{hub3} = L_3 \quad (3.2c)$$

Hub 4 $$P_{hub4} = L_4 - P_{gen2} \quad (3.2d)$$

Hub power with losses $$P_{net,h} = 0.00019{P_{hub,h}}^2 + 1.012P_{hub,h} \quad (3.3)$$

The power losses are small and similar to using a small, constant efficiency (~4%), but the advantages of using this method are twofold. First, this method attempts to estimate actual line losses and cause dispatch optimization to prefer local power production, especially at high power. Secondly, using a constant efficiency causes a discontinuity at zero power (the transition between importing and exporting power). This

discontinuity can cause numerical difficulty for nonlinear programming algorithms. The quadratic power loss model gives a smooth transition between power import and export as shown in Fig. 3.4.

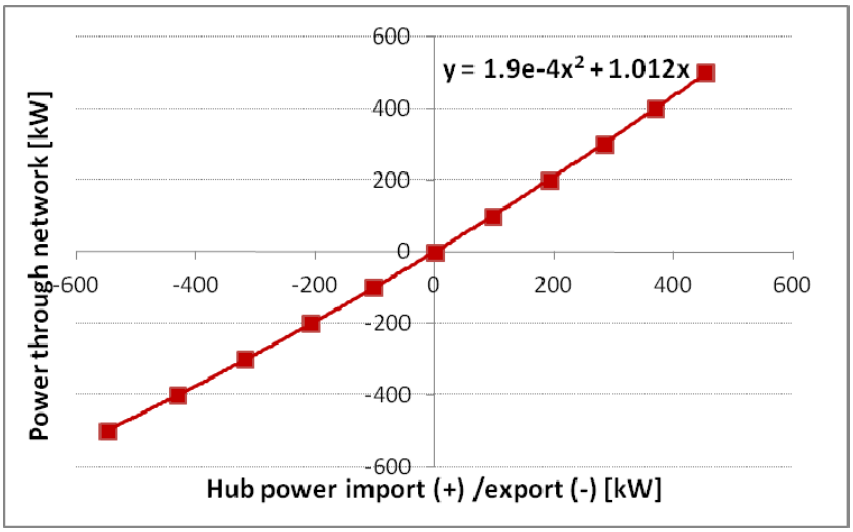

Figure 3.4 – Quadratic power import/export model on microgrid network

3.4.1.2 Generators

Performing design optimization of generator sizing requires a fuel-use model that varies both with the size (rated power) of the generator and with the load on the generator. Generator fuel use data at various loads were gathered for fifty Cummins diesel generators in rated powers from 10 – 300 kW [Cummins 2011]. A response surface model was created to calculate the generator efficiency as a function of generator rated power and load. The available data gave fuel use per hour at 25%, 50%, 75%, and 100% load. Data were added for 0% load, where it was assumed the generator would be turned off (not idling) so the fuel use was set to zero.

One of the goals of the response surface model was to be constantly increasing with load, so polynomial models were not suitable as they typically have inflection points between the two extremes, 0% and 100% load. Instead, a logarithmic model was chosen of the form:

$$Fuel \text{ (liters/hr)} = a\, P_{gen} \log(1 + L_{gen}) \qquad (3.4)$$

where a is the model fit parameter, P_{gen} is the rated power of the generator in kW, and L_{gen} is the generator load as a fraction of its rated load (0 – 1.0). The second goal of the response surface model was to ensure zero fuel use at 0% load, which is accomplished by adding 1 to the L_{gen} variable in the logarithm. This model form was suggested by Yi Ren at the Optimal Design Laboratory, University of Michigan.

After fitting the model using Matlab's *nlinfit* function, the resulting fit parameter was a = 3.95. The model produces contours of fuel use vs. load and rated power as shown in Fig. 3.5.

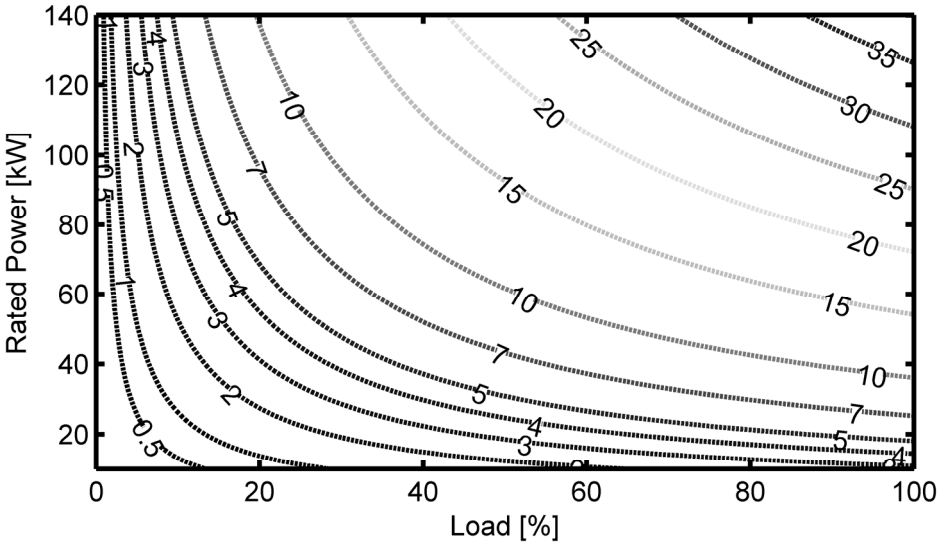

Figure 3.5 - Model of diesel generator fuel use (liters/hr) as a function of generator rated power and load

3.4.1.3 Batteries & photovoltaic array

The efficiencies of charging the batteries were assumed to be linear with a 95% efficiency for either charging or discharging. The power output from the photovoltaic array scaled linearly with solar irradiation and rated power, which was based on a 1 kW/m^2 peak solar irradiance. The PV panel inverter efficiency was assumed to be a constant 95% efficiency.

3.4.1.4 Power load

The electrical power load was based upon the number of soldiers at the forward operating base (50) and the estimated average and peak power loads per soldier (1.5 kW

per soldier). Due to lack of measured data, the daily power load was generically represented by a base load with an afternoon peak and night-time trough. The total daily power load was split amongst the hubs according to the following percentages: Hub 1: 10%, Hub 2: 20%, Hub 3: 40%, Hub 4: 30%.

The nominal power load was modified for a given day by seasonal average temperature data for the chosen region using Eq. (3.5), where the deviation from a "goal" temperature is used to approximate heating and cooling load changes.

$$L_d = L_b[0.65 + 0.023max(0, T_{av} - T_g) + 0.016\max(0, T_g - T_{av})] \quad (3.5)$$

In this equation, L_d is the daily power load, L_b is the average power load over the year, T_{av} is the average air temperature for a given day (°F), and T_g is the goal temperature, chosen to be 65 °F. The average daily temperature for the region was taken from historical data, as shown in Table 3.1.

Table 3.1 – Average monthly high and low temperature for Kabul, Afghanistan (°F) [weather.com]

	Jan	Feb	Mar	Apr	May	Jun	Jul	Aug	Sep	Oct	Nov	Dec
High	40	41	54	66	75	86	89	89	83	72	59	46
Low	19	21	33	42	47	54	59	57	48	39	29	23

Combining the seasonal variation with the nominal power load curve results in daily power load curves as shown in Fig. 3.6.

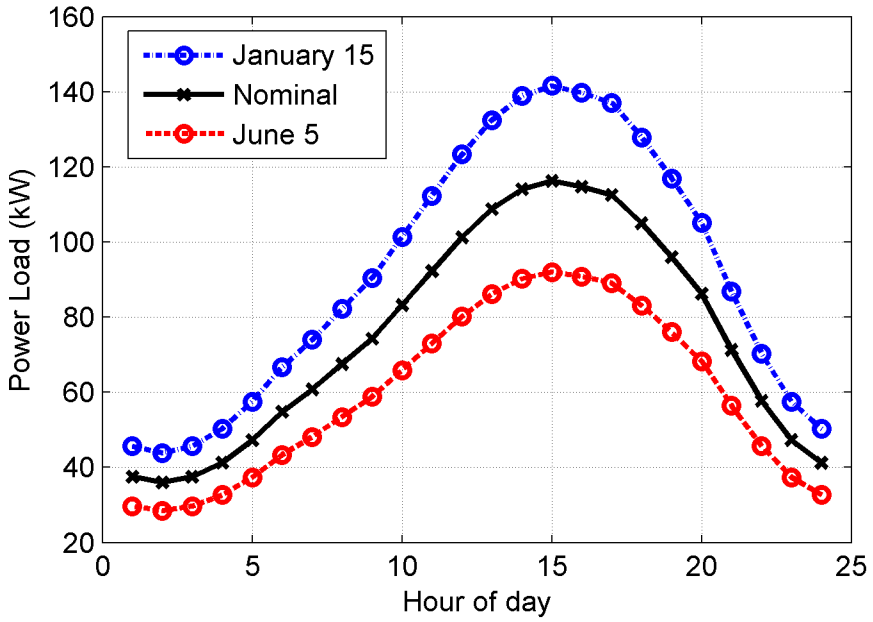

Figure 3.6 - Nominal power load and specific days showing seasonal variation

3.4.1.4 Solar irradiance

The solar irradiance for Kabul is taken from HOMER, which can estimate the solar irradiance at global locations by specifying the latitude and longitude of the location. Due to the high variability of solar supply (e.g., due to clouds), the hourly solar irradiance was averaged using two weeks before and after the days studied to smooth out the supply and represent an average day at that time of year. The averaged solar irradiance is shown in Fig. 3.7.

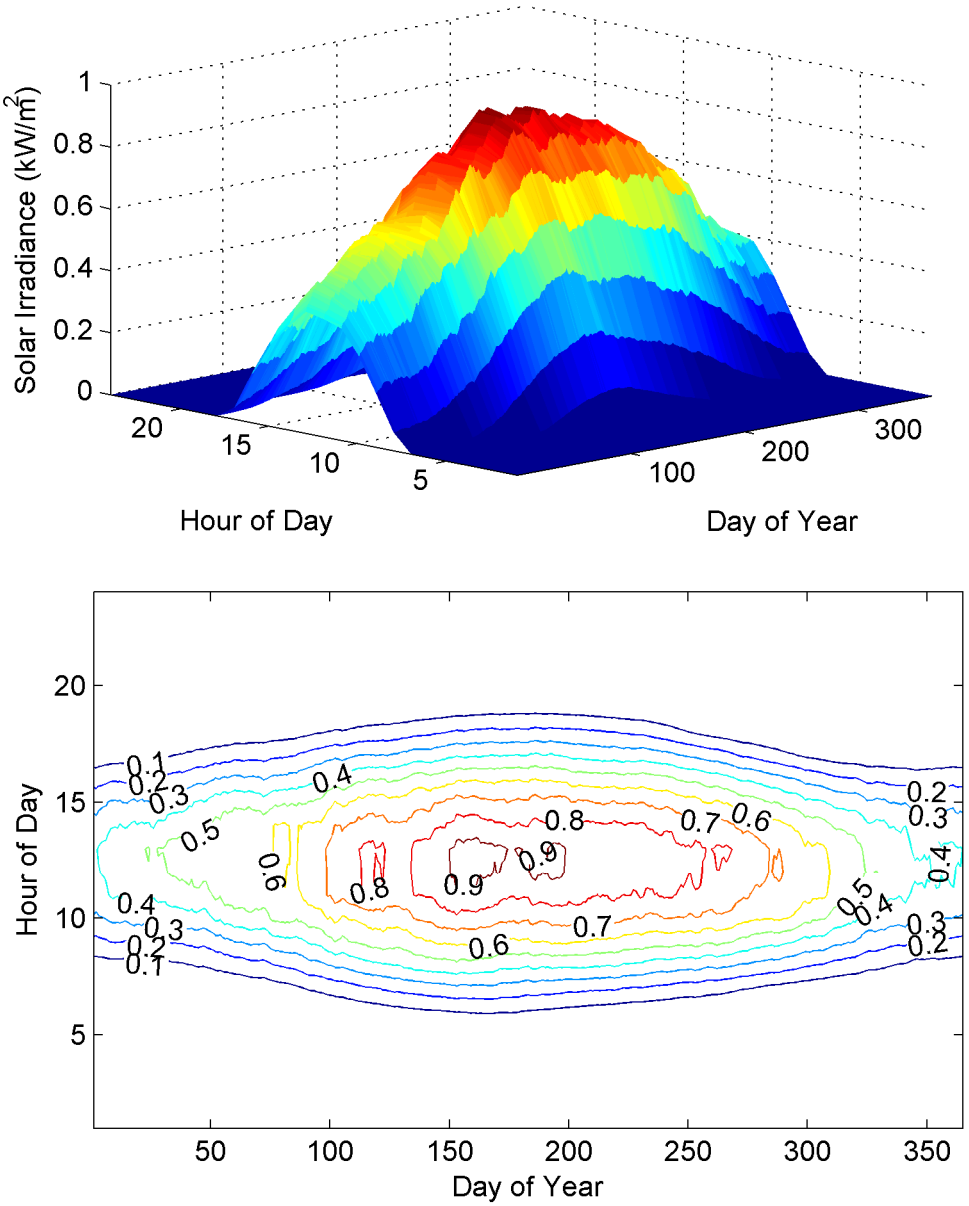

Figure 3.7 – Averaged solar irradiance for one year in Kabul, Afghanistan

3.4.1.5 Fuel cost

The fully-burdened cost of fuel for the U.S. military can range upwards from $5 per gallon ($1.32/liter), with one study estimating the average fully-burdened cost of a gallon of JP-8 at $13.68/gallon ($3.61/liter) [Hartranft et al. 2007]. Thus, the capital investment in renewable energy could be justified to reduce fuel cost. The variation in fuel cost varies widely depending on base location, method of transport, and other

factors, and different fuel costs will result in different optimal designs. Therefore, a parametric study of fuel cost is often included to show the range of optimal designs.

3.4.1.6 Capital costs

The capital costs of the microgrid components are functions of their sizes and the capital costs were "annualized" to enable combination with annual operating cost. To properly annualize the capital cost, the net present value (NPV) of the capital should be calculated. However, this requires knowledge of the investing entity's discount rate, the lifetime of the project (different than the total life of the capital), and the salvage or re-sell value of the equipment at the end of the project. The life of a forward operating base can range from months to years and the depreciation of the equipment is unknown. Therefore, it was assumed that the depreciation of the equipment was a linear function of its total lifetime. Also, the U.S. government has a low discount rate that is tied to the interest rate on U.S. Treasury bonds (currently ~2.2%), versus the discount rate for companies, which is typically assumed to be between 8 – 10%. As the discount rate approaches zero the NPV calculation collapses to the cost of the equipment divided by its lifetime. Therefore, given the large uncertainties in capital lifetimes and the low discount rate, the annualized capital cost calculation was simplified to be the total capital cost divided by its expected lifetime.

The capital cost of diesel generators and photovoltaic arrays are functions of their maximum power, p (kW), and lead-acid battery costs are a function of their capacity, C (kWh), as shown in Table 3.2. The equations are taken from various references, also listed in the table.

Table 3.2 – Capital cost equations as a function of component size

Component	Capital Cost Equation ($)	Reference
Generators	$1352(p^{0.631})$	[LBNL 2010]
PV array	$8431(p^{0.983}) + 3000$	[LBNL 2010]
Lead-acid Battery	$190C$	[Vyas et al. 1997]

The lifetimes were estimated based upon lifetimes reported by Lawrence Berkeley National Labs [LBNL 2010], but the PV array life was reduced from 20 to 15 years based on the rigors of military use and portability. These lifetimes are summarized in Table 3.3.

Table 3.3 - Lifetime estimates for capital equipment

	Diesel Generator	PV Array	Lead-Acid Battery
Lifetime (yr)	10	15	8

3.4.2 Optimization problem statements

The optimal design problem statement for this example is listed in Eqs. (3.6) and the accompanying optimal dispatch problem statement is listed in Eqs. (3.7).

$$\underset{\boldsymbol{x}}{min} \quad \sum_{c} \frac{1}{L_c} p_c x_c + \sum_{t=1}^{T_{Final}} p_{fuel} E_{fuel}^{t} \qquad \text{Annualized Capital Cost + Annual Fuel Cost} \qquad (3.6a)$$

w.r.t.:

$$x_1 = \bar{P}_{gen1} \qquad \text{Generator 1 rated power (kW)} \qquad (3.6b)$$

$$x_2 = \bar{P}_{gen2} \qquad \text{Generator 2 rated power (kW)} \qquad (3.6c)$$

$$x_3 = \bar{E}_{batt} \qquad \text{Storage battery capacity (kWh)} \qquad (3.6d)$$

$$x_4 = \bar{P}_{PV} \qquad \text{PV array rated power (kW)} \qquad (3.6e)$$

subject to:

$$\boldsymbol{g}\left(\boldsymbol{x}, \hat{\boldsymbol{u}}(\boldsymbol{T}, \boldsymbol{x})\right) \leq \boldsymbol{0} \qquad \text{Optimal dispatch problem feasibility} \qquad (3.6f)$$

$$\boldsymbol{h}\left(\boldsymbol{x}, \hat{\boldsymbol{u}}(\boldsymbol{T}, \boldsymbol{x})\right) = \boldsymbol{0} \qquad (3.6g)$$

$$35 \leq \bar{P}_{gen1} \leq 150 \qquad (3.6h)$$

$$30 \leq \bar{P}_{gen2} \leq 140 \qquad (3.6i)$$

$$50 \leq \bar{E}_{batt} \leq 2000 \qquad (3.6j)$$

$$50 \leq \bar{P}_{PV} \leq 400 \qquad (3.6k)$$

In the above formulation, $\boldsymbol{x}$ is the vector of design variables; L_c is the lifetime and p_c is the unitized capital cost of microgrid component c; $\bar{P}_{gen1}$ and $\bar{P}_{gen2}$ are rated powers of Generators 1 and 2, respectively; $\bar{E}_{batt}$ is the capacity of the stationary battery; and $\bar{P}_{PV}$ is the rated power of the PV panel array. All other symbols are used as previously described.

The optimal dispatch formulation is a problem-specific version of the one presented in Section 2.3.2, with all symbols as previously defined.

$$\underset{\boldsymbol{u}(t)}{min} \sum_t \sum_i p_{fuel} f(u_i^t, \bar{P}_i) \qquad \text{fuel cost for time horizon} \qquad (3.7a)$$

w.r.t.:

u_i^t dispatch of generator *i* at time *t*, $\forall i, \forall t$ (3.7b)

u_j^t dispatch of storage *j* at time *t*, $\forall j, \forall t$ (3.7c)

subject to:

$0.3\overline{E}_j \le E_j^t \le 0.95\overline{E}_j$ storage energy capacity limits, $\forall j, \forall t$ (3.7d)

$E_j^{t+1} = E_j^t + u_j^t \overline{P}_j$ storage energy balance, $\forall j, \forall t$ (3.7e)

$\sum_h P_{net,h}^t \le 0$ network power balance, $\forall t$ (3.7f)

$0 \le u_i^t \le 1$ generator power limits, $\forall i, \forall t$ (3.7g)

$-0.5\overline{E}_j \le u_j^t \le 0.5\overline{E}_j$ storage power limits, $\forall j, \forall t$ (3.7h)

$$\boldsymbol{u}(t) = \left[\boldsymbol{u}_i(t)\, \boldsymbol{u}_j(t)\right];\ t \in \{1,..,18\};\ h \in \{1,2,3,4\};\ i \in \{1,2\};\ j \in \{1\}$$

The network power balance Eq. (3.7f) is found according to the modeling Equations (3.2) in Section 3.4.1.1. In this case, rather than a strict equality the total power import for all hubs, *h*, must be less than or equal to zero (any excess power production is assumed to be dissipated). The problem-specific dispatch formulation places limits on the power and energy available from the storage battery. The maximum and minimum SOC are limited to 95% and 30%, respectively, and the maximum power is limited to a 0.5C charge/discharge rate, as shown in Eq. (3.7h).

Again, it should be noted that this problem formulation, with its nonlinear transmission losses, falls under Case 4 as presented in Section 2.8. Therefore, no simplifications can be applied to decompose the solution of the power generation and energy storage. However, the time reduction strategies (18-hour time horizon, 6-hour time step between horizons, and partial-year solution) were all applied to reduce the computation time.

3.4.3 Results and discussion

The optimal designs, costs, and fuel uses are shown in Table 3.4. A parametric study of fuel cost was performed, with levels from $1.6 – $2.6 per liter ($6.05 - $9.85 per gallon).

Table 3.4 – Results of microgrid design optimization for different fuel costs

	$1.6/lit	**$2.1/lit**	**$2.6/lit**
Total Cost ($1k)	282.5	336.4	384.9
Fuel Cost ($1k)	167.4	198.4	165.1
Capital Cost ($1k)	115.1	138.0	219.8
Generator-1 (kW)	39	41	37
Generator-2 (kW)	41	37	28
Battery (kWh)	676	869	775
PV Array (kW)	190	224	395
Fuel Use (kiloliters)	105.6	93.9	62.5

The results show that as fuel price increases the optimal microgrid design increases the size of the PV array and slightly decreases the sizes of the generators. The PV array, though expensive, dramatically reduces fuel use and thus overall cost. Smaller generators will operated at higher load and thus higher efficiency. The size of the battery does not vary monotonically with fuel price, though each design chooses a fairly large battery. This suggests that a larger battery does not monotonically reduce fuel use, but some minimum level of battery storage is preferred by the system.

The practicality of installing large solar panel arrays and battery banks may be limited by the footprint of these components or by transportation issues. Barring these restrictions, the purely economic dispatch shows that significant installation of energy storage and solar power is justified to reduce fuel use and operating cost.

It is notable that the total generator power (65 – 80 kW, depending on the case) can provide the average power load (~65 kW), but cannot provide the peak power load of the system (~140 kW). The microgrid designs must rely on the solar power, which peaks in the mid-day, to supply most of the remaining power load, which also peaks in mid-day. However, these optimal microgrid designs were based upon averaged solar irradiance. Actual solar irradiance varies widely by hour and by day. Thus, these microgrid designs,

with their small dispatchable generators, may not supply power reliably in an actual implementation. Uncertainties in the solar irradiance and the power load must be considered in the design process, as will be discussed in Chapter 4.

3.5 Summary

This chapter introduced a method to optimize the design of a microgrid to balance capital investment and operational costs. The method is coordinates an optimal design problem with a nested optimal dispatch problem to size individual microgrid elements simultaneously with their dispatch strategy. The approach presented thus far is deterministic: all inputs are assumed to be known perfectly, with no variation. The next chapter will discuss how to include parametric uncertainty into the optimal design problem.

Chapter 4: Optimal design of a microgrid under uncertainty

Modeling any system involves many types of uncertainty. Even given a hypothetical, "perfect" physical model, the modeler must make assumptions on the correctness of input values (parameters), though inevitably there will be errors and temporal variation in these inputs. Furthermore, the modeler assumes that a real device or system will be built exactly as designed using the model, though precision, tolerances, and error will lead to deviations from the design. For a microgrid, uncertainty appears within the system inputs, such as power load and renewable energy supply. Designing a reliable microgrid requires accounting for these uncertainties.

4.1 Sources of parametric uncertainty in microgrid design problem

Various sources of uncertainty can affect the design problem directly or through the dispatch problem, cascading upward into the design problem.

4.1.1 Uncertain parameters that affect inner loop (dispatch problem)

The dispatch problem has multiple input parameters that are stochastic and time-variant: renewable energy inputs (e.g., wind speed and solar radiance) and power load. In addition, if the microgrid has electric vehicles, the plug-in schedules and states-of-charge of vehicle batteries are also stochastic and time-variant. The system may be modeled using the expected values of these stochastic parameters, but the actual system performance will deviate from this expectation due to the uncertainty.

Depending on the problem objective formulation, fuel price may affect the inner loop (dispatch) problem, or it may only affect the outer loop (design) problem. Throughout this dissertation we have only considered minimization of operating costs in the dispatch problem. In addition, the operating costs are limited to a single source: liquid

diesel fuel to run generators and potentially to run vehicles as well. In this single-fuel case, the fuel price can be removed from the optimal dispatch objective and the resulting solution would be the same. Thus, fuel price uncertainty would not affect the optimal dispatch problem in this single-fuel case.

However, if multiple fuels are used, if the microgrid is grid-connected, or if additional costs (e.g., maintenance costs) are considered in the optimal dispatch objective, then the fuel price(s) cannot be removed from the objective and fuel price uncertainties will affect the solution of the optimal dispatch problem.

4.1.2 Uncertain parameters that affect outer loop (design problem)

Any uncertainty that affects the inner loop dispatch problem will affect the outer loop design problem because the output of the dispatch problem (objective and constraints) will be stochastic inputs to the design problem. As mentioned previously, calculating these distributions is a major issue, which motivated the linearization approach of Chan [2006]. The design problem can also be affected by other parametric uncertainties that do not affect the dispatch problem, e.g., capital cost, lifetime, and fuel prices.

Capital costs and capital lifetimes are contained within the design problem objective function but do not occur in the dispatch problem objective (Eq. 3.7a). Therefore, their uncertainty will only affect the solution of the design problem. As mentioned in the previous section, uncertain fuel prices may or may not affect the dispatch problem, but will affect the design problem because they appear in the objective.

4.2 Characterization of uncertainty distributions

4.2.1 Solar irradiance

The solar irradiance measurement used for fixed photovoltaic panels is the Global Horizontal Irradiance (GHI), which is the sum of the total direct radiation and diffuse radiation coming from other parts of the sky as they strike a flat panel, horizontal to the ground [Lambert et al. 2006]. Other corrections must be made for PV panels that follow the sun, but only fixed PV panels are considered in this dissertation. The data are

typically measured by sensors on the ground but some data for remote locations are estimated by satellite data.

The data used in this dissertation comes from HOMER Energy's worldwide data set, which uses satellite data measured by NASA, taken for a site near Kabul, Afghanistan. Solar irradiance varies diurnally and also throughout the year, so modeling the variation in solar irradiance should ideally include multiple years of data to show the variation of a specific hour of the year. Lacking this data, it was assumed that the variation of a single hour could be correlated to the same hour in the two weeks preceding and following a particular day. Using these twenty-nine data points, the mean irradiance was calculated for each hour of the year. A typical day is shown in Fig. 4.1, with the mean irradiance plotted versus time as the solid line, and the actual data for all twenty-nine days plotted as dashed lines.

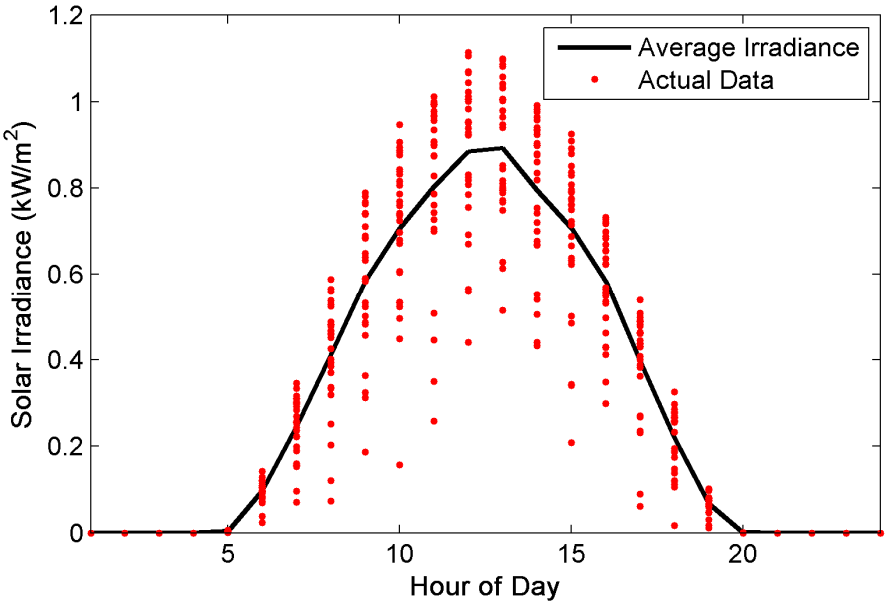

Figure 4.1 – Mean and actual solar irradiance and for two weeks around July 1st

The distribution of irradiance for a given hour was estimated using these same data groupings and a distribution was fit to the data, as shown for 12pm on July 1st in Figure 4.2. Multiple times of day and days of the year were examined this way and seven of nine data sets examined showed a unimodal distribution with a long tail towards zero irradiance. The other two data sets showed a smaller mode at low irradiance, most likely due to increased cloudiness during those months. For all the data sets, it was found that a

generalized Extreme Value (EV) distribution best fit the data. An EV distribution was fit to each hour of the year and the resulting distributions were used to randomly generate solar irradiance for use in the uncertainty analysis.

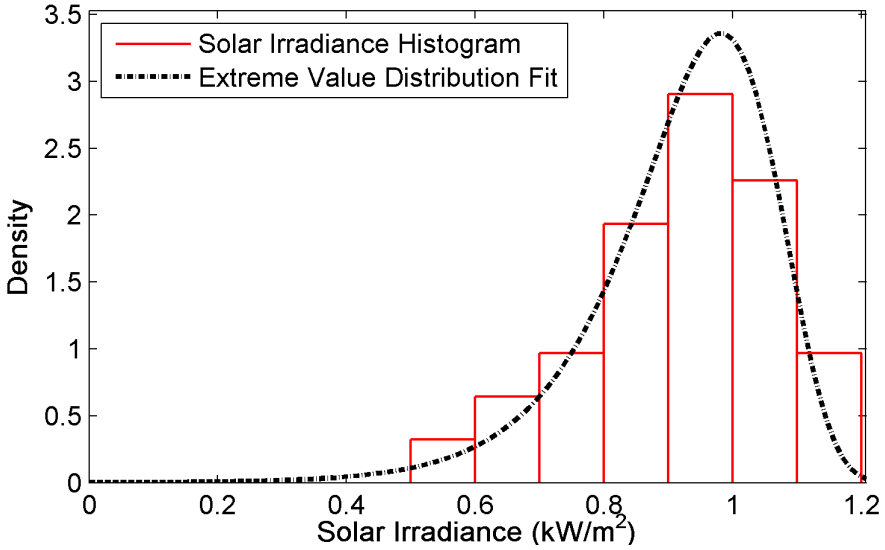

Figure 4.2 – Distribution of solar irradiance at noon for two weeks around July 1st

While this distribution worked well to represent the variation for a single hour, in reality the solar irradiance of one hour is partially correlated to the irradiance during the previous hour, due to the presence of clouds (or lack of clouds). This hour-to-hour correlation is not modeled here. Thus, the stochastic variation modeled here will be more volatile from hour to hour, and the energy storage devices will be necessary to smooth this volatility.

4.2.2 Power load

Similar to the solar irradiance data, the power load data will also follow a circadian cycle and also vary throughout the year. Ideally, data from multiple years would be used to understand the variation for each hour of the year. No power load data was available to analyze, so instead the power load was assumed to have a normal distribution centered around a nominal power load with a standard deviation that was a constant percentage of the mean load during any specific hour, $\sigma_L = x(\mu_L)$. An example is

shown in Figure 4.3 for $\sigma_L = 0.15\mu_L$. The mean power load is plotted for July 1st – 3rd with +/- one standard deviation and an example random power load.

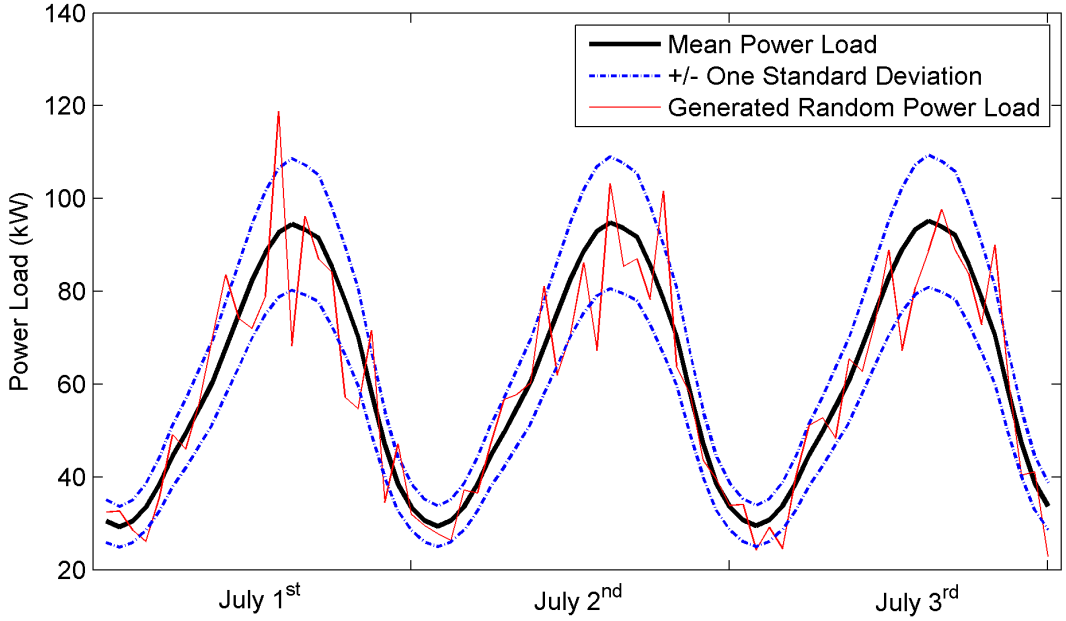

Figure 4.3 – Mean power load with standard deviation for July 1 - 3

Like the solar irradiance model, the power load during one hour should be correlated to the power load during the previous hour due to daily ambient temperature and other environmental conditions. This hour-to-hour correlation is not modeled here.

4.3 Uncertainty in design problems

Engineering design often uses safety factors to account for uncertainties because they are difficult to characterize, requiring significant data from a system that may not exist, and the way uncertainties propagate through a system is difficult to understand without significant modeling and sampling. However, safety factors risk oversizing a system, resulting in operating inefficiencies and increased capital costs, or potentially undersizing a system, risking system failure.

4.3.1 Robust design

Robust design seeks to address the large number of possible uncertainties in the design process, from manufacturing and material variation to uncertainty in the environment where the product/system is used. The manufacturing and material variations are often referred to as *stochastic variables*, because the designer is determining their nominal characteristics, whereas the environmental uncertainty is referred to as *parametric uncertainty*, because it is an input to the designed artifact or system.

Robust design seeks to minimize the variation from a nominal performance (refer to Taguchi's methods for quality improvement via statistical analysis, e.g., [Roy et al. 1990]). In essence, robust design seeks to minimize the spread of a distribution, where that distribution represents the possible range of a product's performance. Robust design methods can be focused on minimizing variation in the objective function (optimality robustness), meeting some level of reliability of the constraints (feasibility robustness), or both.

The formulation of optimality robustness problems typically involves minimizing some weighted sum of the mean and standard deviation of the objective function. This is a common problem solved in product manufacturing to improve product quality. Design for feasibility robustness seeks to generate optimal design solutions that will not fail in the presence of expected variation, within some specified level of reliability. Formulations of optimal feasibility robustness problems usually include probabilistic constraints, because design optimization will often find a design that is optimal on constraint boundaries (active constraints), and any deviation from that point due to random variables or parameters can result in violation of the active constraint(s). Some robust design methods (e.g., Six Sigma Design), consider both optimality robustness and feasibility robustness, typically by design of experiments and sampling, to minimize product variation within a manufacturing process.

4.3.2 Reliability-based design optimization

Robust design that considers only feasibility robustness is sometimes called Reliability-Based Design Optimization (RBDO) [Tu et al. 1999]. RBDO can include stochastic design variables, stochastic parameters, or both. A generalized RBDO problem has a formulation as shown in Eq. (4.1), where the design variables, $\boldsymbol{x}$, or the input parameters, $\boldsymbol{p}$, may be uncertain.

$$\min_{\boldsymbol{x}} \quad f(\boldsymbol{x}, \boldsymbol{p}) \tag{4.1a}$$

subject to:

$$\Pr\left[g_m(\boldsymbol{x}, \boldsymbol{p}) > 0\right] \leq P_{f,m} \tag{4.1b}$$

In this formulation, each constraint g_m is now formulated as a probability of failure (infeasibility) being less than or equal to some probability, $P_{f,m}$, for each constraint m. Solving the above problem typically involves a two-loop process: the outer optimization loop and an inner loop to estimate the probability of failure of each of the constraints. The problems here are threefold: (1) the distributions of the stochastic parameters may be unknown, or only limited data may be available, (2) calculating the distributions of the probabilistic constraints in the above formulation is challenging, and (3) calculating the distributions of the constraints for each design evaluated results in a two-loop optimization problem structure, which can be computationally expensive.

Addressing the first problem, in the ideal case there will exist a large amount of measured data over a long period of time for all of the stochastic parameters. This data often does not exist, so probability distributions must be assumed around an expected mean value. However, if the wrong type of distribution is assumed, or the spread of the distribution does not match the actual distribution, the reliability calculations will be inaccurate and the resulting system design may be sized incorrectly.

For the second problem, the probability distributions of the constraints can be estimated using sampling methods such as Monte Carlo sampling (MCS) or Latin Hypercube Sampling (LHS), though large numbers of samples may be required to

accurately estimate high probability levels (the tails of the distributions). Other methods attempt to approximate the probability of violating constraints using first- and second-order Taylor series expansions at the constraint boundaries. These methods are known as the first-order second moment method (FOSM), the first-order reliability method (FORM) and the second-order reliability method (SORM), though these methods require normal (Gaussian) distributions of stochastic variables and parameters. Chan extended the FORM and SORM methods to non-normally distributed random quantities by transforming them into normal distributions. However, he notes that this is computationally intensive because these methods require their own optimization process, and the transformations applied may cause convergence difficulties [Chan 2006].

Addressing the third problem, much research has focused on reducing the computation required for the two-loop RBDO problem structure. The two-loop problem structure is shown for reference in Fig. 4.4.

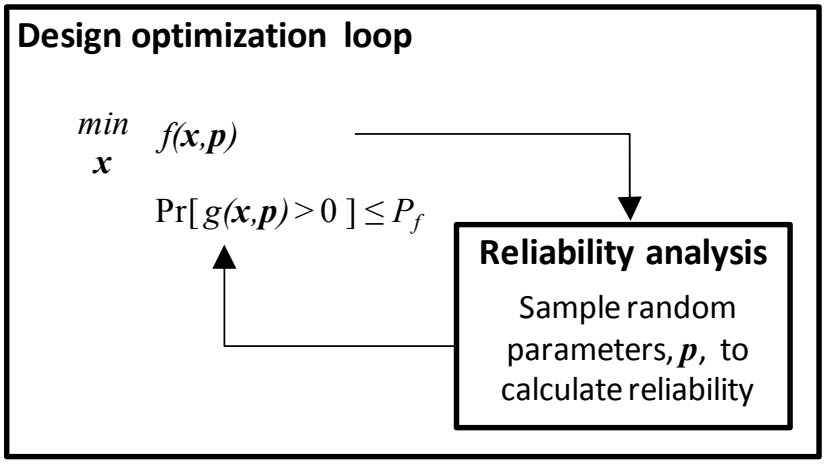

Figure 4.4 – Typical two-loop RBDO problem structure

Improved methods often seek to either reduce the number of samples required to evaluate the reliability in the inner loop, or eliminate the sampling completely by explicitly calculating the probability distributions of the constraints. Some examples include the advanced mean value method, the hybrid mean value method [Youn et al. 2003], sequential optimization and reliability analysis [Du and Chen 2004], the design potential method [Tu et al. 2001], and Chan's sequential linearization method [Chan 2006]. For

this dissertation the sequential optimization and reliability analysis (SORA) method was chosen. The SORA method places the reliability analysis at the end of the optimization, resulting in the modified RBDO problem structure shown in Fig. 4.5. The design reliability from the reliability analysis is used to update the constraints within the design optimization problem, until the design converges with the desired reliability. This method will be explained in detail in Section 4.4.

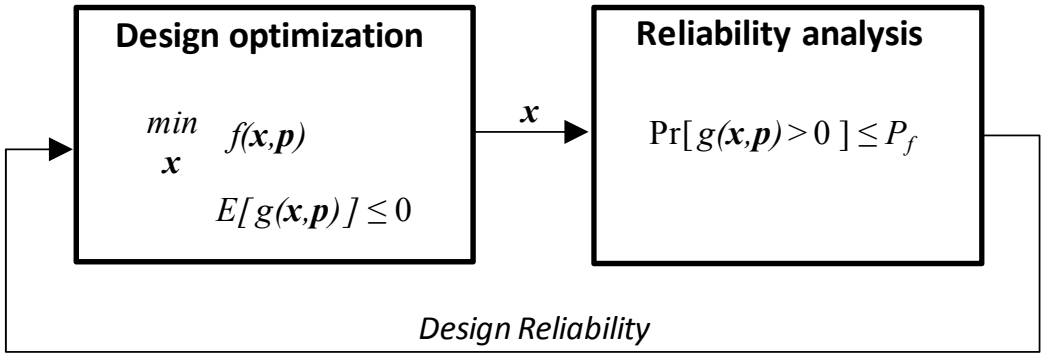

Figure 4.5 – Sequential RBDO problem structure of the SORA method

4.3.3 Microgrid design under uncertainty

Adding stochastic renewable energy resources to the electrical grid introduces significant uncertainties that must be addressed by new research and methods [Mills et al. 2009]. The effect of uncertainty is even more severe when a lack of available dispatchable power can lead to loss-of-load situations, such as those that can occur with an islanded microgrid. In spite of this, little research has specifically addressed how to handle uncertainty on a microgrid in a rigorous way and how to design a microgrid to be robust and reliable without oversizing the system. This research is described below.

Most microgrid research uses sensitivity analysis to capture some trends of parametric uncertainty. For example, research by Firestone and Lawrence Berkeley National Laboratories use sensitivity analysis to study the effects of different levels of carbon taxes and electricity tariffs on microgrid design [Firestone 2007, Stadler et al. 2009]. The research mentioned in Chapters 2 and 3 by HOMER Energy handles microgrid design under uncertainty through sensitivity analysis. The user can specify a range of parameter values around some nominal value, and HOMER will simulate each

value. For time-variant parameters, such as wind speed or solar irradiance, HOMER will scale all data over the entire time period with respect to the mean value of the parameter [NREL 2005]. Similarly, del Real et al. [2009b] propose performing similar sensitivity studies to account for uncertainties. These sensitivity methods are useful to identify worst-case scenarios and give the designer a sense of how the system will respond, but do not directly address the issue of how to design for a specified level of reliability.

The research mentioned in Chapter 2 and 3 by Lu et al. [2011] uses Markov chains to incorporate renewable energy uncertainty into their method for finding the optimal design (sizing) of a hybrid energy system, including energy storage, solar power, and wind power. Their objective is minimizing the capital cost of the system and they solve the dispatch of energy storage for each design at one-hour increments using stochastic Markov chains to minimize the probability of loss-of-load (LoL). As mentioned previously, their formulation does not include solving an optimal dispatch problem, nor solution over a time horizon.

4.4 Method used: Sequential Optimization and Reliability Analysis (Du/Chen)

The Sequential Optimization and Reliability Analysis (SORA) method, developed by Du and Chen [Du et al. 2006], is implemented here to perform design optimization of microgrids under parametric uncertainty. This method eliminates the need to perform reliability analysis of every design during the optimization process, e.g., via Monte Carlo sampling, and instead only evaluates the reliability of designs at the end of each optimization iteration. This significantly reduces the number of function evaluations during the optimization.

The SORA method first performs deterministic design optimization to generate an initial design. At the end of the optimization, the active constraints are identified. The active constraints that are a function of uncertain parameters are selected for reliability analysis, typically by Monte Carlo sampling or some other procedure. Once the reliability of the design is quantified with respect to the active constraints, the method follows one of two paths. If the actual reliability is lower than the desired reliability, the bounds of the active constraints are shifted to be more conservative and the SORA method iterates. If the actual reliability is greater or equal to the desired reliability, and the design is not

significantly changed from the previous iteration (within some tolerance), the SORA method exits. This operation is explained in the flowchart of Fig. 4.6. The implementation of this method is detailed in sub-sections 4.4.1 – 4.4.4.

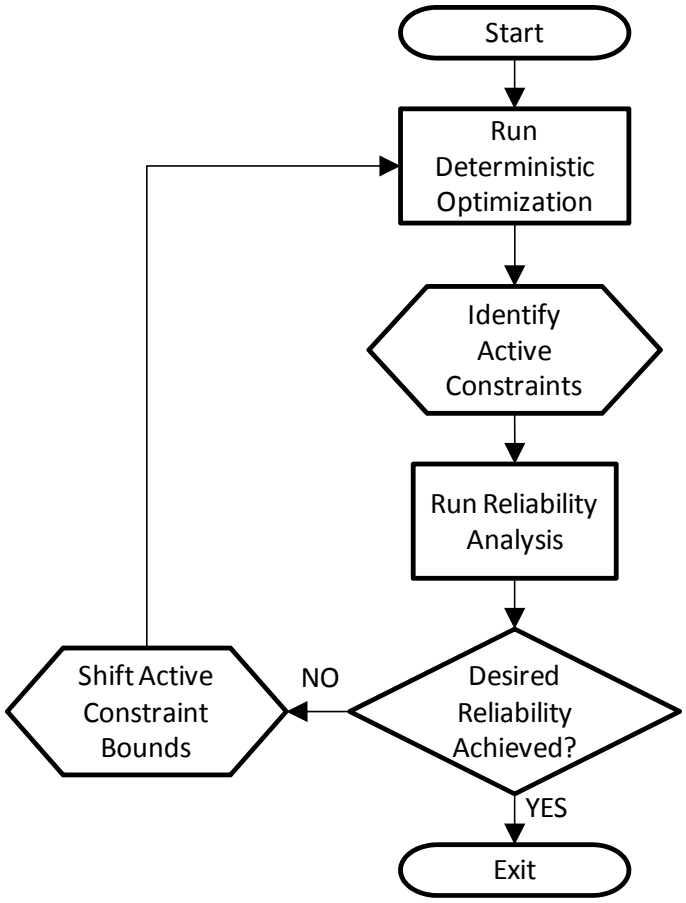

Figure 4.6 – Flowchart of Du and Chen's Sequential Optimization and Reliability Assessment (SORA) method

4.4.1 Deterministic optimization

Deterministic design optimization is performed by setting the uncertain parameters (electrical power load or solar irradiance) to their nominal, expected values. The optimization algorithm chosen is the same used for deterministic design optimization in Chapter 3, the DIRECT algorithm. DIRECT has no convergence criteria, so it is run for a pre-determined number of function evaluations as specified by the expert user. For a

four-variable design problem, 200 function evaluations were shown to be sufficient. For a more general implementation, the rate of change of the objective function could be tracked and when it is sufficiently small the DIRECT algorithm could terminate, though this method was not implemented here.

4.4.2 Calculation of design reliability

The final design from the deterministic optimization is simulated with random sampling of the chosen random parameter(s) to calculate design reliability. It is assumed that the effect of the random parameters does not result in an identifiable distribution at the output, so the reliability is calculated simply as the number of successful samples (feasible designs) over the total number of samples. If the uncertain parameters were known to generate identifiable distributions of the output (e.g., normal distributions, Weibull distributions, or other distributions), then "smart sampling" methods could be used to generate the output distributions with the sampling procedure to reduce the total number of samples needed to calculate the design reliability. For generalization, this was not implemented here.

The sampling method used will affect the required number of samples as well as the error in the resulting reliability calculation. For example, for Monte Carlo sampling (MCS), Chan quotes Shooman who estimates the error in MCS by Eq. (4.2).

$$\varepsilon(\%) = \left[\frac{1 - p_{Tf}}{N_{MCS} p_{Tf}}\right]^{0.5} \text{x } 200\% \tag{4.2}$$

where p_{Tf} is the true probability of failure and N_{MCS} is the number of samples [Chan 2006]. The true probability of failure is usually unknown, so calculating this error involves multiple iterations. MCS is run for some number of samples to calculate an approximate probability of failure. Based on the result, one can calculate the N required to obtain desired accuracy and then run MCS for this number of samples. The probability is then updated and N is calculated again until the desired error is reached and converged. The prediction error for various probabilities of failure is plotted as a function of the

number of MC samples in Fig. 4.7. As seen in the figure, even for 20% probability of failure, 1500 samples are required to reach 10% error in the prediction.

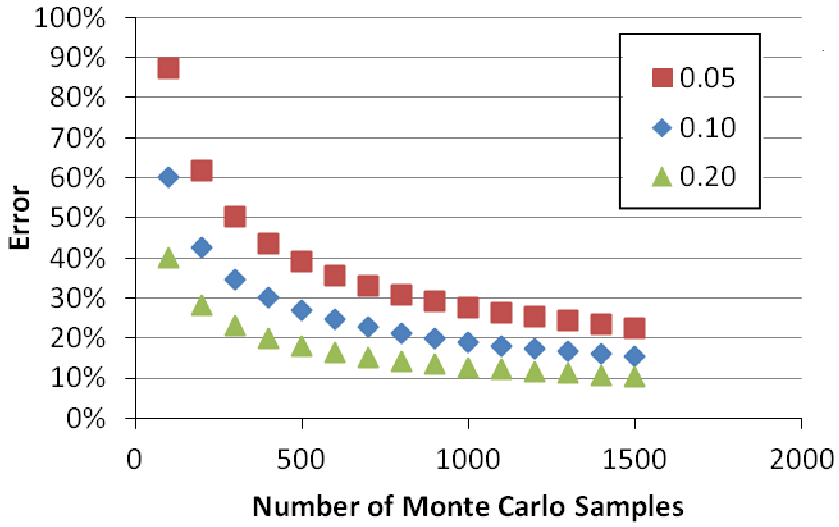

Figure 4.7 – Error in failure probability estimations using Monte Carlo sampling

Drawing thousands of samples to evaluate the reliability of a microgrid design is computationally prohibitive. Instead, various "smart sampling" methods can be used to reduce the number of samples required to accurately estimate a probability distribution. These methods include quasi-Monte Carlo sampling, latin hypercube sampling, importance sampling, and adaptive importance sampling [Chan 2006]. For this dissertation, latin hypercube sampling (LHS) is used to generate the random parameters during the reliability analysis. Latin hypercube sampling seeks to spread the random samples over the sampling space by creating intervals and only sampling once within a given interval. This is especially useful when sampling in multiple dimensions, as the number of samples required to "cover" the space increases linearly with dimension rather than quadratically. However, no relation such as Eq. (4.2) is known to the author for determining a sufficient number of LH samples required to achieve some level reliability. Instead, empirical studies showed that the calculated reliability of a system converged within ±3% after 150 LH samples, as shown in Fig 4.8. Thus, 200 LH samples were used to evaluate reliability for the studies in this dissertation. Whether this is an appropriate number is an area for future research.

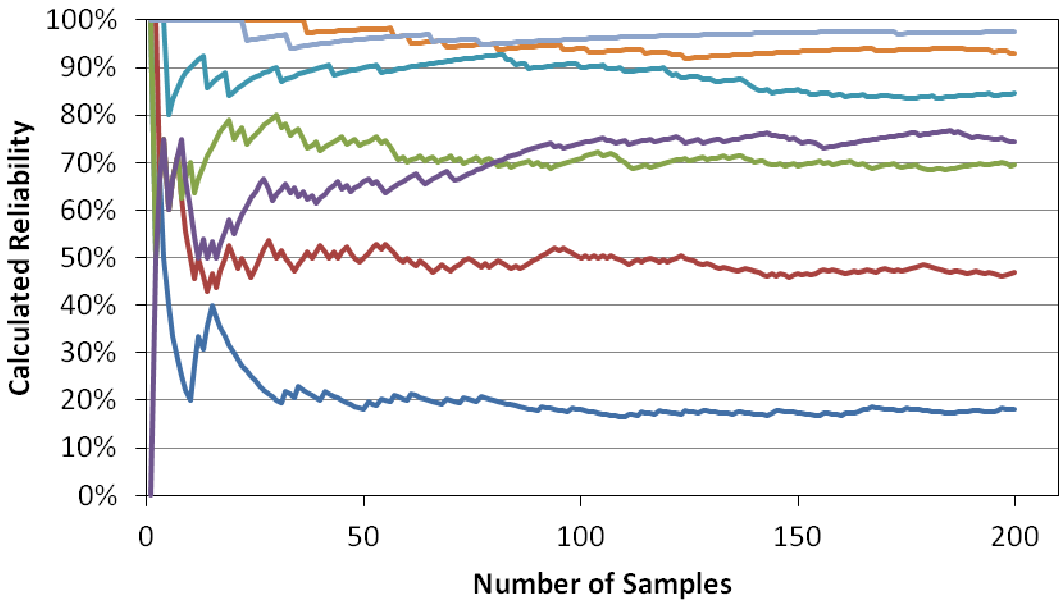

Figure 4.8 – Change in reliability calculation with increasing number of samples (7 independent cases)

4.4.3 Identifying active constraints for bound movement

The only constraint in the design problem that is not a variable bound is the constraint ensuring feasibility of the dispatch problem, Eq. (3.6f). Therefore, to identify the active constraints, we must examine the activity within the dispatch problem. Within the dispatch problem, many of the constraint bounds are fixed by the design problem, e.g., the limits on battery power are determined by the battery design (size, chemistry, electrode geometry, and other battery design variables). Therefore, it is not possible to move these bounds to improve the reliability of the design. In fact, the "movement" of these bounds is implicitly handled by the optimal design problem when it attempts to achieve a feasible design.

The same is true for the generator power limits and battery energy capacity limits, leaving only one set of constraints where the bounds can be moved: the network power balance at each time step (Eq. 3.7f). By moving the bound on these constraints, the optimal design problem will be forced to oversize the system, thus leaving reserve capacity that can handle the uncertainty in the power load, renewable energy supply, or other system variability.

These constraints are equality constraints and thus, by definition, they are all active constraints, so in keeping with the SORA method one should move the constraint bounds uniformly for all of these constraints. However, doing so will require the microgrid to produce extra energy at all time instances which will result in artificially high energy and fuel use for each design. Instead, it is preferred to identify only those network constraints where the microgrid cannot meet the power load because its dispatchable power devices are operating at their limits, or within some range from their limits.

The most practical way to address this is to create a new constraint that calculates the "operating reserve" of the microgrid. We will define the operating reserve as the additional power potential that is not being produced by the microgrid. Such a constraint is shown in Eq. (4.3) and will be added to the optimal dispatch problem.

$$\bar{P}_{gen} + P_{PV}^{t} + \bar{P}_{batt}^{t} - P_{ls}^{t} - P_{ld}^{t} \geq P_{reserve} \ , \forall t \tag{4.3}$$

In the above equation, $P_{reserve}$ is a constant value of reserve power desired on the network, $\bar{P}_{gen}$ is the combined rated power from the generators, P_{PV}^{t} is the power available from the PV array at time *t*, $\bar{P}_{batt}^{t}$ is the maximum power available from the storage battery at time *t*, P_{ls}^{t} is the total power lost during transmission at time *t*, and P_{ld}^{t} is the total microgrid power load at time *t*. This equation is similar to the network power balance Equation (2.2d), except instead of using the actual power produced by each device, it uses the maximum power possible from each device. Note (1) that the maximum possible power for generators is independent of the time period, whereas the power available from energy storage may be limited by the current state-of-charge; and (2) that the renewable power potential is limited by the renewable input (e.g., solar radiance or wind speed) in each time period.

The operating reserve, $P_{reserve}$, will be changed for each iteration of the SORA method in order to ensure a reliable microgrid. By dynamically changing this parameter, we can attain the desired reliability level analytically without arbitrarily setting the

operating reserve or using heuristic rules that may excessively oversize the system (resulting in increased cost) or undersize the system (resulting in poor reliability).

4.4.4 Calculating amount of bound movement

The initial operating reserve is set to zero for the first iteration of the SORA method. After the reliability assessment, the amount of increase in operating reserve is calculated by first calculating the number of designs that must shift to the feasible region to meet the desired reliability level. All of the designs are ranked by increasing level of constraint violation (operating reserve deficit). Designs with some amount of constraint violation are counted until reaching the desired number to shift to the feasible region. The constraint violation of the last design counted is used to set the new operating reserve.

4.4.5 Termination criteria

Once the design has achieved the desired reliability, the objective function value of the current design is compared to the objective of the previous design. If they are within a 0.5% tolerance from each other, the process terminates.

4.5 Example: Optimization of military microgrid under uncertainty

The approach described in this chapter to perform optimal microgrid design under uncertainty was applied to the same military microgrid case from Chapter 3. The basic problem remains the same, except that the power load and/or the solar irradiance are represented by probability distributions rather than their nominal values. The changes in the problem statement will be described in section 4.5.2. This example has four goals:

(1) Show the effect of microgrid design optimization while considering solar and power load uncertainty in comparison to the deterministic case shown in Chapter 3;
(2) Compare the SORA method to optimal design using Monte Carlo sampling;
(3) Show the effect of energy storage on reliability;
(4) Analyze the effect of different levels of power load variation.

4.5.1 Uncertainty propagation through the optimization problem

Understanding how uncertainty will affect the microgrid design optimization requires an understanding of how the uncertainty will propagate through the problem. The parametric uncertainties for solar irradiance and power load enter the optimization problem through the dispatch subproblem in the hub power balance equations. From there the uncertainties are propagated to the outer design problem via the variation in operating cost. As an example, the hub power balance Equations (3.2a – d) can be re-written to include the expected value of power load, *E[L]*, as follows:

Hub 1 $$P_{hub1} = E[L_1] - P_{gen1} - \eta_{PV} P_{PV} - P_{batt} \quad (4.4a)$$

Hub 2 $$P_{hub2} = E[L_2] \quad (4.4b)$$

Hub 3 $$P_{hub3} = E[L_3] \quad (4.4c)$$

Hub 4 $$P_{hub4} = E[L_4] - P_{gen2} \quad (4.4d)$$

As a result of this uncertainty, the power required at each hub, P_{hubi}, also becomes uncertain, which causes the network power balance constraint from the optimal dispatch problem, Eq. (3.7f), to be uncertain. The new probabilistic constraint is shown in Eq. (4.5).

$$Pr\left[\sum_{h} P_{net,h} > 0\right] \leq P_f \quad (4.5)$$

To satisfy this constraint, the dispatchable components (generators and battery) must modify their operation from the expected value to meet any variation in power load. This variation in generator output will propagate into the optimal dispatch objective, which is to minimize fuel cost, Eq. (3.7a), and this cost is then propagated out to the objective of the optimal design problem, Eq. (3.6a). A similar propagation can be shown for the solar uncertainty.

These uncertainties create variation in the fuel use and operating cost of the microgrid, with an example shown in Fig. 4.9 for a power load standard deviation of 30%

of the mean (σ_L=0.3μ_L). The variation of the output (operating cost) due to the variation of the load also has an approximately normal distribution for this example case with 200 Monte Carlo samples.

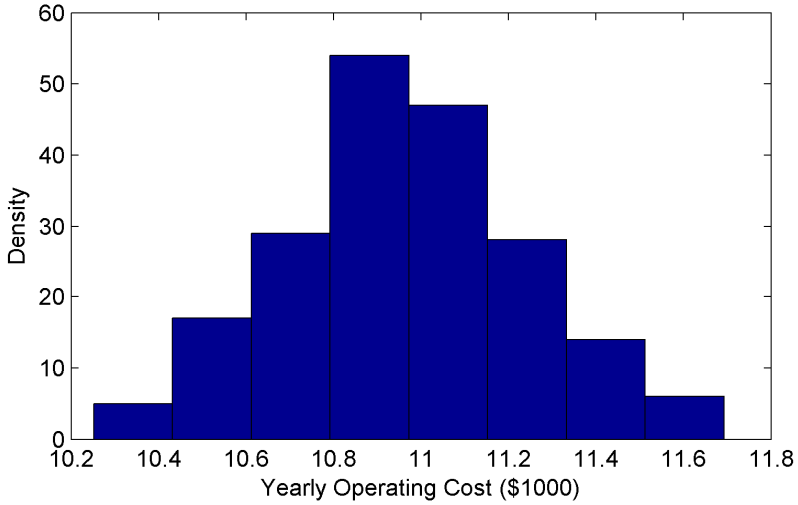

Figure 4.9 – Operating cost variation due to one level of load variation (σ=0.3μ)

4.5.2 Updated optimal dispatch problem statement

There are two different optimal dispatch problem statements used with the SORA method. The first is the deterministic problem statement, used during the Design Optimization portion of the SORA method. This optimal dispatch problem statement is the same as the one presented in Eqs. (3.7), with the addition of the operating reserve constraint for each time *t*, as shown in Eq. (4.3). The deterministic optimization only uses the mean values of the uncertain parameters to generate the optimal designs.

The second optimal dispatch formulation is used during the Reliability Analysis portion of the SORA method. In this formulation, the operating reserve constraints are excluded, but the network power balance constraint is probabilistic, as shown in Eq. (4.5). All other equations in the formulation remain as in Eqs. (3.7). The Reliability Analysis uses parametric inputs that are sampled from the previously described distributions for power load and solar irradiance. However, while the parameter inputs vary for each sample, they are still "known" exactly over the time horizon: that is, there is no "prediction error" as might be seen using a forward-predictive feedback controller.

4.5.3 SORA flowchart for microgrid optimization under uncertainty

The flowchart presented in Fig. 4.6 can be updated to include the microgrid-specific elements described above. This flowchart is shown in Fig. 4.10.

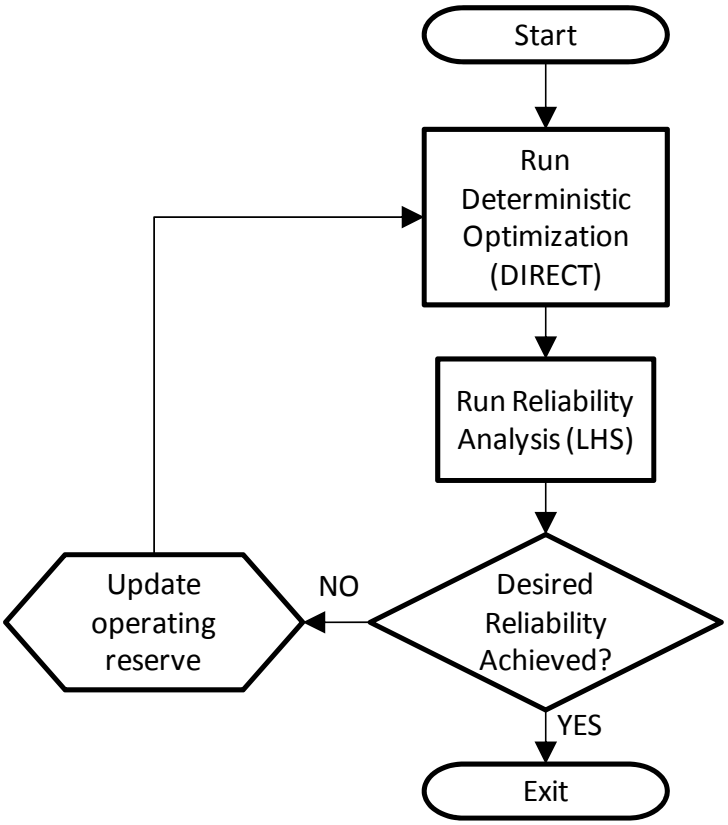

Figure 4.10 – SORA flowchart for microgrid optimization

4.5.4 SORA method efficacy vs. optimal design using Monte Carlo sampling

The first goal of the example is to ensure that the SORA method has similar or improved results compared to design optimization with Monte Carlo sampling (MCS), while significantly reducing the computation time. Thus, the example was run using both approaches for two cases: with solar irradiance uncertainty and no power load uncertainty, and for power load uncertainty of $\sigma_L=0.1\mu_L$ with no solar uncertainty. The reliability goal was set to be >90% and the optimal design for both methods was run for 120 design evaluations with 100 Monte Carlo samples to evaluate design reliability.

The results for power load uncertainty and solar uncertainty are shown in Table 4.1. As seen in the table, the designs generated by the SORA method and optimal design

using MCS are similar, and the SORA method results in designs with slightly improved objectives. By only performing reliability analysis at the end of a design optimization run, rather than for each design, the SORA method reduced the number of function evaluations and computation time by ~98%.

Table 4.1 – Comparison of SORA method and MCS for optimal design with power load uncertainty or solar uncertainty

	Load Uncertainty		Solar Uncertainty	
	MCS	**SORA**	**MCS**	**SORA**
Objective Function ($1k)	268.6	268.4	269.8	268.7
Gen 1 (kW)	46	47	53	56
Gen 2 (kW)	40	35	62	50
Battery (kWh)	676	676	655	647
PV array (kW)	169	169	173	167
Reliability	100%	100%	98%	100%
Num. Function Evals	12700	221	13700	227
Calculation time (hrs)	143.0	1.6	104.9	2.9

These trials show that the SORA method is successful at generating reliable designs, similar to the Monte Carlo approach, but saving a significant number of function evaluations, which will become important as the problem is scaled up. However, for these cases the SORA method only required one iteration to find designs that met the required reliability level. That is, the initial deterministic design optimization, which is the first step of the SORA method, was able to meet the required reliability with an operating reserve of zero. This will be investigated further in the next section.

4.5.5 Optimization under uncertainty vs. deterministic optimization

As shown in Section 4.5.2, when the microgrid design is allowed to choose a large battery and PV array the resulting reliability is 100% during the first iteration. This means that the initial, deterministic design optimization using mean values of power load and solar irradiance was sufficient. However, the resulting battery and PV arrays are impractically large. In practice they would be limited by their footprint for the PV array and footprint, weight, and/or volume for the battery. This is especially true for the

military case, where they must transport all of their equipment through potentially hostile environments to some remote location.

Lacking specific limits on the sizes of these two components, arbitrary limits were set on each to analyze the effects. The PV array was limited to 100 kW, which is a medium-large array of 430 m^2 for rigid PV panels or 1500 m^2 for flexible PV panels. This is equivalent to the footprint of 1.6 and 5.7 tennis courts, respectively. The lead-acid storage battery capacity was limited to 400 kWh, which would have an approximate weight of 11,400 kg and a cell volume of 5.3 m^3 [Larminie et al. 2003], excluding controls, spacing of cell racks, cooling, and other associated equipment. Assuming a 50% increase for actual installed volume, the resulting installed volume would be 8.0 m^3, which would result in a footprint of 4.0 m^2 for a 2 m tall system enclosure.

Using these new constraints, the SORA method was re-run for power load variation $\sigma_L=0.4\mu_L$ and fuel price of \$2.1/liter with a goal of >90% reliability. For these runs, DIRECT was run for 200 function evaluations for each optimization and 200 latin hypercube samples were used to evaluate design reliability. The SORA method took four iterations to converge to the desired reliability (up to 5% greater reliability was allowed) as shown in Table 4.2.

Table 4.2 – Optimal design with $\sigma_L=0.3\mu_L$ and limited battery and PV panel sizes

SORA Iteration	1	2	3	4
Operating reserve (kW)	15.0	48.5	44.5	45.5
Reliability	23%	99%	88%	95%
Total cost (\$1k)	348.2	349.9	349.4	349.4
Capital cost (\$1k)	59.7	61.6	60.6	60.7
Operating cost (\$1k)	288.5	288.3	288.8	288.7
Gen 1 (kW)	93	109	113	112
Gen 2 (kW)	61	79	64	70
Battery (kWh)	183	243	206	217
PV array (kW)	100	100	100	100

The results show that limiting the storage battery and PV panel sizes causes the initial deterministic design to have only 23% reliability. The SORA method then overshot the desired reliability on the second iteration and required two additional iterations to

reach the desired reliability window with an operating reserve of 45.5 kW. The total computation time was 13 hours. If oversizing the system was not a concern, the method could be terminated once the desired reliability was surpassed, saving computation time. The final design shows a 19% larger battery and 18% greater total generator power than the initial design, and all designs reached the maximum allowable PV array size. The capital costs increased by less than 2% and operating costs were almost unchanged. Overall, the investment in reliability is fairly inexpensive and does not cause a noticeable reduction in system efficiency.

A similar study was performed for solar irradiance variation with limits on battery capacity and solar panel size; results are shown in Table 4.3. However, in this case the initial deterministic design with zero operating reserve achieved the reliability target (>90%), suggesting that the solar variance (as modeled) is not enough to reduce the reliability of the resulting microgrid design. Therefore, for simplicity, only power load variation will be considered for the rest of the studies in this chapter.

Table 4.3 – Optimal design with solar irradiance uncertainty and limited battery and PV array sizes

SORA Iteration	1
Operating reserve (kW)	0
Reliability	100%
Total cost ($1k)	347.6
Capital cost ($1k)	288.3
Operating cost ($1k)	59.3
Gen 1 (kW)	88
Gen 2 (kW)	45
Battery (kWh)	183
PV array (kW)	100

4.5.5.1 Comparison of sensitivity analysis and RBDO

As mentioned in the literature review, most microgrid design including uncertainty uses sensitivity analysis of the uncertain parameters to analyze the effects of uncertainty. To compare this approach to design using the SORA method, sensitivity analysis was performed by running deterministic optimization using increasing levels of

the power load instead of using the mean power load. Assuming a normal distribution of power load with standard deviation of $\sigma_L=0.3\mu_L$, three levels were chosen at the 70th, 84th, and 90th percentiles of the distribution's CDF. This is shown graphically for a CDF of power load with a mean of 100 kW and a standard deviation of 30 kW in Fig. 4.11.

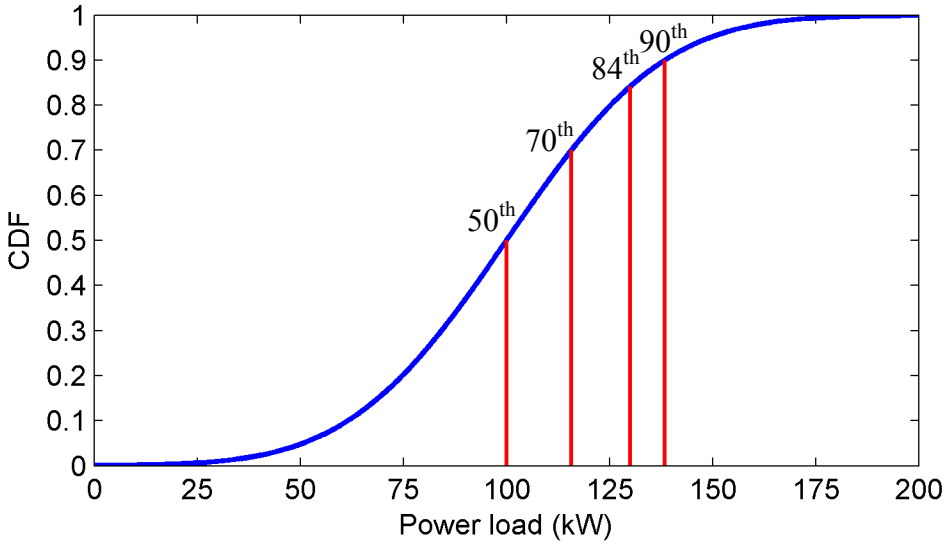

Figure 4.11 – Power load cumulative density function showing the mean and 70th, 84th, and 90th percentiles

The second case, the 84th percentile of the CDF, was chosen to capture one standard deviation higher than the mean power load; the other two levels were chosen to bracket that percentile. A graph of the mean power load and the three levels above it is shown in Fig. 4.12 for example days around July 1st.

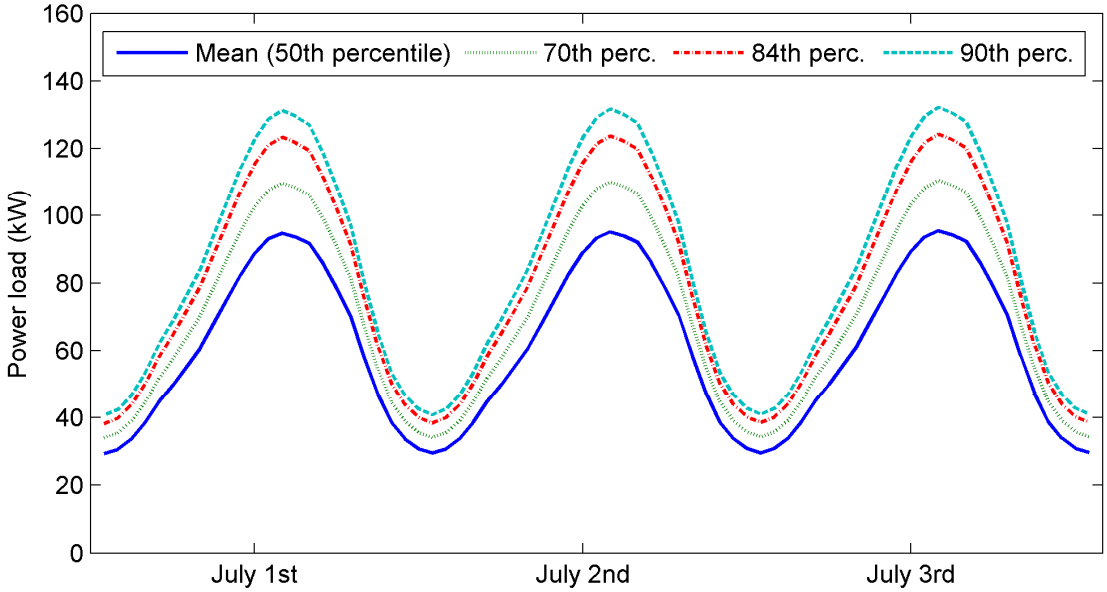

Figure 4.12 – Example power load inputs used for sensitivity analysis

The deterministic optimization was re-run as before as well as a reliability analysis using LH sampling for the final design in order to compare the reliability of these designs to the one generated using the SORA method. For these results, the fuel cost was set at $2.1/liter. The results are summarized in Table 4.4.

Table 4.4 – Optimization results from sensitivity analysis compared to SORA result

	SORA Method	Deterministic Optimization w/ Sensitivity Analysis		
Power load CDF	-	70.0%	84.2%	90.0%
Total cost ($1k)	348.8	349.6	349.8	350.9
Reliability	90%	86%	100%	100%
Operating Reserve (kW)	20.0	-	-	-
Gen 1 (kW)	94.6	96.3	111.8	116.2
Gen 2 (kW)	60.9	63.9	65.4	75.5
Battery (kWh)	183.3	183.3	216.7	183.3
PV array (kW)	99.5	99.5	99.9	99.5

The results show that the SORA result is most similar to the deterministic result using power load scaled up to 70% of the CDF of the power load distribution. The result using SORA has a slightly better objective and higher reliability; however, the difference

in reliability is not significant. The sensitivity analysis results using higher power loads show the expected increase in generator sizes necessary to meet the higher power requirements, approximately 10% larger for every 10% increase in power load CDF, and a requisite increase in total cost.

The result of this shows that it is possible to design using sensitivity analysis instead of a formal RBDO method. However, this requires an understanding of where to set the level of power load in order to achieve the desired system reliability. This in itself is an iterative optimization problem, which may be as computationally costly as using the RBDO method. It may be possible to develop a design heuristic relating CDF percentage to desired reliability, but this heuristic may not hold for a wide variety of scenarios. Furthermore, if high levels of reliability are desired, it will be necessary to sample the extreme tails of the distribution, which a sensitivity analysis may not reach. As such, the RBDO method is the most general method to guarantee a level of reliability for microgrid design under uncertainty.

4.5.6 Effect of different levels of power load variation

The actual power load variation is unknown due to lack of data. To address this, a parametric study was performed using three levels of power load variation, with the standard deviation (σ_L) ranging from 30% - 50% of the mean power load. The final results using the SORA method are shown in Table 4.4.

The results show that as power load uncertainty distribution widens, the operating reserve required to meet the 90% reliability level also increases. To meet this increasing requirement, the total generator power and battery capacity increase by up to 24% and 45%, respectively, but annualized capital cost only increases by 3.5% because most of the capital cost is invested in the PV array, which is already at its maximum size. Interestingly, the operating cost remains essentially unchanged. One possible reason for this is that the increase in energy storage increases system efficiency enough to offset the efficiency loss due to increasing generator size.

Table 4.4 – Optimal design with three levels of power load uncertainty and limited battery and PV array sizes

Power Load St. Dev (%)	30%	40%	50%
SORA Iterations	2	4	4
Operating reserve (kW)	20	46	60
Reliability	90%	95%	91%
Total cost ($1k)	348.4	349.4	350.3
Capital cost ($1k)	59.8	60.7	61.9
Operating cost ($1k)	288.6	288.7	288.4
Gen 1 (kW)	95	112	120
Gen 2 (kW)	61	70	73
Battery (kWh)	183	217	265
PV array (kW)	100	100	100

To understand better the effect of operating reserve on reliability, operating reserve was swept at 5 kW increments for the two power load variations: $\sigma_L = 0.4\mu_L$ and $\sigma_L = 0.5\mu_L$. By plotting the iterations of the SORA method versus operating reserve, we can observe the trend of reliability improvement, as shown in Fig. 4.13.

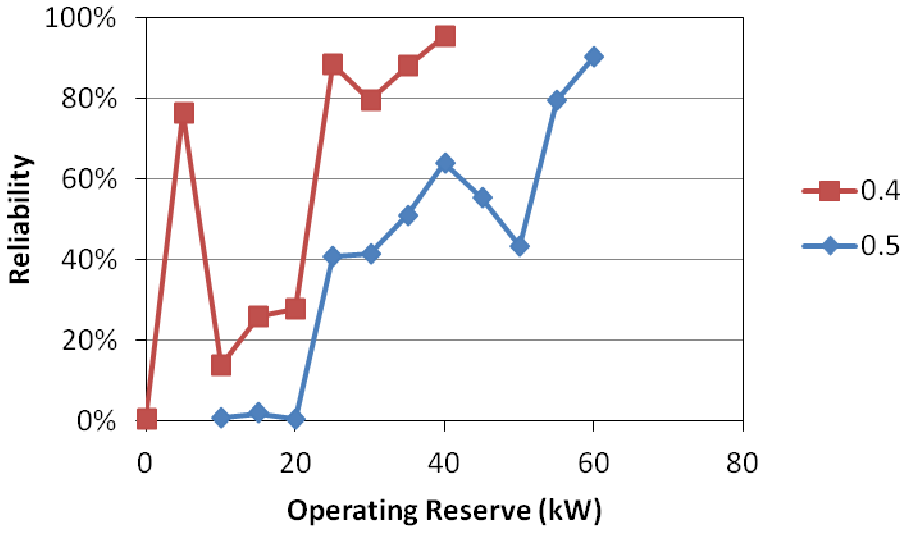

Figure 4.13 – Reliability trends as a function of operating reserve

The figure shows that reliability is not necessarily monotonic with increasing operating reserve, which is unexpected. In fact, the discontinuous responses suggest that specific details of the microgrid design can affect reliability more than the overall

operating reserve. The effect of the operating reserve is to change the design of the microgrid so that the network constraints are satisfied with some "reserve," but the goal of the optimization is still to minimize costs without directly considering reliability. It is possible that the goal of improving reliability is somewhat independent of the goal of objective function improvement and each goal may be served by changing different elements of the microgrid design.

To inform this question, we can also plot the trend of reliability improvement with respect to battery capacity and total generator power, as shown in Fig. 4.14.

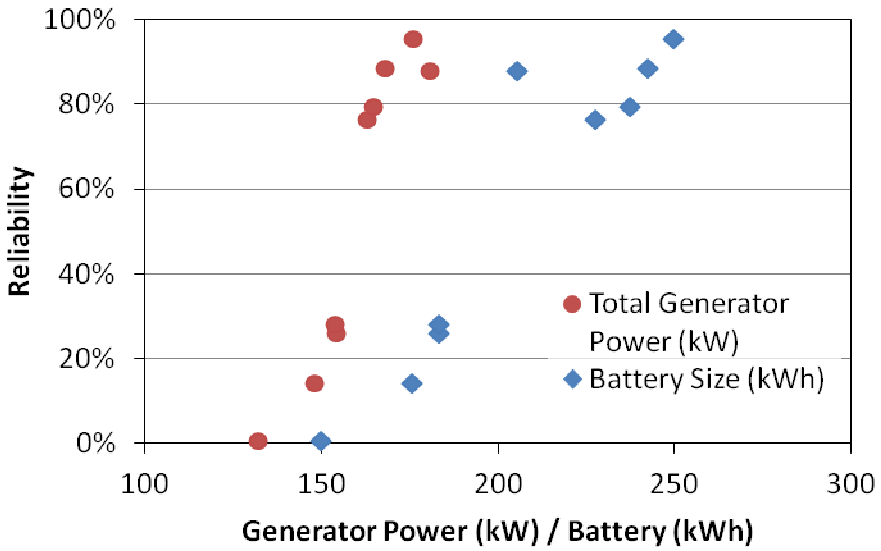

Figure 4.14 – Reliability trends as a function of total generator power and battery capacity

Observing these results, it is difficult to decide correlation of reliability to each variable, as they are changing simultaneously for each iteration. Most likely each has some effect on total system reliability and operating cost. The following section will discuss the variation of reliability and objective function with respect to battery size only. Battery size is chosen because it can be increased without significantly affecting the fuel use and operating cost, whereas increasing generator size monotonically increases these outputs.

4.5.7 Effect of energy storage on reliability

The previous study showed that increased operating reserve did not directly increase the reliability of the microgrid. It was observed that increased reliability was correlated to increased battery capacity. It is expected that increasing the battery capacity will generally improve the reliability of microgrid operation because a larger battery has increased ability to buffer spikes in power load or drops in solar power. To study this effect, the battery size was swept while the rest of the microgrid design was held constant. A Monte Carlo sample was taken for each step in battery size with the standard deviation of load set to 50% of mean load. The fixed design values were: Generator 1 = 120 kW, Generator 2 = 65 kW, PV panel = 100 kW. The results are shown in Fig. 4.15.

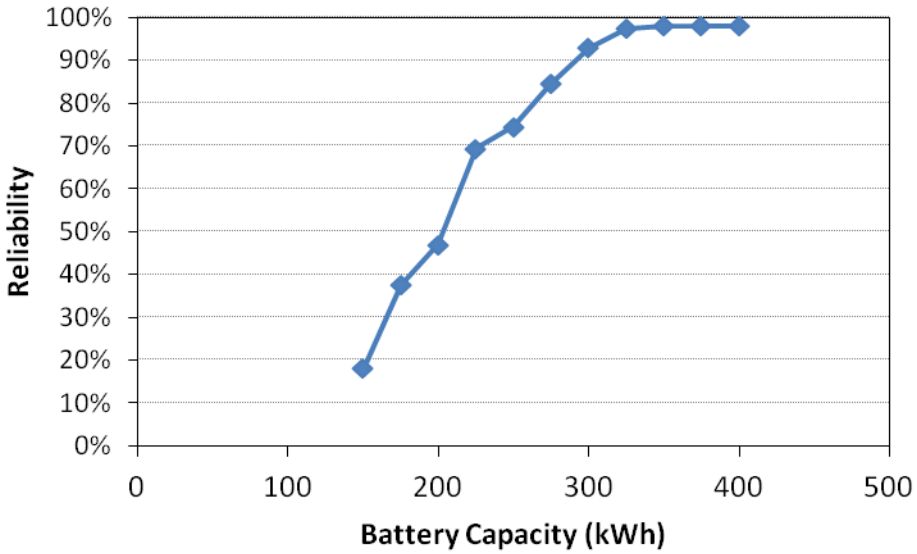

Figure 4.15 – Effect of battery capacity on reliability for $\sigma_L = 0.4\mu_L$

The figure shows that the battery size has a significant role in microgrid reliability, up to a point. For this design, the reliability was not able to improve beyond 98%, which suggests that higher reliability would require changing other design variables. However, it has been previously noted that battery size only weakly affects the overall optimal design objective. Lead-acid batteries are relatively inexpensive, so increasing their size does not dramatically increase the total capital cost relative to other, expensive components (e.g., solar panels). Also, some battery storage helps reduce operating costs, but that benefit flattens out as storage increases.

This will have an effect on iterations of the SORA method. The operating reserve may be increased to improve reliability, and the optimal design problem re-solved multiple times. However, a simple heuristic rule could be to increase the battery capacity to achieve the desired reliability, while holding the rest of the design fixed. This could result in improved operating cost, if it allows the generators to remain smaller rather than increasing in size to meet the increased operating reserve requirement. Additionally, it could save time by reducing the number of iterations of the SORA method.

4.5.8 Summary and conclusions

Accounting for uncertainties in microgrid design is important in order to design reliable systems. Using analytical methods can generate reliable microgrids that have lower cost and higher efficiency because they are not unnecessarily oversized. The methods shown in this chapter can account for power load uncertainty and renewable energy uncertainty in the design process. Using the Sequential Optimization and Reliability Assessment (SORA) method of Du and Chen can efficiently design for these uncertainties, while requiring less than 10% of the computation time of using Monte Carlo sampling of every design.

The initial studies showed that allowing very large energy storage and PV arrays results in economically optimal designs that are also very reliable. Note, though, that this optimum occurs because the fuel cost is relatively high ($2.1/liter), so the addition of large PV arrays can be cost-justified. However, these large PV arrays and storage batteries may not be practical for implementation at remote military bases due to their sizes and weights. Practical upper limits are necessary to properly optimize these system designs, and when their sizes are limited the microgrid reliability is reduced.

The results of the various studies showed that the goals of system reliability and minimizing costs are opposed to each other. Thus, deterministic optimization to minimize costs will not necessarily result in a reliable microgrid design, as increasing reliability will increase capital costs. However, simply adding operating reserve to the deterministic optimization does not guarantee an increase in system reliability. This occurs because increasing battery capacity will improve system reliability, but battery size is not

monotonic with respect to minimizing costs, which is the goal of the optimization. Adding a heuristic design rule of increasing energy storage capacity to improve reliability could save design computation time.

The studies performed here showed that power load uncertainty has a greater effect on system reliability than solar uncertainty. This can be explained because solar supply, at the extreme low side of its distribution, can only approach zero, whereas power load uncertainty can spike to very high values. The same would be true for other uncertain renewable energy supplies, e.g., wind speed. However, the solar irradiance in one hour may be correlated to preceding and following hours, rather than independent as modeled here. These correlations, e.g., a series of cloudy days, could cause long droughts of solar power that the energy storage may not be able to buffer. This is an area for further study.

Chapter 5: Co-design of electric vehicles and a microgrid

Until now this dissertation has been solely concerned with methods and strategies for the optimal design of microgrids. This chapter will examine the addition of electric vehicles to the microgrid and consider how the two can be co-designed to maximize benefits. The question of how vehicles interact with a microgrid has been studied in some detail, both as a variable charging load as well as the possible benefits offered by vehicle-to-grid (V2G) support. However, no research has investigated how the physical *designs* of vehicles and microgrids can improve or hinder their interactions. Likewise, these studies have not considered the optimal design of electric vehicles and microgrids in a single, system-level problem. This co-design problem is the subject of this chapter.

The chapter will first overview vehicle design optimization, focusing on electrified vehicle powertrains. A model of an all-electric military light tactical vehicle (LTV) will be described, along with its optimization problem formulation. The chapter will continue by discussing various co-design problem formulations and suggest a preferred formulation. The co-design problem will be solved with uncertain power load (as in Chapter 4) and the results will be discussed to generate insights into the interactions of vehicle design and microgrid design.

5.1 Vehicle powertrain optimization

Vehicle powertrain optimization is an important early-stage design tool that can include sizing the powertrain components, the design of the powertrain controller, and/or the location of components within the vehicle. The basic vehicle geometry and mission are often considered as givens, with the goal usually set to maximize some performance measure (fuel economy, vehicle range, or another metric) while satisfying various performance constraints (acceleration time, towing ability, maximum velocity, vehicle dynamics, or packaging). Powertrain optimization is especially useful for design of

electrified and other non-conventional powertrains, where there are multiple tractive power sources, multiple energy storage elements (batteries, liquid fuel), and a complicated energy management strategy. For these vehicles there are too many components to easily capture the design tradeoffs among them by using heuristic design rules and separated design of each component.

5.1.1 Literature review

The availability of system-level vehicle simulation models and computing power improvements combined with increased interest in hybrid vehicles to make vehicle powertrain optimization a topic of research in the late 1990s. For example, hybrid vehicle analysis tools were developed at national laboratories, PSAT at Argonne National Laboratory and ADVISOR at the National Renewable Energy Laboratory, and these tools were used for study of hybrid vehicle benefits [Cuddy et al. 1997]. These simulation tools were used with design optimization methods to efficiently design complex, hybrid powertrains simultaneously with their controllers [Assanis et al. 1999, Fellini et al. 1999, Guzzella et al. 1999, Whitehead 2001, Wipke et al. 2001, Filipi et al. 2004, Hu et al. 2004, Guenther and Dong 2005]. Throughout the past decade, improvements in computing power have allowed these methods to be used with higher-fidelity component submodels (e.g., for the battery pack, fuel cell, electric motor, and engine). Examples include studies of HEV power management [Kim et al. 2007], fuel cell vehicle powertrain and optimal control design [Rodatz et al. 2005, Kim and Peng 2007, Han et al. 2008b], power-split hybrid powertrain design [Ahn et al. 2008, Whitefoot et al. 2010], dual-mode hybrid vehicle optimization [Ahn et al. 2011b], and PHEV control optimization with varying all-electric range [Karbowski et al. 2008].

Since the early 2000s, plug-in hybrid electric vehicles (PHEVs) and battery electric vehicles (BEVs) have been a larger topic of research. PHEVs are more practical than BEVs for wide deployment in the near future due to their smaller battery cost, so there has been an associated larger amount of research on these vehicles. The research on PHEVs can be divided mainly into two areas: optimal powertrain/energy management control and optimal design. The optimal control literature is often focused on minimizing

the power consumption per mile of a given vehicle, maximizing all-electric distance, and/or minimizing degradation of the battery packs during charging and discharging. Moura et al. showed results for optimal power management of a PHEV using Markov chains [Moura et al. 2008] and also studied the effect of battery sizing of PHEVs on the optimal power management strategy [Moura et al. 2010]. The optimal design literature typically has addressed the tradeoff of battery pack size and petroleum displacement, especially from a cost/benefit point-of-view for the consumer. Shiau et al. studied the optimal design of PHEVs to minimize consumer cost, greenhouse gas emissions, and petroleum consumption [Shiau et al. 2010a, 2010b]. University of Michigan researchers used GPS driving data in Southeast Michigan to create naturalistic driving cycles [Adornato et al. 2009, 2010] and used them to study PHEV designs [Patil et al. 2009], showing how their performance varies dramatically on different driving cycles.

Much of the research on PHEVs applies to all electric vehicles as well, especially any research relating to battery degradation and charging algorithms. However, these studies do not typically consider the electric grid side of the system, though some of them do consider the charging controllers. They do not address the potential to concurrently design a microgrid, nor design the battery packs of the vehicles to support a microgrid. While this chapter focuses on all-electric vehicles, some of the methods and results can be extended to plug-in hybrid vehicles.

5.1.2 Military EV optimization

Optimization of an all-electric, tactical military vehicle has been previously studied in [Alexander 2011]. Alexander optimized the design of an all-electric Light Tactical Vehicle (LTV), which is the U.S. Army's upcoming replacement for the High Mobility Multipurpose Wheeled Vehicle (HMMWV). It is a four-person vehicle designed for convoy escort and urban assault missions. Additionally, the vehicle would be used internally on military bases, so it is a viable candidate for military microgrid support. The design goal was to maximize the range of the vehicle by changing the design of the four in-hub electric motors along with the battery pack design and placement and transmission gear ratios. The constraints on the problem included limitations on battery pack volume,

limits on battery and motor power draw (design-dependent), vehicle dynamic stability, and vehicle protection from improvised explosive devices (IEDs).

5.1.2.1 EV model description

The electric vehicle (EV) model used by Alexander was a modification of the EV model developed by [Allison 2008]. Alexander's dissertation explains this model in great detail and only a brief summary is given here to introduce the level of modeling. This model was used as given: all modeling of the electric vehicle is solely by Alexander and other researchers. For a more in-depth description including more modeling equations, please refer to [Alexander 2011].

As seen in the top-view of Fig. 5.1, the vehicle has four traction motors, one at each wheel, with a gearbox to reduce the motor speed to wheel speeds. The battery pack is centrally-located with limits on maximum width and length, and the center of mass of the battery is also a variable.

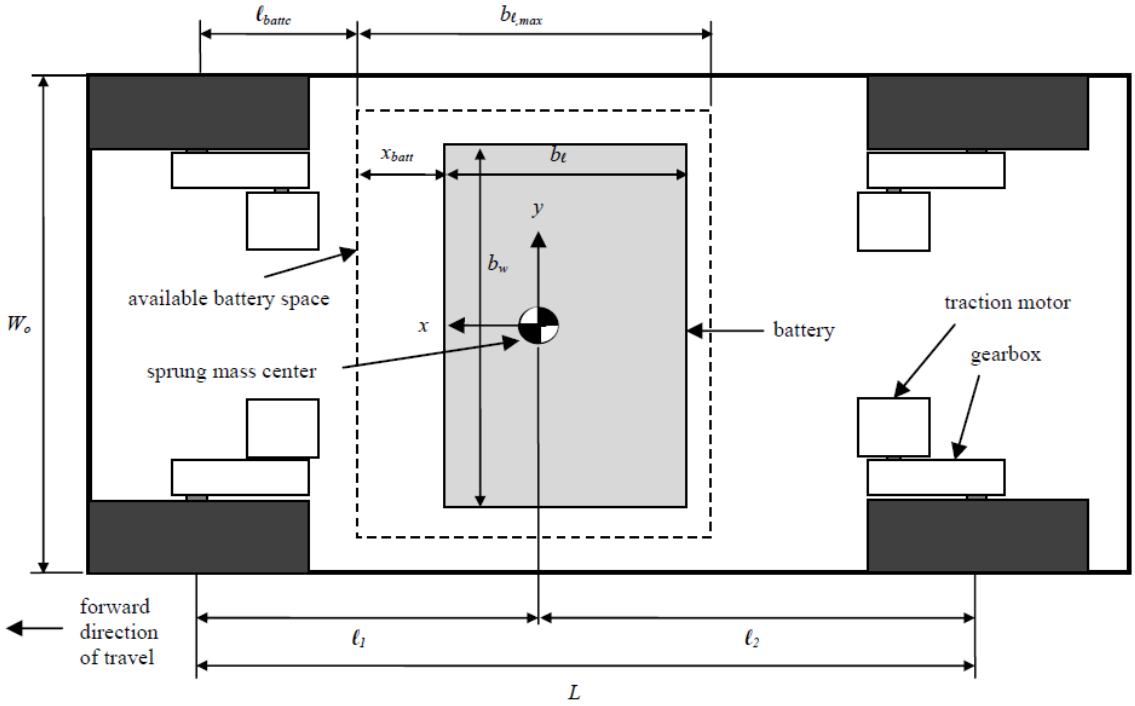

Figure 5.1 – Top view of all-electric military light tactical vehicle [from Alexander 2011]

The dimensions of the LTV were based upon the dimensions of the existing HMMWV M1025A2, though the mass of the vehicle was modified to exclude the internal combustion engine and fuel tank and include the electric machines and battery pack. Alexander developed relations between the motor, battery, and gearbox variables and the mass of each, so that as the vehicle design changes the vehicle mass will change accordingly. This is important because the vehicle dynamics, electricity use, and blast protection are all mass-dependent.

The vehicle energy efficiency simulation uses a backward-looking calculation and is implemented in Simulink. The backward-looking simulation calculates the necessary motor torque, motor speed, and battery power at each time step to follow a prescribed military drive cycle, with outputs of vehicle range and electricity use per kilometer. Using a backward-looking calculation requires the addition of power limit constraints to the optimization problem that ensure the motors and battery can supply the torque and power requested during the simulation. The vehicle efficiency is tested on a military-specific convoy escort cycle, which covers a total distance of 42 miles (69.0 km) in approximately 1.14 hours (4100 seconds) with an average speed of 37 mph (60.8 kph). The acceleration simulation is forward-looking and uses the same power limits on the motors and battery along with the other vehicle parameters to determine the vehicle acceleration performance from 0 to 50 mph (82.1 kph). The vehicle design parameters are listed in Table 5.1.

Table 5.1 – Military electric LTV model parameters [Alexander 2011]

Parameter	Description	Value
m_b	Baseline vehicle mass	1930 kg
m_{occ}	Occupant mass	100 kg
L	Wheelbase	3.30 m
W_o	Overall vehicle width	2.18 m
C_d	Drag coefficient	0.70
A_f	Frontal area	3.58 m^2
ρ_a	Air density	1.10 kg/m^3
m_{us}	Unsprung mass	440 kg
ζ	Damping ratio per wheel	83500 N-s/m
k_s	Suspension stiffness per wheel	16000 N/m

g_h	Geared hub ratio	1.92
r_{go}	Gearbox output gear radius	0.0508 m
$r_{go,i}$	Gearbox output idler gear radius	0.0254 m
$r_{gi,i}$	Gearbox input idler gear radius	0.0762 m
I_{yt}	Tire/wheel assembly spin inertia per axle	14.22 kg-m^2
C_r	Tire rolling resistance	0.01
r_t	Tire radius	0.470 m
P_{acc}	Accessory power load	11200 W

Battery submodel

The vehicle battery consists of two parallel packs, with each pack containing 48 prismatic Li-ion cells in series (the electrode and electrolyte materials are not specified in the documentation). The battery performance parameters are determined via a surrogate model (radial-basis function artificial neural network) developed by Alexander, which was generated from the output of a 1-D Li-ion electrochemical diffusion model developed in [Han 2008a]. Han's battery simulation is based on studies by Doyle, Fuller, and Newman on a single Li-ion cell undergoing a hybrid pulse power characterization (HPPC) test [Doyle et al. 1993; Fuller et al. 1994; PNGV 2001]. This test determines the cell capacity, internal and polarization resistances, open circuit voltage, and polarization time constant as a function of cell state-of-charge. The inputs to the model are the battery electrode insertion scale, battery width and length.

The battery electrode insertion scale, B_I, defines the thickness of the electrodes and the separator. The battery cell width scale, B_W, determines the electrode and cell width as shown in Fig. 5.2. The battery is mounted transversely in the LTV; thus, this variable affects the overall battery length, b_l. The number of windings (folds) in the cell are given by the variable B_L. The cell height is set to a constant 11cm.

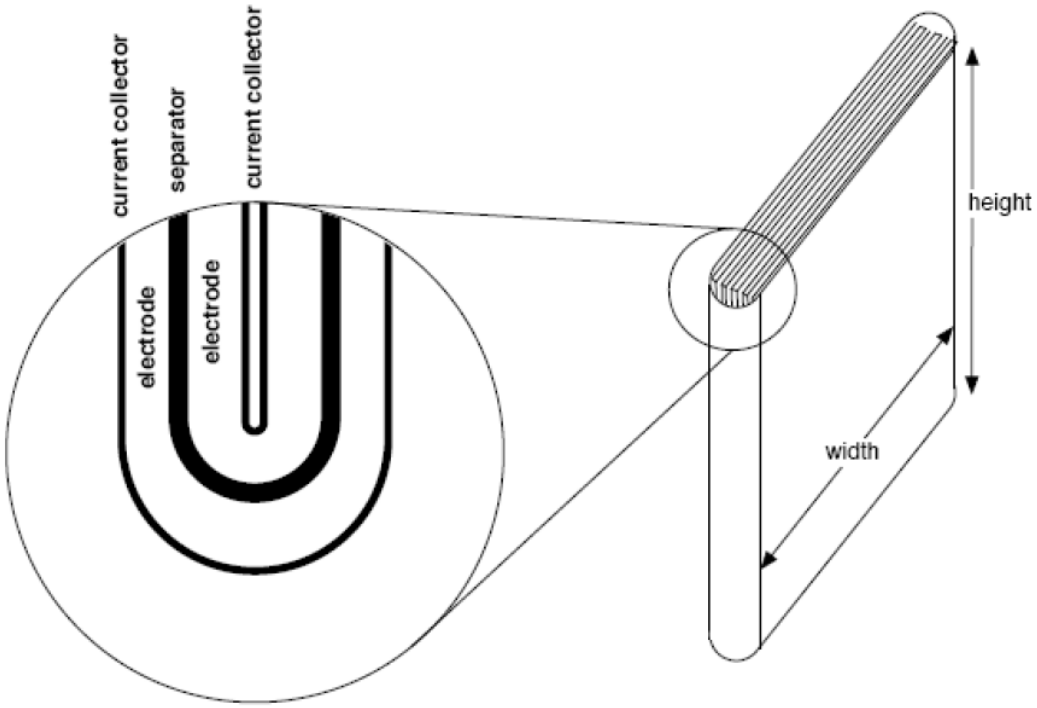

(a) Cell windings (b) Flat-wound lithium-ion cell

Figure 5.2 – Typical flat-wound lithium-ion battery cell [Han 2008a]

Electric motor submodel

The four electric traction motors are three-phase AC induction motors. Induction motors (IM) were chosen over permanent magnet motors due to their lower cost. Hybrid-electric vehicles often use permanent magnet (PM) motors due to their higher power density, but the larger electric power requirements of an EV tends to make PM motors cost-prohibitive. Thus, induction motors are used in commercially-available EVs, such as the Chevrolet Volt extended-range electric vehicle and the Nissan Leaf electric vehicle.

Each phase of the motor is modeled as an equivalent electrical circuit as shown in Figure 5.3, where V_s is the RMS AC source voltage, L_m is the mutual inductance between the stator and rotor, R_s is the winding resistance of the stator, L_{ls} and L_{lr} are the leakage inductances of the stator and rotor respectively, and R_r is the variable electric resistance through the rotor. The electromagnetic interaction between the stator and rotor

is modeled by dividing the slip s into R_r. This model was originally developed by [Bose 2002], implemented by [Allison 2008] and modified by [Alexander 2011]. For additional modeling details, refer to those references.

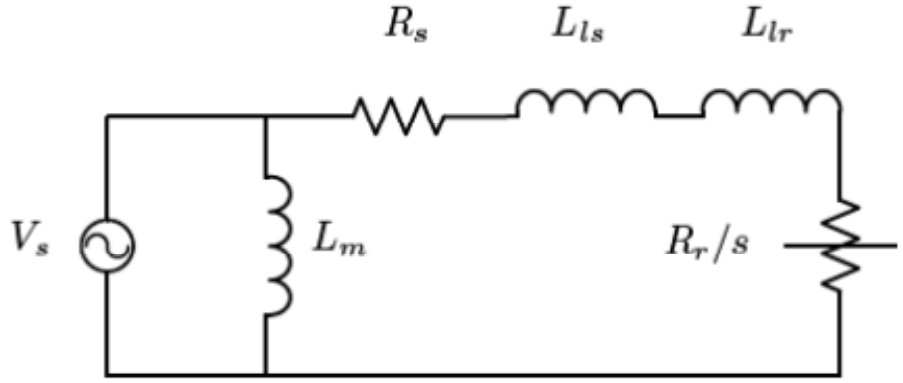

Figure 5.3 – Equivalent circuit model of one phase of an induction motor [Bose 2002]

The input variables to the motor model are the rotor stack length, rotor radius, number of turns per coil in the stator, and rotor resistance (l_s, r_m, n_c, R_r). These variables are used with the parameters in Table 5.2 to determine the motor performance.

Table 5.2 – Induction motor parameters [Alexander 2011]

Parameter	Description	Value
V_{sm}	Maximum stator voltage	460 V
p	No. of stator poles	4
q	No. of slots per phase per pole	3
m_1	No. of motor phases	3
σ_{Yr}	Rotor yield stress	300 MPa
ν	Rotor Poisson ratio	0.30
SF	Rotor safety factor	4
ω_{inv}	Maximum inverter frequency	1510 rad/s
ρ_{fe}	Iron density	7870 kg/m^3
C_{m1}	1st *cm* parameter	0.062
C_{m2}	2nd *cm* parameter	0.998
C_{m3}	3rd *cm* parameter	0.94
C_{m4}	4th *cm* parameter	0.0513
n_a	Slot volume ratio	0.8
n_p	Wire packaging ratio	0.5
t_s	Stator radius proportionality factor	0.5

k_e	End effect ratio	1.5
ρ_{cu}	Copper resistivity	1.72 x 10-8 Ω-m
C_{I1}	Constant I_{sm} parameter	0.0564
C_{I2}	Linear I_{sm} parameter	-0.0237
C_{I3}	Quadratic I_{sm} parameter	2.21

The outputs from the motor model are the maximum and minimum torque curves as a function of motor speed, as well as the power loss map. An example output map is shown in Fig. 5.4. The final output from the motor submodel is the motor mass.

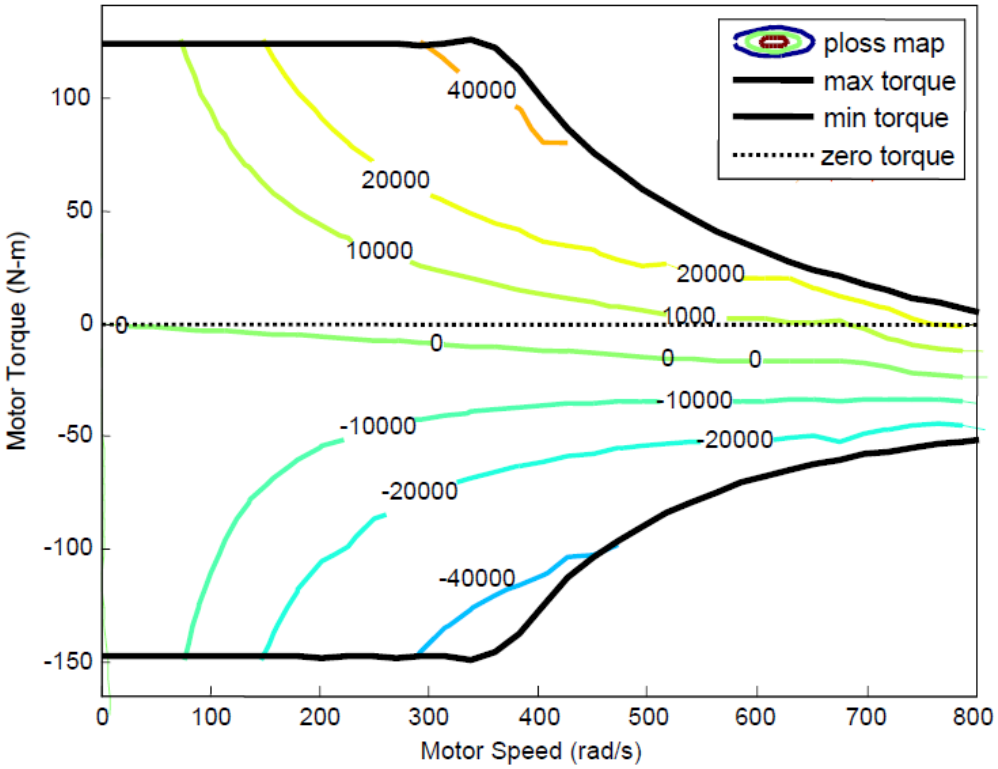

Figure 5.4 – Example power loss map of induction motor model [Alexander 2011]

Directional stability

Under specified vehicle design parameters and driving conditions, the directional stability analysis determines whether the vehicle would remain stable (i.e., not "spinning out") at a specified maximum stable speed, herein set as 113 kph (70 mph). The directional stability submodel has inputs of the sprung mass, longitudinal center of mass

location, tire stiffness, and the average front and rear tire normal forces to computes the directional stability based on a model in [Wong et al. 2001].

Blast resistance

Based on the large number of roadside bomb attacks causing numerous casualties in recent conflicts, the U.S. Army has set design targets that require future LTVs to protect against a 10% chance of severe injury on the abbreviated injury scale (AIS) for the neck, lumbar/spine, and tibia of occupants. Light military vehicles such as the electric LTV described herein run a greater risk of injury due to their low mass and light armor; however, these vehicles maintain the mobility required for certain military missions. A metric was developed to address this tradeoff between the probability of exceeding the injury thresholds and mobility. This equation is a nonlinear function of total vehicle mass, m_T, as shown in Eq. (5.1) [Hoffenson 2012].

$$Pr_{inj} = 1 - 0.5\left(1 + erf\left(\frac{1757 - \frac{4e10^6}{m_T^{1.02}}}{\sqrt{2\left(\frac{2e10^6}{m_T^{1.04}}\right)^2}}\right)\right) \tag{5.1}$$

5.1.2.2 EV optimization problem formulation

The objective of the military EV optimization problem is to maximize the vehicle range by varying the design of the electric motors, battery pack, battery pack location, and reduction gear ratios. The constraints on the system include the acceleration time, maximum battery capacity, torque and speed limits for the motors, power limits for the battery, vehicle directional stability, and vehicle blast protection. The problem formulation is listed in Eqs. (5.2).

$\underset{\boldsymbol{x}}{max}$	r_v	EV range	(5.2a)
w.r.t.:	$0.7 \leq x_1 \leq 2.0$	Battery electrode insertion scale	(5.2b)
	$0.5 \leq x_2 \leq 2.8$	Battery cell width scale	(5.2c)
	$15 \leq x_3 \leq 30$	Number of cell windings	(5.2d)
	$0.0 \leq x_4 \leq 0.5$	Longitudinal battery pack placement from reference point (m)	(5.2e)
	$0.75 \leq x_5 \leq 2.00$	Gearbox ratio, front gearboxes	(5.2f)
	$0.75 \leq x_6 \leq 2.00$	Gearbox ratio, rear gearboxes	(5.2g)
	$0.05 \leq x_7 \leq 0.13$	Motor stack length (m)	(5.2h)
	$0.01 \leq x_8 \leq 0.19$	Motor rotor radius (m)	(5.2i)
	$8 \leq x_9 \leq 22$	Number of turns per stator coil	(5.2j)
	$0.05 \leq x_{10} \leq 0.30$	Rotor resistance (ohms)	(5.2k)
subject to:			
	$b_w \leq 1.5$	Battery pack width packaging limit (m)	(5.2l)
	$b_l \leq 2.1$	Battery pack length packaging limit (m)	(5.2m)
	$t_{0-50} \leq 20$	Acceleration time 0 – 50mph (s)	(5.2n)
	$T_{frnt} \leq T_{max}$	Torque limit – front motors (N-m)	(5.2o)
	$T_{rear} \leq T_{max}$	Torque limit – rear motors (N-m)	(5.2p)
	$N_{frnt} \leq N_{max}$	Speed limit – front motors (rad/s)	(5.2q)
	$N_{rear} \leq N_{max}$	Speed limit – rear motors (rad/s)	(5.2r)
	$P_{vbatt} \leq P_{max}$	Power limit of battery (W)	(5.2s)
	$E_{vbatt} \leq \{350, \ldots, 650\}$	Capacity limit of battery (A-h)	(5.2t)
	$D_s \leq 1$	Directional stability metric	(5.2u)
	$Pr_{inj} \leq 0.1$	Probability of injury due to blast	(5.2v)

The only differences between this formulation and Alexander's are that his formulation allowed different designs for the front and rear motors and used a fixed upper limit on battery capacity to limit battery cost. In this formulation, multiple limits were used for the maximum battery capacity and the problem was solved for each limit. This was done because Alexander's results showed this constraint was always active, which is expected because the design problem is maximizing vehicle range. In the co-design problem, battery cost will be included in the overall cost minimization objective so this constraint can eventually be eliminated and the co-design problem can determine the optimal battery capacity.

5.1.2.3 Possible objectives of EV optimization problem

The most common objective for vehicle optimization is to minimize its energy consumption per unit distance (e.g., liters of fuel per 100 kilometers or electric watt-hours per kilometer) subject to constraints on the vehicle's performance, such as vehicle range, acceleration time, top speed, and handling dynamics. The range constraint is especially important for an EV, because the energy density of electrochemical batteries is low compared to liquid fuels and batteries are expensive.

For an EV, it makes sense to formulate the problem with a different objective: range maximization with a constraint on the maximum battery size to limit the battery cost. This is the formulation used in Section 5.1, as proposed by [Alexander 2011]. However, for an EV the range maximization problem and energy consumption minimization problem can be shown to be equivalent, under certain ranges of the design variables. For a given battery size, *b,* electrical energy use per kilometer, E_{km}, and vehicle range, r_v, are related through Eq. (5.3).

$$r_v = \frac{b}{E_{km}} \tag{5.3}$$

Thus, reducing electrical energy use per kilometer will increase vehicle range, and the objectives of the two possible formulations are aligned. However, for the first formulation, minimizing E_{km}, we must include a constraint to ensure that vehicle range meets a minimum value (lower bound), lest the optimization seek to reduce the battery size to reduce vehicle weight (thus improving the objective). Due to this relationship, the minimum range constraint will be active at the optimum.

Conversely, for the range maximization formulation, we must include an upper bound on the battery size, lest the optimization seek to continuously increase the battery size to increase the vehicle range. As Alexander showed, this constraint is expected to be active at the optimum because vehicle range monotonically increases with increasing battery capacity [Alexander 2011]. We can show these two formulation tradeoffs graphically, as presented in Fig. 5.5. In this figure, an example function is plotted showing the monotonic relationship between EV range and battery capacity.

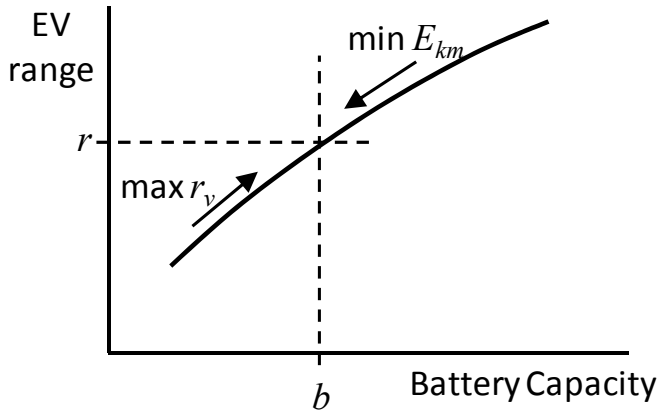

Figure 5.5 – Equivalency of range and efficiency objectives for an EV

For a given battery size, b, we can expect a particular range for the vehicle, r_v. If the range constraint of the first problem formulation (min E_{km}) is set to r, and the battery size constraint of the second problem formulation (max r_v) is set to b, we can see that the two problems will generate the same optimal solution, albeit forcing the design in different directions. Thus, we can see that the solutions to the two problems are equivalent. This insight is only applicable in the variable range where increasing battery size will monotonically increase vehicle driving range, and decreasing battery size will improve vehicle efficiency. It is possible that there exist extreme values of battery size where this monotonicity is not present.

We can exploit this feature to simplify the co-design problem. By solving the range-maximization EV optimization for multiple levels of maximum battery size, we can generate a tradeoff curve of battery size to vehicle range, with an accompanying relationship for electricity use per kilometer. This tradeoff curve can then be used in the microgrid optimization problem in place of concurrent vehicle optimization, thus simplifying the co-design problem significantly. This sequential process is possible because the performance of the vehicle is independent of the microgrid design, but the microgrid performance is dependent on the vehicle design. This type of interaction between two linked problems is known as unidirectional coupling [Fathy et al. 2001, Peters et al. 2009]. However, the microgrid must ensure that the vehicle has enough battery energy to perform its driving tasks. Therefore, the microgrid design and dispatch

problems must contain constraints that account for each vehicle's driving requirements and state-of-charge of the batteries. This problem decomposition will be explained further in Section 5.3.

Solving the co-design problem this way has an additional advantage in that it "modularizes" the combined microgrid and EV optimization problem: multiple vehicles can be implemented within the microgrid design problem without the need to include all of the design variables from each within the AiO problem. This is accomplished by generating the EV tradeoff curves for multiple types and sizes of vehicles, and these results can be implemented into any number of different microgrid design problems.

5.1.2.4 Military EV optimization results

The military EV design was optimized to maximize vehicle range for seven levels of the battery capacity constraint. This capacity constraint was always active at the optimum, which matches Alexander's result. The vehicle range is plotted versus battery size in Fig. 5.6 along with a linear-fit model. Here, battery amp-hours were converted to kWh by assuming a constant battery pack voltage of 210 V. The vehicle energy consumption for all runs ranged from 530 – 545 W-h/km, with an average value of 540 W-h/km.

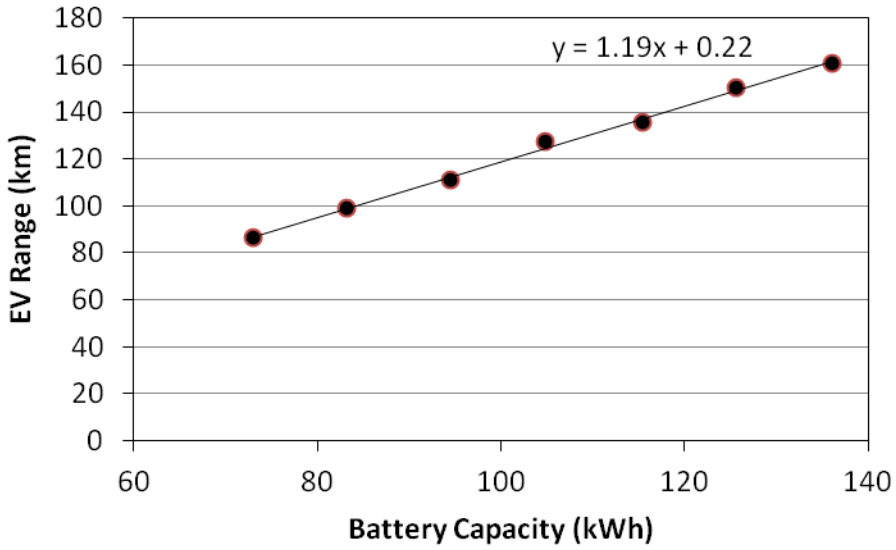

Figure 5.6 – Light Tactical Vehicle range versus battery capacity

The complete results are shown in Table 5.3. As seen in the final row, the battery capacity constraint, *g9*, was always active at the optimum.

Table 5.3 – Electric LTV optimization for different battery capacity constraints

Max. battery capacity (A-h)	350	400	450	500	550	600	650
Objective: Range (km)	86.4	99.0	111.2	127.6	135.6	150.1	160.8
x1 - Battery electrode scale	0.92	0.92	1.49	1.84	1.37	1.40	1.83
x2 - Battery cell width scale	1.63	1.62	1.63	1.63	2.38	1.63	1.63
x3 - Number of cell windings	24.4	27.7	19.4	17.5	17.7	27.5	22.7
x4 - Battery pack placement (m)	0.18	0.20	0.25	0.40	0.06	0.08	0.14
x5 - Gearbox ratio, front	1.47	1.50	1.51	0.77	1.64	1.47	1.23
x6 - Gearbox ratio, rear	1.45	1.56	1.61	0.77	1.64	1.51	0.96
x7 – Motor stack length (m)	0.13	0.13	0.12	0.05	0.12	0.13	0.06
x8 – Motor rotor radius (m)	0.10	0.10	0.10	0.16	0.10	0.10	0.14
x9 - Number of turns per coil	9.9	10.2	8.9	18.6	11.7	8.3	16.6
x10 - Rotor resistance (ohms)	0.05	0.09	0.19	0.12	0.27	0.06	0.20
g9 - Battery capacity constraint	-0.01	-0.01	-0.00	-0.00	-0.00	-0.00	-0.00

5.2 Vehicle interaction with microgrid

Plug-in vehicles, both all-electric and plug-in hybrid, can interact with a microgrid either with one-way power flow (solely as a charging load) or with two-way power flow, including vehicle-to-grid (V2G) power flow. Two-way power flow requires increased communication and control equipment, but can offer additional benefits to the microgrid. However, V2G may not offer enough benefits to justify the additional costs of controls equipment and vehicle battery degradation.

5.2.1 Literature review

Of the existing V2G literature, the vehicles are typically modeled as a simple power source/sink combination and the focus is often on the control strategies or required communications infrastructure. Also, the vehicles are generally assumed to follow a fixed connection schedule. No research has studied the issues of modifying vehicle design to improve V2G benefits or how to design for stochasticity in vehicle charging scheduling.

Much of the research on V2G has focused either on the practical, technological aspects or the economic aspects of V2G. Kempton and Tomić developed models of the economic potential of using electrified vehicles for grid support, though their work was focused on the macrogrid. They discussed the multiple possibilities for the owner of a plug-in vehicle to generate revenue through power supply during peak load times and through ancillary support services (acting as a "spinning reserve" or via frequency regulation) [Kempton et al. 2005]. They also looked into the revenue potential of a company or other entity with a fleet of plug-in vehicles to provide frequency regulation [Tomić et al. 2007]. Gage performed tests using a converted PHEV based on a Volkswagen Jetta to test PHEV capability as well as the practical aspects of V2G capability, including the communication necessary to remotely control the vehicle to supply energy back to the grid [Gage et al. 2003]. More recently, Galus studied agent-based control strategies to maximize the economic benefits of plug-in vehicles for grid support [Galus et al. 2008]. Waraich et al. studied the details of how PHEVs might affect the load on a grid using a micro-simulation model of thousands of PHEVs in Berlin [Waraich et al. 2009].

Other research by Peterson et al. questioned the economic viability of using PHEVs for grid support, especially in areas with low electricity pricing and given the costs of battery pack degradation and replacement [Peterson et al. 2010a]. Peterson et al. also studied the economics of battery degradation of PHEVs when used for V2G applications, concluding that it rarely makes economic sense for a vehicle owner to allow their vehicle to be used to support the grid [Peterson et al. 2010b].

There are many papers that discuss the communication protocols and hardware required to allow V2G to work, e.g., [Hiskens et al. 2009]. This area of research is critical for the actual implementation of V2G, but it is out of the scope of this dissertation and will not be reviewed here.

5.2.2 Charging only

If no V2G power flow is allowed, consideration of plug-in vehicles attached to a microgrid only requires including an additional load to the system. The major differences

are that this load can be controllable, allowing for charging at optimal times of day, e.g., during periods of high renewable energy supply or during periods of low load, such as late at night. Adding vehicle loads to the system can thus change the typical diurnal power load curve, as shown previously in Fig. 3.6, and result in high overnight loads. For a microgrid with diesel generators and a PV array, this may increase fuel use due to the absence of solar power at night.

5.2.3 V2G capability

The more complicated case for adding plug-in vehicles to a microgrid is when the vehicles have the ability to return power to the microgrid. Many possible benefits arise, as now the vehicles appear as both a controllable load and a controllable power supply. However, additional controls are necessary and the degradation of vehicle batteries must be balanced against the possible benefits to the grid.

5.2.3.1 Possible benefits from V2G

Various potential benefits have been suggested for adding plug-in vehicles to a grid or microgrid. Among these include acting as a controllable load to balance renewable energy variability [Ahn et al. 2011a], spinning reserve to maintain line frequency and voltage [Tomić et al. 2007, Peterson et al. 2010], and as a vessel for arbitrage, storing energy when electricity is cheap and returning it when it is expensive [Momber et al. 2010, Stadler et al. 2010]. For most electric grids, which have high reliability and low marginal costs, it is difficult to make an economic case to justify vehicle-to-grid benefits of plug-in vehicles [Peterson et al. 2010a]. The high cost of vehicle batteries and the resultant battery degradation are higher than the value of using the vehicle as spinning reserve or as arbitrage. However, economic benefits can be realized by using communication technologies to control the charging load of the vehicles [Ahn et al. 2011a], but this does not require any V2G capability.

The economic situation for military microgrids and other remote, islanded grids is significantly different than for a regional-level macrogrid. Microgrid power generation is much more expensive on the margin, as the power often comes from a high-energy

density fuel, e.g., petroleum-based fuels. Additionally, the power outputs tend to vary widely and the power generation efficiency will suffer at low loads. Furthermore, microgrids rarely have significant redundancy or operating reserve, resulting in lower reliability. Thus, plug-in vehicles may offer a wider range of benefits to a microgrid than to the macrogrid.

The remainder of this chapter will study the benefits of controlling power flow to and from electric vehicles and a microgrid. The possible benefits for voltage and frequency regulation will not be considered as those require short time-scale simulation (~1 ms to 1 sec), whereas this dissertation only studies bulk power flows on hourly time increments.

5.2.3.2 Control algorithm for V2G

The V2G control algorithm used in this dissertation was previously mentioned in Section 2.4.1.1. The algorithm, from [Peters et al. 2011], attempts to balance the state-of-charge (SOC) of all the connected vehicles, either in charging or discharging. This controller is a rule-based approach that splits the total power command between attached vehicles depending on their individual states-of-charge. Thus, when the lumped charging station command is negative (charging) it prioritizes charging the vehicles with lowest SOC, and when the command is positive (discharging) it prioritizes the vehicles with the highest SOC. The charge priority and power flow to/from each vehicle are calculated by Eqs. (5.4).

$$Priority_k = c_k * (\bar{E}_v - E^t_{v,k}) \quad (5.4a)$$

$$Priority_k = c_k * (E^t_{v,k} - \underline{E}_v) \quad (5.4b)$$

$$P^t_{veh} = P^t_{v,k} * \frac{Priority_k}{\sum_k Priority_k} \quad (5.4c)$$

In these equations, c_k is a binary variable that specifies whether a vehicle is connected (c_k =1) or disconnected (c_k =0). The first equation calculates priority for each vehicle k when the lumped command is to charge and the second equation calculates the priority during discharge. The third equation calculates the power to each vehicle k as a

function of the total lumped charging station power, P_{veh}^{t}, and the priority of each vehicle relative to the other vehicles.

This control strategy does not contain constraints to ensure that the battery SOC is maintained within certain bounds, nor does it ensure that the battery will have enough SOC to drive its scheduled cycle. These constraints will be added within the microgrid optimization problem formulation.

5.3 Formulation of co-design problem

The co-design problem can be solved by combining the EV optimization problem and the microgrid optimization problem into a single problem, known as the All-in-One (AiO) approach. Theoretically, solving this problem will give the optimal co-design solution. However, the clear separation between these two systems, the vehicle and the microgrid, provides the possibility of decomposing the AiO problem into two subproblems, which can be solved sequentially to reduce computation time and provide for a modular, generalized structure for solving the co-design problem. The resulting structure of the decomposed co-design problem may or may not provide the same solution as the AiO problem. Under certain conditions, though, the structure can be proven to provide the overall optimal solution.

5.3.1 Decomposed co-design problem formulation

To decompose the co-design problem, we must first understand how the electric vehicle and microgrid subproblems interact. The EV optimization problem does not depend on its interaction with the microgrid. However, the microgrid optimization problem will depend on the vehicle battery size, vehicle energy use per mile (which will vary how much energy the microgrid should supply to the vehicle), and the vehicle plug-in schedule. This is referred to as a co-design problem with unidirectional coupling [Fathy et al. 2001, Peters et al. 2009]. Therefore, it could be possible to solve the EV optimization problem first and then solve the microgrid optimization problem in an iterative, sequential optimization loop.

The vehicle plug-in schedule is an exterior parametric input to the system and is independent from either the vehicle design or the microgrid design; it is, rather, part of the "environment" where the system exists. (An argument could be made that vehicles designed with very small or large battery packs may change their plug-in schedules, but that will be ignored here.) Thus, we can say that the microgrid design will depend on the vehicle design through the battery size and energy use per kilometer. The new problem structure is shown graphically in Fig. 5.7.

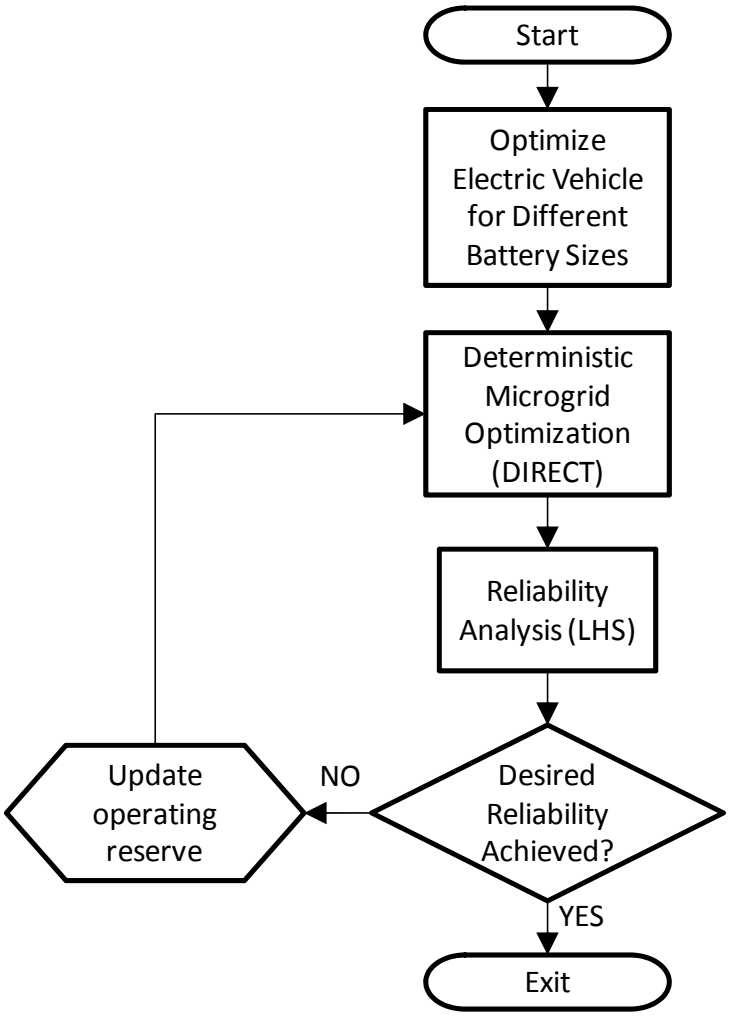

Figure 5.7 – Microgrid and vehicle co-design problem structure

In this structure, the microgrid design could select the number of electric vehicles but would not be able to directly affect the design of the vehicles, e.g., the size of the batteries. Thus, the microgrid design may be sub-optimal in that it can only increase the

storage capacity of the microgrid by discretely selecting additional vehicles, which may be more expensive than simply adding additional battery capacity. For example, if the optimal microgrid design would prefer 150 kWh of storage, and the vehicles have 100 kWh packs, the design is limited to selecting one or two vehicles, neither of which is optimal for the microgrid.

One possible solution to this problem is to generate optimal vehicle designs over a range of battery pack sizes, and this information can be used by the microgrid problem to choose the battery pack size as well as the number of vehicles, which should result in a better design. These results were generated in Section 5.1.2.4 as a linear model of EV range as a function of battery size.

5.3.2 Modeling connected electric vehicles

Using the microgrid topology described in Chapter 3, the EVs are assumed to all plug in at a single charging station in Hub 2 (as shown in Fig. 5.8) and they follow a fixed plug-in/driving schedule. The lead-acid storage batteries previously in Hub 1 have been removed.

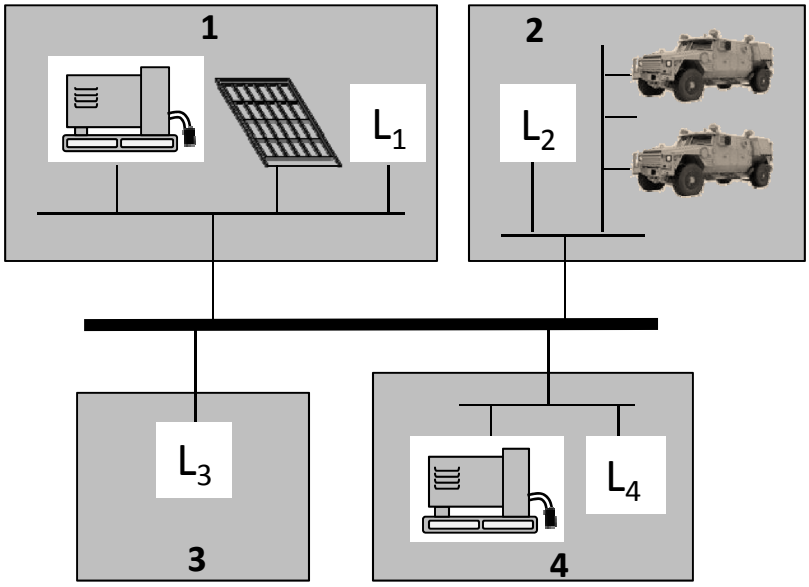

Figure 5.8 – Microgrid topology with vehicle charging station

This schedule was initially randomly-generated but then held fixed to allow for direct comparison between different system designs. Each vehicle was assigned a driving

"cycle" according to the probabilities in Table 5.4. When driving, the vehicles were assigned a random driving distance in the ranges specified in the table. The probabilities varied diurnally, where the vehicles were more likely to be driving from 5am to 9pm than during the overnight hours. Lacking actual driving behavior data for military vehicles, these probabilities and distances were set to roughly approximate the expected use of vehicles during a given day. The overall probability of any vehicle being parked during any hour was ~75%.

Table 5.4 – Driving schedule and distance probabilities

Cycle	Probability (5am – 9pm)	Probability (9pm – 5am)	Driving Distance Range (km)
Parked/plugged-in	60%	90%	0
Driving 1 hour trip	30%	10%	3 – 30
Driving 2 hour trip	8%	0%	5 – 40
Driving 3 hour trip	2%	0%	10 - 50

An example day's plug-in schedule using the probabilities in Table 5.4 is shown in Fig. 5.9, where white squares signify a vehicle that is driving (not plugged-in) and a filled-in square represents a parked and plugged-in vehicle. This plug-in schedule will vary for different days.

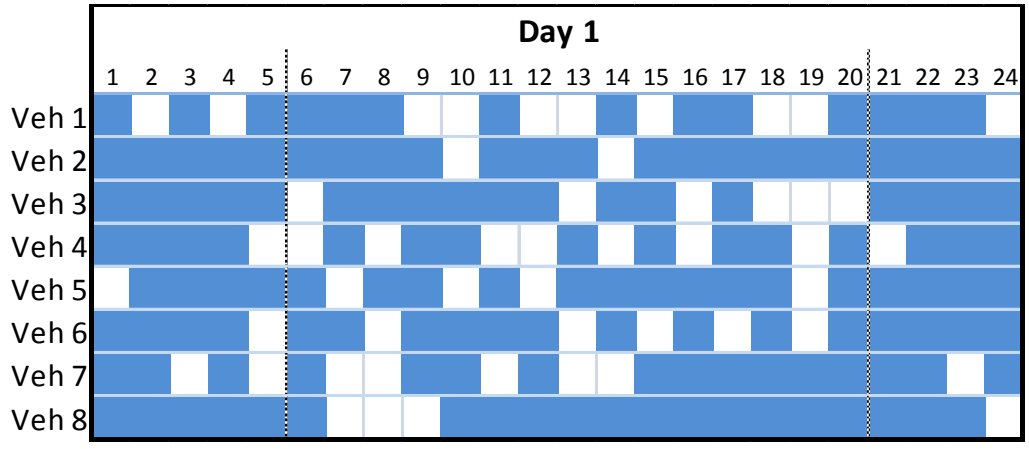

Figure 5.9 – Example vehicle plug-in schedule for one day

When the vehicles are attached to the microgrid, the optimal dispatch problem is free to decide when to charge and discharge the vehicles, as long as the vehicles can maintain enough charge to complete their driving requirements. This can roughly approximate a smart-charging scheme where the vehicle operators can input future driving information to the charge controller. However, in order to allow for some unexpected vehicle use, the vehicle state-of-charge was constrained to always allow for enough charge to drive 15km at any time. Thus, the minimum vehicle battery SOC is set as a function of the EV's energy use per kilometer, which can vary depending on the vehicle design.

A total of eight vehicles are assumed to be assigned to the military base, and any vehicles that are not chosen to be EVs are assumed to have typical internal combustion engines. It is necessary to account for this fuel use in the design problem, otherwise the optimization problem will favor IC engine vehicles over EVs. The U.S. Army specifications for a HMMWV list the highway fuel economy at 14 miles per gallon of diesel fuel. Assuming a mixture of driving, the overall fuel economy of the diesel-powered LTV was set at 12 mpg, which is equivalent to a fuel consumption of 19.6 liters/100km.

5.4 Case Study: Co-design of a military microgrid with attached EVs and uncertain system parameters

The co-design formulation was tested on a similar system to the one presented in Chapter 4. The military microgrid specifications remain the same, including the power load variability and desired reliability. However, instead of stationary lead-acid storage batteries the design includes the number of electrified military LTVs as well as the size of their Li-ion battery packs. The objective remains the same: minimizing combined capital costs and operating costs, but as mentioned previously the operating costs now include the charging of the electric LTVs and the fuel use of the diesel-powered LTVs. Note: lacking cost data converting from a diesel powertrain to an electric powertrain, it is assumed that the only additional cost for an electric LTV is the cost of the battery pack.

5.4.1 Description of case study

For this case study, capital lifetimes were reduced to reflect expected reduced lifetimes on a military base, as listed in Table 5.5.

Table 5.5 – Updated capital lifetimes for a military base

	Diesel Generator	PV Array	Li-ion Battery
Lifetime (yr)	8	10	5

The base is equipped with eight vehicles, though the optimization can choose how many of them are electrified. The design is optimized to meet a reliability of 90% with a power load variability of $\sigma_L = 0.2\mu_L$. The fuel price was set at a medium level of \$8/gallon (\$2.11/liter). Three levels of EV range constraint were chosen as a parametric study: 80, 100, and 120 km. To reduce solution time, the time horizon was reduced from 18 hours to 12 hours and the time step between sequential optimal dispatch problems was increased from 4 hours to 6 hours.

The formulation of the MG+EV co-design problem allows for ease of selecting a different type of vehicle, with a modular change in the model. Therefore, a second, larger vehicle was simulated to show the effect of different vehicles on the design problem. The only additional information needed for the second EV is the vehicle range as a function of battery size and the electrical energy use per kilometer. Likewise, the fuel consumption for the conventional vehicle needs to be updated as well.

The vehicle was assumed to be a larger LTV, with 1.5 times the mass and size of the original vehicle. For the purposes of this study, the larger vehicle will be referred to as the Medium Tactical Vehicle, or MTV. The simulated vehicle range as a function of battery size is shown in Figure 5.10 and the vehicle electricity use per mile is 733 W-h/km. The fuel consumption for the conventional version of this vehicle was scaled with the same proportion as the electricity consumption, resulting in a fuel consumption of 26.5 liters per 100 km.

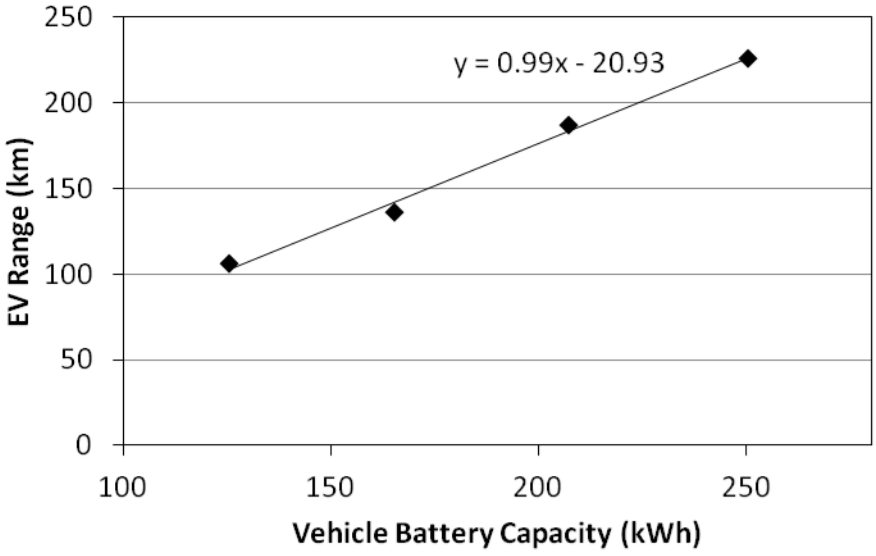

Figure 5.10 – Medium Tactical Vehicle range versus battery capacity

5.4.2 Optimization problem statement

The co-design problem structure with uncertainty is similar to the one presented in Chapter 3, with the modifications for uncertainty as described in Chapter 4 and additional changes to include the vehicles and eliminate the stationary battery storage. The two-stage SORA method requires different optimization problem statements for the deterministic optimization and reliability analysis (refer to Fig. 5.7 for the problem structure). These will be described below.

The deterministic optimal design problem statement is a modification of the one presented in Chapter 3 in Eqs. (3.6). The changes include replacing the stationary battery capacity variable with the vehicle battery capacity variable, $\bar{E}_v$; adding an integer variable for the number of vehicles, N_v; and changing the lower bound of the vehicle battery size to be a function of the required vehicle range, r_v. Also, the constraint to ensure feasibility of the optimal dispatch problem, Eq. (5.5g), is now a function of the operating reserve.

$$\min_{\boldsymbol{x}} \quad \sum_{c} \frac{1}{L_c} p_c x_c + \sum_{t=1}^{T_{Final}} p_{fuel} E_{fuel}^{t} \qquad \text{Annualized capital cost + annual fuel cost} \qquad (5.5a)$$

w.r.t.:

$x_1 = \bar{P}_{gen1}$ Generator 1 rated power (kW) (5.5b)

$x_2 = \bar{P}_{gen2}$ Generator 2 rated power (kW) (5.5c)

$x_3 = \bar{P}_{PV}$ PV array rated power (kW) (5.5d)

$x_4 = N_v$ Number of electrified vehicles (5.5e)

$x_5 = \bar{E}_v$ Vehicle battery capacity (kWh) (5.5f)

subject to:

$\boldsymbol{g}\left(\boldsymbol{x}, \hat{\boldsymbol{u}}(\boldsymbol{T}, \boldsymbol{x})\right) \leq 0$ Feasibility of optimal dispatch (5.5g)

$35 \leq \bar{P}_{gen1} \leq 190$ (5.5h)

$30 \leq \bar{P}_{gen2} \leq 160$ (5.5i)

$50 \leq \bar{P}_{PV} \leq 150$ (5.5j)

$2 \leq N_v \leq 8$ (5.5k)

$f(r_v) \leq \bar{E}_v \leq 200$ (5.5l)

The optimal dispatch problem statement for the deterministic optimization is a modified version of the one presented in Eqs. (3.7). In this formulation, the changes included the addition of the operating reserve constraints (as explained in Chapter 4), new limits on vehicle battery SOC, where the lower limit is set to allow for 15km of range at all times, and the fuel cost in the objective is now also a function of the fuel energy consumed by the non-electrified vehicles, E_{vIC}. By including constraints on the battery minimum and maximum SOC, the optimization problem ensures that the vehicles have enough energy to perform their various driving cycles. For example, if a vehicle returned from a trip with an SOC below the requirement, the dispatch strategy would be infeasible and a new strategy would be sought.

$$\min_{\boldsymbol{u}(t)} \sum_{t} \sum_{i} p_{fuel}[f(u_i^t, \bar{P}_i) + E_{vIC}^t] \quad \text{fuel cost for time horizon} \qquad (5.6a)$$

w.r.t.:

u_i^t dispatch of generator *i* at time *t*, $\forall i, \forall t$ (5.6b)

u_v^t dispatch of connected vehicles at time *t*, $\forall t$ (5.6c)

subject to:

$f(r_v) \leq E_{v,k}^t \leq 0.95\overline{E}_v$	battery energy capacity limits, $\forall k, \forall t$	(5.6d)
$E_{v,k}^{t+1} = E_{v,k}^t + f(u_v^t)$	battery energy balance, $\forall k, \forall t$	(5.6e)
$\sum_h P_{net,h} \leq 0$	network power balance, $\forall t$	(5.6f)
$\bar{P}_{gen} + P_{PV}^t + \bar{P}_{veh}^t - P_{ls}^t - P_{ld}^t \geq P_{reserve}$	operating reserve requirement, $\forall t$	(5.6g)
$0 \leq u_i^t \leq 1$	generator power limits, $\forall i, \forall t$	(5.6h)
$-0.4\overline{E}_v \leq u_v^t \leq 0.4\overline{E}_v$	battery power limits, $\forall t$	(5.6i)

$t \in \{1,..,12\};\ h \in \{1,2,3,4\};\ i \in \{1,2\};\ k \in \{1,..,N_v\}$

Finally, the optimal dispatch problem statement for the reliability analysis portion of the SORA method is presented in Eqs. (5.7). The changes between this problem statement and the deterministic optimization problem statement are the elimination of the operating reserve constraints, Eq. (5.6g), and formulating the network power balance, Eq. (5.7f) as a probabilistic constraint.

$\underset{\boldsymbol{u}(t)}{min} \sum_t \sum_i p_{fuel}[f(u_i^t, \bar{P}_i) + E_{vIC}^t]$	fuel cost for time horizon	(5.7a)

w.r.t.:

u_i^t	dispatch of generator *i* at time *t*, $\forall i, \forall t$	(5.7b)
u_v^t	dispatch of connected vehicles at time *t*, $\forall t$	(5.7c)

subject to:

$f(r_v) \leq E_{v,k}^t \leq 0.95\overline{E}_v$	battery energy capacity limits, $\forall k, \forall t$	(5.7d)
$E_{v,k}^{t+1} = E_{v,k}^t + f(u_v^t)$	battery energy balance, $\forall k, \forall t$	(5.7e)
$Pr\left[\sum_h P_{net,h}^t > 0\right] \leq P_f$	network power balance, $\forall t$	(5.7f)
$0 \leq u_i^t \leq 1$	generator power limits, $\forall i, \forall t$	(5.7g)
$-0.4\overline{E}_v \leq u_v^t \leq 0.4\overline{E}_v$	battery power limits, $\forall t$	(5.7h)

$t \in \{1,..,12\};\ h \in \{1,2,3,4\};\ i \in \{1,2\};\ k \in \{1,..,N_v\}$

5.4.3 Results: two sizes of electric vehicle

The results from optimization of the microgrid with electric LTVs are shown in Table 5.6 and the results using the electric MTVs are shown in Table 5.7. The total optimization time for each case ranged from 28 to 76 hours. The fuel price for these optimization runs is set at $2.1 per liter ($8 per gallon) and the power load distribution has a standard deviation of 20% of the mean ($\sigma_L = 0.2\mu_L$).

Table 5.6 – Co-design optimization results using LTVs

Range Constraint (km)	80	100	120
SORA iterations	3	2	1
Operating Reserve (kW)	79.3	26.3	0
Reliability	92%	98%	92%
Total Cost ($1k)	369.4	387.0	404.9
Operating Cost ($1k)	213.3	207.4	202.5
Capital Cost ($1k)	155.1	179.6	202.4
Generator 1 (kW)	80	160	69
Generator 2 (kW)	84	47	83
PV Array (kW)	98	100	107
Number of Vehicles	8	8	8
Veh. Battery Capacity (kWh)	68	86	101

Table 5.7 – Co-design optimization results using MTVs

Range Constraint (km)	80	100	120
SORA iterations	2	1	1
Operating Reserve (kW)	20	0	0
Reliability	100%	99%	100%
Total Cost ($1k)	378.3	401.0	423.8
Operating Cost ($1k)	191.7	181.1	178.4
Capital Cost ($1k)	186.6	219.9	245.4
Generator 1 (kW)	145	99	167
Generator 2 (kW)	81	70	91
PV Array (kW)	83	98	99
Number of Vehicles	8	8	8
Veh. Battery Capacity (kWh)	103	123	144

Looking at the LTV case first, the optimal design generally chooses larger generators to increase system reliability because generators are the least-expensive way to increase operating reserve. However, when larger vehicle batteries are required to meet the minimum vehicle range constraint, these batteries increase the reliability of the system. Therefore, the designs with the 120 km vehicle range constraint meet the desired reliability with smaller generators and an operating reserve of zero. The resulting capital cost is 13% higher than the 100km range case, due mainly to the Li-ion batteries, but the operating cost is 3% lower due to the large PV array and downsized generators.

The optimal design of the vehicle battery pack for all cases is reduced to its minimum value in order to meet the vehicle range constraint. However, the optimal design always features the maximum number of electrified vehicles in order to reduce the cost of fuel, mainly during driving relative to the diesel-powered vehicles, which outweighs the additional cost of the Li-ion battery packs. These results are highly dependent on the fuel price, as shown previously in Chapter 3. For actual use in design a parametric study should be performed over the range of expected fuel prices.

When moving from the LTV to the MTV, we see similar trends as the LTV case. The major difference is that the MTVs always require larger battery packs due to the increased weight of the vehicles, and microgrid system reliability is improved accordingly. In fact, only the 80 km range case required more than one SORA iteration to meet the desired reliability. The larger battery packs also resulted in 10 – 12% lower operating costs for the MTV-supported microgrids as compared to the LTV-supported microgrids. However, the capital costs were ~20% greater for the MTV-supported microgrids because of the larger battery requirements. Relative to the LTV+microgrid system designs, the MTV cases featured smaller PV arrays. This is due to the increased capital cost required for the larger battery packs, which is offset during the optimization by specifying a smaller PV array.

The designs of the vehicles are relatively unchanged compared to when they were designed independently of the microgrid. In both cases, the vehicle battery pack size is minimized to meet the required range (refer to Section 5.1 for the discussion on EV optimization). This further strengthens the assumption that vehicles can be initially designed for different range requirements, and the microgrid design problem can then

choose the vehicle(s) which meet its requirements. A further extension of this would be to allow the microgrid design to choose different vehicles with various battery pack sizes (e.g., a mixture of MTVs and LTVs). The heterogeneity allowed by this approach could meet system reliability at reduced cost relative to the cases presented here.

5.4.4 Results: effects of fuel price and battery cost

The results from the previous study showed that the optimal vehicle designs generated using the co-design approach are the same designs as would be generated if the vehicles were separately optimized from the microgrid. In order to determine whether the vehicle design during co-design would ever deviate from the separately-optimized vehicle design, a parametric study was performed using two parameters that were expected to cause significant change in the optimal design. The two parameters chosen were fuel price and the unit cost of the lithium-ion batteries. Three levels were chosen for fuel price: \$1.32, \$2.64, and \$3.96 per liter (\$5, \$10, and \$15 per gallon). Two levels were chosen for Li-ion battery cost: \$700 and \$350 per kWh. The optimizations were performed using the LTV with a required 80km minimum driving range. Power load uncertainty was assumed with the standard deviation of the distribution set at 20% of the mean ($\sigma_L = 0.2\mu_L$). The results from the optimization are shown in Table 5.8 for the battery cost of \$350 per kWh and in Table 5.9 for the battery cost of \$700 per kWh.

Table 5.8 – Co-design of LTVs with varying fuel cost and battery cost of \$350/kWh

Fuel Price (\$/liter)	1.32	2.64	3.96
Operating Reserve (kW)	65	65	6
Reliability	94%	100%	97%
Total Cost (\$1k)	243.3	388.0	499.6
Operating Cost (\$1k)	157.9	228.0	336.0
Capital Cost (\$1k)	85.5	160.0	163.7
Generator 1 (kW)	115	86	118
Generator 2 (kW)	66	125	47
PV Array (kW)	52	144	144
Number of Vehicles	8	8	8
Veh. Battery Capacity (kWh)	68.9	72.4	82.7
Resulting vehicle range (km)	81.9	86.1	98.3

Table 5.9 – Co-design of LTVs with varying fuel cost and battery cost of $700/kWh

Fuel Price ($/liter)	1.32	2.64	3.96
Operating Reserve (kW)	54	0	0
Reliability	96%	89%	91%
Total Cost ($1k)	280.6	421.1	539.7
Operating Cost ($1k)	158.9	244.6	340.7
Capital Cost ($1k)	121.8	176.5	199.0
Generator 1 (kW)	107	92	75
Generator 2 (kW)	80	67	81
PV Array (kW)	50	122	144
Number of Vehicles	8	8	8
Veh. Battery Capacity (kWh)	67.8	67.8	72.4
Resulting vehicle range (km)	80.6	80.7	86.1

Three of the six cases run resulted in a co-designed vehicle battery that is the same as for the separately-designed vehicle. However, as fuel price increases the vehicle battery chosen by the co-design approach increases in capacity. This occurs for both levels of battery price, but the effect happens at a lower fuel price when the battery price is low. For the $700/kWh battery scenario, the breakpoint where the co-designed EV differs from the separately-designed EV happens between fuel prices of $2.64 and $3.96 per liter ($10 and $15 per gallon). For the $350/kWh battery scenario, the breakpoint happens between fuel prices of $1.32 and $2.64 per liter. These breakpoints clearly show when co-design can generate a better design than when separately designing the vehicle and microgrid systems.

Comparing across battery prices, we see that along with the larger batteries for the $350/kWh case, the operating cost (which is a proxy for fuel use) is lower, even though the total generator power tends to be higher. Thus, we can see the effect of increased energy storage in the vehicles on system fuel use and the sensitivity of the optimal designs to capital equipment costs.

To analyze the effects of vehicles on the microgrid operation in detail, we can examine the hourly power balance for a single design over time. The design chosen for this analysis was the optimal co-design generated using $350/kWh batteries and $3.96/liter fuel from Table 5.8. For this design, the rated powers of Generator 1 and 2 are 118 kW and 47 kW, respectively; the rated power of the PV array is 144 kW; and there

are 8 electric vehicles, each with a 82.7 kWh battery pack. This design was chosen because it represents a design where the co-design solution chooses a larger vehicle battery than if the vehicle was designed separately.

The power balance of the system is shown for hours 1 – 30 in Fig. 5.11 and for hours 30 – 60 in Fig. 5.12. These figures show the output power from each generator and the power to/from the vehicle charging station, where negative power means that vehicles are charging (absorbing power). The heavy black line shows the power load minus the power from the PV array. Thus, the power goal of the system reduces to meeting this remaining power load. If the output power from the generators is greater than the 'Load less PV' line, the generators are also supplying power to the vehicle charging station (as shown in hours 5 and 6 in Fig. 5.11).

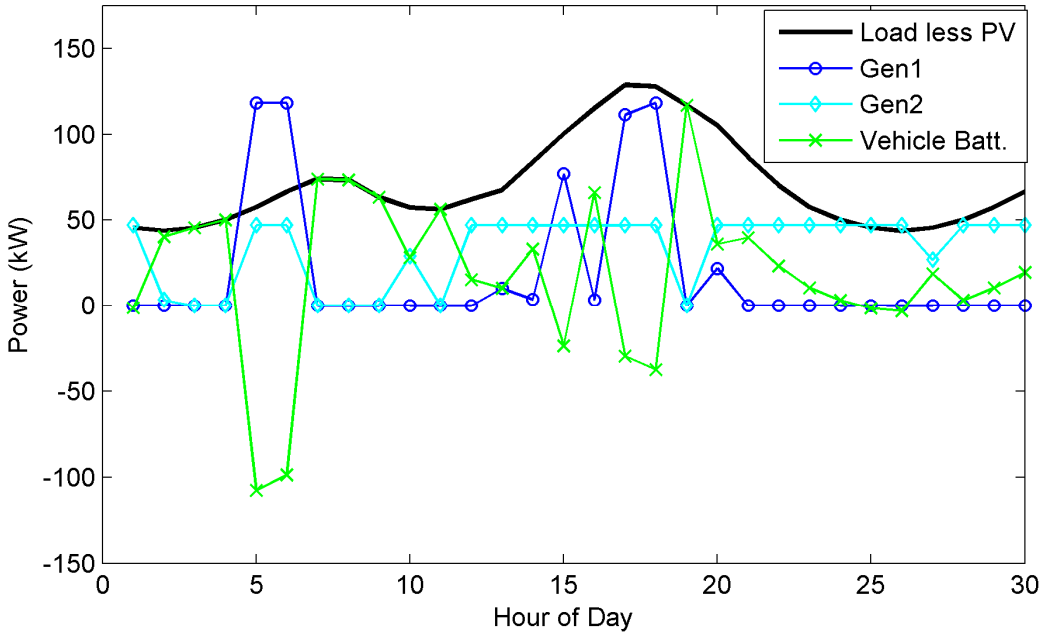

Figure 5.11 – Detailed power balance over time: hours 1 – 30

Looking first at the first day in Fig. 5.11 we can see that the power load is initially low in the early morning hours. In hour 1, the smaller generator (Gen2) is sufficient to supply the load and is operating because it is more efficient than Gen1. From hours 2 – 4, both generators are shut down and the entire load is supplied by the plugged-in vehicles. At 5am, the SOC of the plugged-in vehicles has been depleted, so they begin charging at a high rate and both generators must be run to supply the load and the vehicles

simultaneously. After this charging period, from hours 7 – 9 the generators are again shut down and the EVs are used to supply the load. From hours 12 – 20 there is a changing mix of generator use, vehicle charging and discharging to meet the peak power of the afternoon and early evening. The mix changes hourly depending on what is the most efficient option. During the overnight period from hours 20 – 30, the smaller generator (Gen2) is mainly used to supply the load, as the vehicle battery capacity is not large enough to supply the entire load for more than a few hours.

Looking at the second day in Fig. 5.12, we can see a different usage of the vehicle batteries. From hours 29 – 37 the power load is greater than can be supplied by Generator 2; however, rather than using Generator 1 to inefficiently supply the remaining power, the vehicles are used to buffer the power fluctuations and supply the rest of the load. By doing this, the larger, less-efficient Generator 1 can remain off until hour 38, which corresponds to 2:00pm.

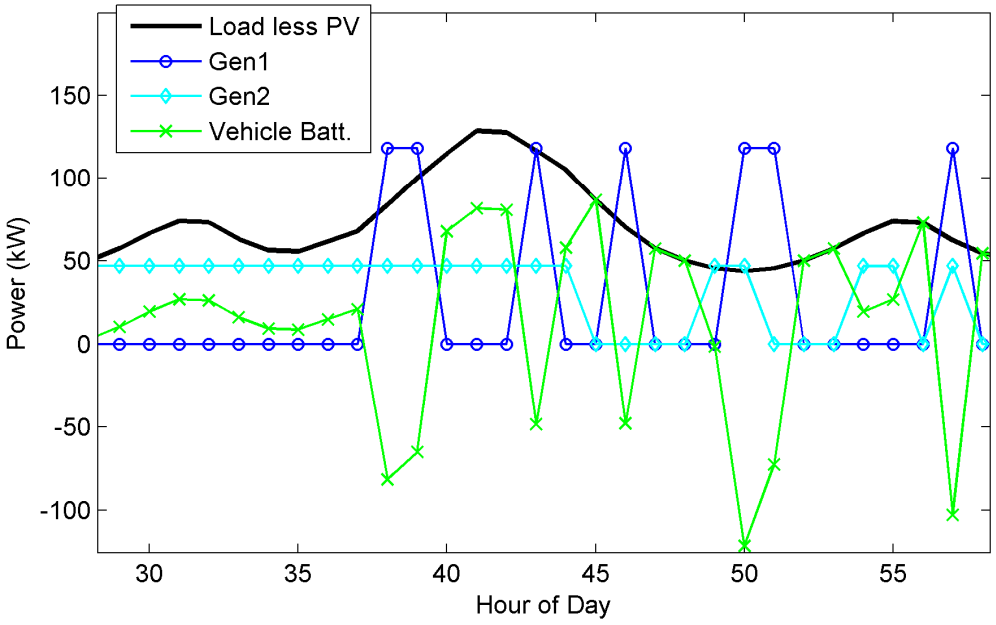

Figure 5.12 – Detailed power balance over time: hours 30 – 60

5.4.5 Results: co-design vs. separated design

The results from the parametric study of fuel price and battery cost showed that under certain conditions the vehicle design resulting from co-design can have a larger

battery than is required to meet the range constraint. If the vehicle were separately designed from the microgrid, the battery pack would be optimized to be the minimum size necessary to meet the range constraint. This shows the effect of co-design but does not quantify the differences between co-design and separate design of the electric vehicles and microgrid.

In order to quantify this difference, one co-design result is compared to the result for separately-designed systems in Table 5.10. For the separately-designed systems, the vehicle was first optimized with a range constraint of 80 km. This vehicle design was then used in the microgrid optimization, where the microgrid design could choose the number of vehicles but could not change any other aspects of the vehicle design (the vehicle battery pack size was fixed). For this comparison, fuel price was set at $5.28 per liter, the battery price was set at $350 per kWh, the minimum vehicle range was 80 km, and the power load distribution had a standard deviation of 20% of the mean ($\sigma_L = 0.2\mu_L$). The third column of the table shows the percent change when moving from the separately-designed systems to the co-designed systems.

Table 5.10 – Difference between co-design and separated design

	Separated design	Co-design	*% change*
Operating Reserve (kW)	80.0	25.9	*-68%*
Reliability	99%	90%	
Total cost (deterministic) ($1k)	615.0	609.0	*-1%*
Mean total cost (LHS) ($1k)	782.4	630.1	*-19%*
Generator 1 (kW)	130	94	*-28%*
Generator 2 (kW)	66	49	*-27%*
PV Array (kW)	145	148	*2%*
Number of Vehicles	8	8	*0%*
Veh. Battery Capacity (kWh)	67	86	*28%*
Resulting vehicle range (km)	80	102	*27%*

The co-designed microgrid features generators that are 27-28% smaller than the separately-designed microgrid, which is made possible because the co-designed vehicles have a 28% larger battery pack than the separately-designed vehicles. As shown in previous results, the larger battery packs allow for improved system reliability with a

lower operating reserve; thus, the generators can be down-sized, which improves the fuel efficiency of the system.

While the total annualized cost of the co-designed system (as evaluated during the deterministic optimization using the mean power load) is only 1% lower than the separately-designed system, the mean total cost (as generated from the LH samples during the reliability analysis) is 19% lower for the co-designed system. That is, the co-designed system is significantly more robust with respect to operating costs than the separately-designed systems. The larger battery capacity, while increasing system reliability, also reduces the operating variability given uncertainty in the power load. This clearly shows the value of co-design for this set of input parameters. However, when the input parameters generate similar systems using co-design and separated design, this advantage will not be seen.

5.4.6 Results: effects of plug-in schedule variation

The microgrid and EV designs are generated using a fixed vehicle plug-in schedule. In reality, the vehicle plug-in schedule and driving distances are stochastic parameters. We wish to understand the consequences of using fixed plug-in schedules during the co-design process on the microgrid reliability and operating cost. Two scenarios will be studied: (1) different schedules with the same probabilities listed in Table 5.4, and (2) schedules generated using lower plug-in probabilities.

For Scenario (1), three new plug-in and driving schedules were randomly generated using the probabilities from Table 5.4. The co-design solution with fuel cost of $2.64/liter and battery cost of $700/kWh (Table 5.8) was simulated using these new driving schedules. Reliability analysis was performed and the resulting reliabilities and mean operating costs for all of the runs are summarized in Table 5.11. The results show that the system is robust to changes in the plug-in schedule and driving distances, assuming the same probabilities that were used to design the system.

Table 5.11 – Co-design of LTVs with different plug-in schedules using the same plug-in probabilities

Cycle	Reliability	Mean Operating Cost ($1k)
Original	89%	424.7
Cycle-1	98%	421.1
Cycle-2	94%	427.6
Cycle-3	91%	419.8

For Scenario (2), more aggressive probabilities for driving distance were assumed, as listed in Table 5.12, and these were used to generate a new schedule. One day of this new schedule is shown in Fig. 5.13, where there is noticeably more driving time than the original schedule shown in Fig. 5.9. The results from this study are shown in Table 5.13.

Table 5.12 – Aggressive driving schedule and distance probabilities

Cycle	Probability (5am – 9pm)	Probability (9pm – 5am)	Driving Distance Range (km)
Parked/plugged-in	45%	75%	0
Driving 1 hour trip	40%	20%	3 – 30
Driving 2 hour trip	10%	5%	5 – 40
Driving 3 hour trip	5%	0%	10 - 50

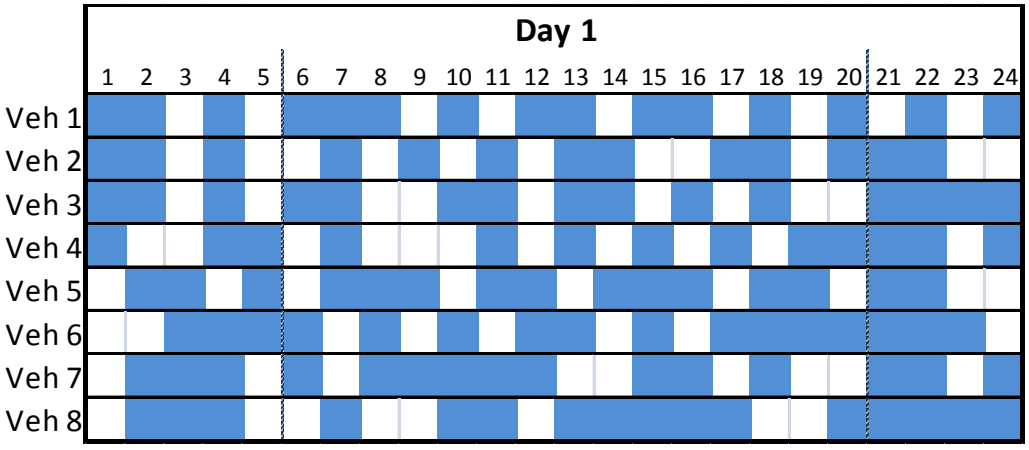

Figure 5.13 – Example vehicle plug-in schedule with higher driving probabilities

The results show that even with a more aggressive driving schedule, with lower probability of plug-in and longer driving distances, the co-designed system still meets the reliability requirements and shows minimal increase in mean operating costs. However, this study does not address whether there is a correlation between vehicles for when they are plugged-in or driving. That is, it may happen that multiple vehicles will be used for a mission simultaneously, depriving the microgrid of their presence. This is not accounted for because the driving schedules are randomly generated.

Table 5.13 – Co-design of LTVs with higher driving probabilities

Cycle	Reliability	Mean Operating Cost ($1k)
Original	89%	424.7
Aggressive	92%	442.1

5.4.7 Summary and conclusions

A microgrid and electric vehicle co-design strategy was developed and implemented for the case of a military microgrid. Analysis of the design problem showed that the electric vehicle optimization could be separated from and solved prior to the microgrid optimization problem. This allowed for significant computation time reduction relative to the all-in-one problem. This also allowed for modular study of the influence of two different vehicles on the microgrid design. However, this problem decomposition may not be applicable when considering plug-in hybrid electric vehicles (PHEVs). The optimization of a PHEV requires simultaneous optimization of its energy management strategy, which will interact with the plug-in frequency, battery state-of-charge, and other factors. This is an area for future research.

The results show that the method performs well for co-design optimization and can generate designs and show design tradeoffs within a reasonable period of time. For example, the optimization shows that requiring increased range from the vehicles will increase overall cost, but with the benefit of improving system reliability and reducing operating costs and fuel use. Also, for these vehicles the benefits of electrification in reduced fuel cost outweighs the significant cost of the battery packs. This result is highly-

dependent on the energy consumption of the electrified and conventional vehicles, but it does allow for high system reliability without the addition of a stationary energy storage system.

One of the outcomes from these studies, and the prior studies in other chapters, is that the designs are highly-dependent on the input parameters, especially pricing parameters. The designer must be careful to perform appropriate parametric studies to understand the sensitivity of the resulting designs to parametric uncertainty. Inclusion of parametric uncertainty is possible, as shown with the uncertain power load used here. However, inclusion of multiple uncertain parameters within the design process can result in an unwieldy and difficult optimization problem with too many random samples required to generate meaningful reliability results.

A parametric study of fuel price and battery cost shows that for low fuel prices and high battery cost the co-design solution is the same as the solution if the two systems, electric vehicles and microgrid, were separately designed. However, as the fuel price increases and the battery price is reduced, a breakpoint is reached where the co-design solution diverges from the separately-designed solution. For these cases, the co-design solution features larger vehicle battery packs, which increases system reliability and reduces operating cost relative to the separately-designed solution. This clearly shows the benefits of co-design for certain scenarios.

While the combined system was designed assuming a fixed plug-in schedule and driving distances, a study shows that the system is robust to modest changes in that schedule. When a single design is simulated with other schedules with increased driving and reduced time spent plugged-in, the system reliability was only slightly reduced and the operating cost remained similar to the baseline case.

Chapter 6: Conclusions and future work

As mentioned in the beginning of this dissertation, the vehicular transportation and electric power systems are converging. These massive systems, long separated and developed in isolation from each other, are beginning to interact directly. As vehicle electrification increases, this interaction will become an area that needs to be addressed in the design of power systems and vehicles. The overall goal of this dissertation is to add a few grains of understanding to this vehicle/grid interaction, provide some guidance for designers of both systems, and generate questions for future research in this direction.

6.1 Summary

The dissertation first addressed the problem of optimal dispatching of multiple power generation and energy storage elements, focusing on long time scale (hourly) economic dispatch to minimize operating costs over a single year (Chapter 2). Multiple problem formulations were identified depending on the available power resources and likewise many problem simplifications were identified to increase the efficiency of solving the optimal dispatch problem. An problem formulation with a finite, moving time horizon was proposed as the best balance of efficiency and accuracy for solving the nonlinear optimal dispatch problem. Short time scale transients and power quality were not evaluated in this analysis, though they may affect the optimal dispatch results, e.g., by placing ramping limits on generators or switching limits on battery storage. The combination of the long time scale economic dispatch problem and short time scale power quality problem is a subject for future research.

Next, Chapter 3 showed how this optimal dispatch strategy could be implemented into an optimal microgrid design framework. A nested optimization problem was formulated and solved for a deterministic example problem. The case studied was a small, islanded military microgrid with diesel generators, a PV array, and a storage

battery. The optimal design with nested optimal dispatch was shown to work well for this example.

In Chapter 4, uncertain parametric inputs were added to the optimal microgrid design problem. The uncertain distributions of solar irradiance and power load were modeled; an extreme value distribution was used for solar irradiance and a normal distribution used for the power load. Two methods were compared for performing design under uncertainty: (1) a two-loop method, where Monte Carlo sampling was performed for each design studied during the optimization, and (2) a sequential method, SORA, developed by Du and Chen, where the reliability of the microgrid design is only evaluated at the end of each optimization. The SORA method was shown to generate similar designs as the two-loop MCS method, but with up to a 98% improvement in efficiency.

Finally, Chapter 5 added electric vehicles to the microgrid in lieu of storage batteries. A co-design problem was formulated and it was shown that the electric vehicle and microgrid optimization problems could be decomposed and solved sequentially. This allowed for computation reduction and modular study of the influence of two different vehicles on the microgrid design. The co-design problem was useful to show various synergies and tradeoffs between the microgrid and electric vehicle designs. For example, the results showed that the presence of electric vehicles can significantly improve the reliability of a microgrid while reducing operating costs and fuel use. The co-design solution was shown to be superior to separately-designed systems for some combinations of input parameters; in this case, fuel price and battery price. This shows how the results are dependent on the costs of fuel and capital equipment, as well as the expected lifetimes of the equipment. This decomposed approach may not be possible when considering plug-in hybrid electric vehicles due to their more complicated energy management strategies.

6.2 Contributions

This dissertation has made three main contributions: (1) developing a categorization of different types of optimal microgrid dispatch problems, (2) a method to

optimally design a microgrid with uncertain parametric inputs, and (3) a method for optimal co-design of electric vehicles and a microgrid including parametric uncertainty. These contributions are described in detail below.

Contribution (1)

The first contribution of this work is developing a categorization of different optimal dispatch problems for microgrids and an explanation of the formulation needed to solve each. In prior work, much effort was given on methods to solve optimal dispatch problems but little emphasis was placed on the different types of formulations. The work presented in this dissertation can guide designers, controls developers, and others needing to solve optimal dispatch problems and help them choose the simplest formulation that meets their particular case.

Contribution (2)

The second contribution of this work is the formulation and solution of an optimal microgrid design problem while accounting for parametric uncertainty. Prior optimal microgrid design research only considered uncertainty by performing sensitivity analysis or other parametric studies, e.g., using best-case and worst-case scenarios for the uncertain parameters. The approach presented here takes into account actual distributions of uncertain parameters using the examples of solar irradiance and power load. The optimal microgrid dispatch and design formulations were combined with the SORA method by Du and Chen to efficiently solve for the optimal microgrid design under parametric uncertainty. Using this method reduced the computation time by up to 98% relative to using Monte Carlo sampling on each design evaluated. This implementation can hopefully provide a new direction for microgrid design research, where uncertainty in the design process is handled in a formal way that can provide actual microgrid reliability predictions.

Contribution (3)

The final and most significant contribution is the development of an approach for co-design of microgrids and electric vehicles. It was shown that the co-design problem

can be decomposed, allowing for faster computation and efficient analysis of the interaction of different vehicles with the microgrid. In some cases, the co-design approach can generate improved system designs as compared to designing the vehicles and microgrid separately. This approach can lead to studies of vehicle fleet mixing and how a range of vehicle types and sizes will interact differently with a microgrid. This is the most-likely scenario for future V2G applications, where consumers who plug-in will not be driving one type of vehicle. Future studies can additionally look at the effects of PHEVs versus BEVs, where the vehicle energy management strategy and difference in battery sizes will affect the V2G interaction.

Looking at the military microgrid case in specific, the current bases in combat areas do not use electrical networks. Typically, each building has its own generator, independent from the other buildings. This is done for practical reasons, as it is easier and more robust, but suffers from severe inefficiencies. The integrated design approach in this dissertation may not generate "field-ready" designs, but is useful to calculate the designs which could be most beneficial for various scenarios. The results from these studies can be used to give impetus to changing military practices to include more renewable energy, network military bases into microgrids, and implement controllers to maximize system efficiency while maintaining reliability. Additionally, the work presented here can be used as a framework to study highly-detailed, practical design issues, such as electrical dynamics and distributed control systems. This capability has been previously demonstrated in the a case study at the University of Michigan's Automotive Research Center [Papalambros et al. 2011].

6.3 Assumptions and Limitations

The modeling and results in this dissertation are performed under the following assumptions:

- all parametric inputs (e.g., capital equipment lifetimes, costs, and other model inputs) are assumed known precisely, unless specifically addressed as stochastic parameters using reliability analysis;

- batteries have fixed, linear charging efficiencies and DC/AC inverters have linear efficiency losses;
- no equipment failure or downtime due to maintenance;
- no battery degradation or other additional costs for V2G;
- the additional cost of an electric vehicle relative to a conventional vehicle is solely due to the battery pack;
- vehicle plug-in schedule and driving needs are known and predictable;
- the vehicle driving model is simple, where vehicle energy efficiency is constant per unit distance (i.e., not a function of the driving cycle);
- reactive power is not considered.

These assumptions present limitations to this work, which lead to possible extensions and future work, as described in the following section.

6.4 Future work

This dissertation studied uncertainty in the parametric inputs to the model; however, the forward-looking dispatch assumed certainty under its time horizon. Thus, the control strategy could perfectly adapt to sudden changes, e.g., a significant drop in solar power. This method is useful for design to account for these uncertainties, especially with regard to balancing system investment cost and operational cost. It is necessary to account for the variation in operation cost in order to know how much to invest, and know how to size components such that expected variation will not result in a loss-of-load.

However, the forward-looking dispatch under a time horizon assumes certainty in its future predictions, at least under the time horizon. Thus, the control strategy is able to perfectly adapt to sudden changes, e.g., a significant drop in solar power. In reality, any future predictions will have error associated with them, and the actual fuel use and probability of LoL will depend on the accuracy of these predictions. Thus, it would be useful to design microgrids using realistic, feedback controllers for the dispatch problem to account for these prediction errors, e.g., model-predictive control or trajectory

methods. Some researchers are studying these controllers for microgrids [Peters et al. 2011, Arnold et al. 2009], but thus far have not used them for system design as well. This is an area for future research.

While this dissertation considered uncertainty in power load and solar power, it assumed the vehicle plug-in and driving schedules were fixed and known. In an actual system, these are uncertain parameters which can significantly affect the system design and performance. For example, if the microgrid assumes the driving distance to be known, it can supply the vehicle with precisely the amount of energy to drive that distance, but additional driving may not be possible. Addition of vehicle driving and plug-in uncertainty would significantly improve the results from this approach.

The methods and results in Chapter 5 only consider all-electric vehicles. If plug-in hybrid vehicles are used instead, the vehicle optimization problem must also include the optimization of the vehicle energy management strategy. This strategy will vary depending on the vehicle battery state-of-charge, which is affected by the battery size, plug-in schedule and the microgrid's dispatch strategy for charging and discharging the vehicles. Thus, the decomposed approach presented herein may not apply for PHEVs.

The analysis and discussion of the possible benefits of vehicle-to-grid (V2G) power flow does not include the negative aspects of V2G, including the costs of battery degradation, additional controls and communication infrastructure, and possible loss of utility for the vehicles drivers. Other studies, e.g., [Kempton and Tomić 2005, Momber et al. 2010, Peterson et al. 2010b], do include aspects of these costs. The inclusion of these costs would generate solutions that are more realistic and give a practical cost/benefit analysis of V2G.

Additionally, the work in this dissertation considered only fixed microgrid topologies and fixed numbers and types of microgrid components, except for changing the number of vehicles. A more generalized microgrid design problem should consider multiple types of renewable power sources, as some may be more economically suitable than others for different locations. Likewise, considering different types of energy storage and power generation can also benefit certain microgrid designs. The number of similar elements should also be used as a variable, as multiple small generators may have better efficiency and reliability than one or two larger generators. Lastly, problem topology is

very important when reliability and robustness are goals of the system and when electrical dynamics are considered in the microgrid design and dispatch.

The analysis of reliability in this dissertation is limited to considering loss-of-load. However, reliability of individual components should also be considered. Using a different formulation, the expected system reliability could be calculated using the mean time to failure and other equipment specifications. This would result in system designs that may have some redundancy in components, but would be more robust to equipment failure and downtime due to regularly scheduled maintenance.

While the nonlinear formulation worked well for the examples presented herein, these were necessarily small design problems with only a few vehicles, power supply, and energy storage resources. Scaling the problem up to larger systems may result in problems that are too large for nonlinear programming algorithms, or simply too large for solving within a practical amount of time. For these cases, the lumping of similar elements can provide some improvement for scaling up, especially if the system being designed has modularity (e.g., a neighborhood where each house has a similar PV array and battery storage). However, at some point linearization should be used to allow for larger problem size and more efficient solution. If loss of fidelity is a concern, sequential linearization or piece-wise linearization can be used to preserve the nonlinear characteristics of the system.

Finally, as mentioned at the beginning of this chapter, the microgrid problems solved in this dissertation only considered the long time scale power flow within the microgrid and vehicles. This is sufficient for capturing the economics of the dispatch problem, but modeling electrical transients and power quality requires simulation on short time scales. The design of microgrids while considering both the long time scale and short time scale dynamics has begun to be studied at the University of Michigan, but is definitely an area for future research.

Bibliography

Adornato, B. (2010) *Prediction of Plug-in Hybrid Electric Vehicle Performance and Potential Charging Scenarios Based on Naturalistic Driving Data*, Master's Thesis, Dept. of Mechanical Engineering, University of Michigan, Ann Arbor, MI.

Adornato, B., Patil, R. and Filipi, Z. (2009) "Characterizing Naturalistic Driving Patterns for Plug-in Hybrid Electric Vehicle Analysis," *5th IEEE Vehicle Power and Propulsion Conference*, September 7-11, Dearborn, MI.

Ahn, C., Li, C.-T., and Peng, H. (2011) "Decentralized Charging Algorithm for Electrified Vehicles Connected to Smart Grid," *American Control Conference*, June 29 – July 1, San Francisco, CA.

Ahn, K., Cho, S. and Cha, S.W. (2008) "Optimal Operation of the Power-Split Hybrid Electric Vehicle Powertrain," *Proceedings of the Institution of Mechanical Engineers, Part D: Journal of Automobile Engineering*, **222**(5), pp. 789-800.

Ahn, K., Whitefoot, J., Atluri, V., Tate, E., and Papalambros, P. (2011) "Comparison of Early-Stage Design Methods for a Two-mode Hybrid Electric Vehicle," *IEEE Vehicle Power and Propulsion Conference*, September 6-9, Chicago, IL.

Alexander, M.J. (2011) *Management of Functional Data Variables in Decomposition-based Design Optimization*, Ph.D. dissertation, Dept. of Mechanical Engineering, University of Michigan, Ann Arbor, MI.

Allison, J. T. (2008) *Optimal partitioning and coordination decisions in decomposition-based design optimization*, Ph.D. dissertation, Dept. of Mechanical Engineering, University of Michigan, Ann Arbor, MI.

Arnold, M., Negenborn, R., Andersson, G. and De Schutter, B. (2009) "Multi-Area Predictive Control for Combined Electricity and Natural Gas Systems," *European Control Conference (ECC)*, 23-26 August, Budapest, Hungary.

Asano, H., Bando, S., and Watanabe, H. (2007) "Methodology to Design the Capacity of a Microgrid," *IEEE International Conference on System of Systems Engineering*, 16-18 April, San Antonio, TX.

Ashok, S. (2007) "Optimised model of a community hybrid energy system," *J. of Renewable Energy*, **32**(7), pp. 1155-1164.

Assanis, D., Delagrammatikas, G., Fellini, R., Filipi, Z., Liedtke, J., Michelena, N., Papalambros, P., Reyes, D., Rosenbaum, D., Sales, A., and Sasena, M. (1999) "An Optimization Approach to Hybrid Electric Propulsion System Design," *J. of Mechanics of Structures and Machines*, **27**(4), pp. 393-421.

Borchers, K. (2011) "Determining a Sample Data Set to Represent a Year," *Optimal Design Laboratory* Report, University of Michigan, Ann Arbor, MI.

Bose, B. K. (2002) *Modern Power Electronics and AC Drives*, Prentice Hall, Inc., Upper Saddle River, NJ.

Braun, R. D. (1996) *Collaborative Optimization: An Architecture for Large- Scale Distributed Design*, Ph.D. dissertation, Stanford University, Stanford, CA.

Carlson, R., Lohse-Busch, H., Duoba, M., and Shidore, N. (2009) "Drive Cycle Fuel Consumption Variability of Plug-in Hybrid Electric Vehicles Due to Aggressive Driving," *Society of Automotive Engineers* Technical Paper 2009-01-1335.

Chan, K.-Y. (2006) *Monotonicity, Activity and Sequential Linearization in Probabilistic Design Optimization,* Ph.D. dissertation, Dept. of Mechanical Engineering, University of Michigan, Ann Arbor, MI.

Colson, C.M., and Nehrir, M.H. (2009) "Review of Challenges to Real-Time Power Management of Microgrids," *IEEE Power & Energy Society General Meeting*, 26-30 July, Calgary, Alberta, Canada.

Cramer, E. J., Dennis, J. E., Frank, P. D., Lewis, R. M., and Shubin, G. R. (1994) "Problem Formulation for Multidisciplinary Optimization," *SIAM J. of Optimization*, **4**, pp. 754–776.

Cuddy, M. and Wipke, K. (1997) "Analysis of the Fuel Economy Benefit of Drivetrain Hybridization," *Society of Automotive Engineers*, Paper 970289.

Cummins Power Generation (2011) "Specifications and Data Sheets," http://cumminspower.com/en/technical/documents, accessed January 10, 2011.

del Real, A. J., Galus, M. D., Bordons, C., and Andersson, G. (2009) "Optimal power dispatch of energy networks including external power exchange," *European Control Conference (ECC)*, 23-26 August, Budapest, Hungary.

del Real, A., Arce, A. and Bordons, C. (2009) "Optimization strategy for element sizing in hybrid power systems," *J. of Power Sources,* **193**(1), pp. 315–321.

Doyle, M., Fuller, T. F., and Newman, J. (1993) "Modeling of Galvanostatic Charge and Discharge of the Lithium/Polymer/Insertion Cell," *Journal of the Electrochemical Society,* **140**(6), pp. 1526–1533.

Du, X. and Chen, W. (2004) "Sequential Optimization and Reliability Assessment Method for Efficient Probabilistic Design," *Journal of Mechanical Design*, **126** (3), pp. 225 - 233.

Energy Information Administration (2011) *International Energy Outlook 2011*, U.S. Department of Energy, DOE/EIA-0484(2011).

Fathy, H. K., Reyer, J. A., Papalambros, P. Y., and Ulsoy, A. G. (2001) "On the Coupling Between the Plant and Controller Optimization Problems," *IEEE American Control Conference*, , June 25-27, Arlington, VA.

Fellini, R., Michelena, N., Papalambros, P., and Sasena, M. (1999) "Optimal Design of Automotive Hybrid Powertrain Systems," *Proceedings of the EcoDesign '99: 1st International Symposium on Environmentally Conscious Design and Inverse Manufacturing*, February 3, Tokyo, Japan,

Filipi, Z., Louca, L., Daran, B., Lin, C.-C., Yildir, U., Wu, B., Kokkolaras, M., Assanis, D., Peng, H., Papalambros, P., Stein, J., Szkubiel, D., Chapp, R. (2004) "Combined optimization of design and power management of the hydraulic hybrid propulsion system for the 6x6 medium truck," *International Journal of Heavy Vehicle Systems*, **11**(3/4), pp.372-402.

Fuller, T.H., Doyle, M., and Newman, J. (1994) "Simulation and optimization of the dual lithium-ion insertion cell", *Journal of The Electrochemical Society*, **141**(1), pp. 1–10.

Firestone, R.M. (2007) *Optimal Real-time Dispatch for Integrated Energy Systems*, Ph.D. dissertation, Dept. of Mechanical Engineering, University of California, Berkeley, CA.

Friedman, N.R., and Stevens, J. (2005) "Characterization of Microgrids in the United States," *Sandia National Laboratories* Report SAND2005-4367.

Gage, T.B., et al. (2003) "Development and Evaluation of a PHEV with V2G power flow," *California Air Resources Board (CARB)* Grant Number ICAT 01-2, Final Report.

Galus, M. and Andersson, G. (2008) "Demand Management of Grid Connected Plug-In Hybrid Electric Vehicles (PHEV)," *IEEE Energy 2030 Conference*, 17-18 August, Atlanta, GA.

Geidl, M. and Andersson**,** G. (2006) "Operational and Structural Optimization of Multi**-**Carrier Energy Systems," *European Transactions on Electrical Power*, **16**(5), pp. 463-477.

Geidl, M. and Andersson, G. (2007) "Optimal Power Flow of Multiple Energy Carriers," *IEEE Transactions on Power Systems*, **22**(1), pp. 145 – 155.

Geidl, M. (2007) *Integrated Modeling and Optimization of Multi-Carrier Systems*, Doctoral dissertation, ETH Zurich, Switzerland.

Griffiths, M. and Coates, C. (2006) "Modelling and Performance of Low Voltage Distributed Generation Systems," *Proceedings of the 2006 Australasian Universities Power Engineering Conference (AUPEC'06)*, 10-13 December, Melbourne, Australia.

Guenther, M. and Dong, Z. (2005) "Modelling and Design Optimization of Low Speed Fuel Cell-Battery Hybrid Electric Vehicles," *Proceedings of the Intl. Green Energy Conference*, 12-16 June, Waterloo, Ontario, Canada.

Gupta, A., Saini, R.P., and Sharma, M.P. (2010) "Steady-state modelling of hybrid energy system for off grid electrification of cluster of villages," *J. of Renewable Energy*, **35**(2), pp. 520-535.

Guzzella, L., Amstutz, A. (1999) "CAE-Tools for Quasistatic Modeling and Optimization of Hybrid Powertrains," *IEEE Transactions on Vehicular Technology*, **48**(6), pp. 1762-1769.

Han, J. (2008) *Sequential linear programming coordination strategy for deterministic and probabilistic analytical target cascading*, Ph.D. dissertation, Dept. of Mechanical Engineering, University of Michigan, Ann Arbor, MI.

Han, J., Kokkolaras, M., and Papalambros, P. Y. (2008) "Optimal Design of Hybrid Fuel Cell Vehicles", *Journal of Fuel Cell Science and Technology*, **5**(4).

Hartranft, T.J., Yeboah, F., Grady, D., and Ducey, R. (2007) "Proceedings of the 1st Army Installation Energy Security and Independence Conference", *Construction Engineering Research Laboratory*, Report ERDC/CERL TR-07-9, U.S. Army Corps of Engineers.

Hawkes, A.D., and Leach, M.A. (2009) "Modelling high level system design and unit commitment for a microgrid," *J. of Applied Energy*, **86**(7-8), pp. 1253–1265.

Hiskens, I., and Callaway, D. (2009) "Achieving Controllability of Plug-in Electric Vehicles," *IEEE Vehicle Power and Propulsion Systems Conference*, Dearborn, Michigan, September 7-10.

Hoffenson, S. (2012) *Safety Considerations in Optimal Automotive Vehicle Design*, Ph.D. Dissertation, University of Michigan, Ann Arbor, MI.

Hu, X., Wang, Z., and Liao, L. (2004) "Multi-Objective Optimization of HEV Fuel Economy and Emissions using Evolutionary Computation," Society of Automotive Engineers, SAE 2004-01-1153.

International Energy Agency (2011) *World Energy Outlook*, http://www.iea.org/weo/, accessed November 15, 2011.

Jiayi, H., Chuanwen, J., and Rong, X. (2008) "A review on distributed energy resources and Microgrid," *Renewable and Sustainable Energy Reviews*, **12**(9), pp. 2472–2483.

Jones, D.R. (2001) "DIRECT Global Optimization Algorithm", *Encyclopedia of Optimization*, eds. C. Floudas and P. Pardalos, Kluwer Academic Publishers, pp. 431-440.

Karbowski, D., Haliburton, C., and Rousseau, A. (2007) "Impact of Component Size on Plug-In Hybrid Vehicle Energy Consumption Using Global Optimization," *The World Electric Vehicle Journal*, **2**(2), pp. 4-12.

Kempton, W., and Tomić, J. (2005) "Vehicle-to-grid power fundamentals: Calculating capacity and net revenue," *J. of Power Sources*, **144**(1), pp. 268–279.

Kim, H. M., Michelena, N. F., Papalambros, P. Y., and Jiang, T. (2003) "Target Cascading in Optimal System Design," *J. of Mechanical Design*, **125**(3), pp. 474–480.

Kim, M.-J., and Peng, H. (2007) "Power management and design optimization of fuel cell/battery hybrid vehicles," *Journal of Power Sources*, **165**(2), March, pp.819-832.

Lambert, T., Gilman, P., and Lilienthal, P. (2006) "Chapter 15: Micropower System Modeling with Homer", in *Integration of Alternative Sources of Energy*, eds. Felix A. Farret and M. Godoy Simoes, John Wiley & Sons.

Larminie, J. and Lowry, J. (2003) *Electric Vehicle Technology Explained*, John Wiley & Sons, p. 31.

Lasseter, R., et al. (2003) "Integration of Distributed Energy Resources : The CERTS Microgrid Concept," *California Energy Commission (CEC)* Report P500-03-089F.

Lasseter, R., Tomsovic, K., and Piagi, P. (2000) "Scenarios for Distributed Technology Applications with Steady State and Dynamic Models of Loads and Micro-Sources," *Consortium for Electric Reliability Technology Solutions (CERTS)* Report, April.

Lasseter, R.H., and Piagi, P. (2006) "Control and Design of Microgrid Components," *Power Systems Engineering Research Center (PSERC)* Final Report, Publication 06-03, University of Wisconsin-Madison.

Lawrence Berkeley National Laboratory (2010) "DER technology Data Used after 2004," compiled by Ryan Firestone, http://der.lbl.gov/der-cam/technology-data-archive, accessed December 6, 2010.

Li, C.-T., Ahn, C., Peng, H., and Sun, J. (2011) "Decentralized Charging of Plug-In Vehicles," *ASME Dynamic Systems and Controls Conference*, Arlington, VA, Oct. 31 – Nov. 2.

Lu, S., Schroeder, N.B., Kim, H.M., Shanbhag, U.V. (2010) "Hybrid Power/Energy Generation Through Multidisciplinary and Multilevel Design Optimization with Complementarity Constraints," *Journal of Mechanical Design*, **132**(10), pp. 101007 – 101019.

Lu, S. and Kim, H.M. (2011) "Hybrid Power Generation System Design Optimization Based on a Markovian Reliability Analysis Approach," DETC2011-48607, *ASME International Design Engineering Technical Conferences*, August 28-31, Washington, DC.

Markel, T., Kuss, M., and Denholm, P. (2009) "Communication and Control of Electric Drive Vehicles Supporting Renewables," *IEEE Vehicle Power and Propulsion Systems Conference*, Dearborn, Michigan, September 7-10.

Meliopoulos, A.P.S. (2002) "Challenges in simulation and design of microgrids," IEEE *Power Engineering Society Winter Meeting*, 27-31 January, New York, NY.

Mills, A., Ahlstrom, M., Brower, M., Ellis, A., George, R., Hoff, T., Kroposki, B., Lenox, C., Miller, N., Stein, J., and Wan, Y-H. (2009) "Understanding Variability and Uncertainty of Photovoltaics for Integration with the Electric Power System," *Lawrence Berkeley National Laboratory*, Report LBNL-2855E.

Mohamed, F.A., and Koivo, H.N. (2009) "System modeling and optimal management of a Microgrid using Mesh Adaptive Direct Search," *J. of Electrical Power and Energy Systems*, **32**(5), pp. 398-407.

Momber, I., Gómez, T., Venkataramanan, G., Stadler, M., Beer, S., Lai, J., Marnay, C., and Battaglia, V. (2010) "Plug-in Electric Vehicle Interactions with a Small Office Building: An Economic Analysis using DER-CAM," *Proceedings of the 2010 IEEE PES General Meeting*, 26-29 July, Minneapolis, MN.

Moura, S., Fathy, H.K., Callaway, D.S., and Stein, J. (2008) "A Stochastic Optimal Control Approach for Power Management in Plug-in Hybrid Electric Vehicles," *Proceedings of the 2008 ASME Dynamic Systems and Control Conference*, 20-22 October, Ann Arbor, MI.

Moura, S., Fathy, H.K., Callaway, D.S., and Stein, J. (2010) "Tradeoffs between Battery Energy Capacity and Stochastic Optimal Power Management in Plug-in Hybrid Electric Vehicles," *J. of Power Sources*, **195**(9), pp. 2979-2988.

National Renewable Energy Laboratory (2005) "Getting Started Guide for HOMER v.2.1", *National Renewable Energy Laboratory,* Golden, CO.

Papalambros, P. Y., and Wilde, D. J. (2000) *Principles of Optimal Design: Modeling and Computation*, 3rd edition, Cambridge University Press, Cambridge, UK.

Papalambros, P., T. Ersal, I. Hiskens, H. Peng, A. Stefanopoulou, J.L. Stein, C. Ahn, A. Mechtenberg, D. Peters, J. Whitefoot, E. Kallio (2011) "Vehicle Supported Military Microgrids: Design, Scheduling, and Regulation for a Forward Operating Base," *Automotive Research Center Conference* presentation, May 24, Ann Arbor, MI.

Patil, R., Adornato, B. and Filipi, Z. (2009) "Impact of Naturalistic Driving Patterns on PHEV Performance and System Design", *Society of Automotive Engineers Technical Paper,* 2009-01-2715.

Peças Lopes, J. A., F.J. Soares and Rocha Almeida, P. M. (2009) "Identifying Management Procedures to Deal with Connection of Electric Vehicles in the Grid," *IEEE Bucharest Power Tech Conference*, June 28 - July 2, Bucharest, Romania.

Pelet, X., Favrat, D., and Leyland, G. (2005) "Multiobjective optimisation of integrated energy systems for remote communities considering economics and CO2 emissions," *Intl. Journal of Thermal Sciences*, **44**(12), pp. 1180–1189.

Peters, D. L., Papalambros, P. Y., and Ulsoy, A. G. (2009) "On Measures of Coupling Between the Artifact and Controller Optimal Design Problems," *ASME International Design Engineering Technical Conferences*, San Diego, CA, Aug. 30 - Sept. 2, DETC2009-86868.

Peters, D.L., Mechtenberg, A.R., Whitefoot, J.W., and Papalambros, P.Y. (2011) "Model Predictive Control of a Microgrid with Plug-in Vehicles: Error Modeling and the Role of Prediction Horizon," *ASME Dynamic Systems and Controls Conference*, Arlington, VA, Oct. 31 – Nov. 2, DSCC2011-6030.

Peterson, S.B., Apt, J., and Whitacre, J.F. (2010) "Lithium-ion battery cell degradation resulting from realistic vehicle and vehicle-to-grid utilization," *J. of Power Sources*, **195**(8), pp. 2385-2392.

Peterson, S.B., Whitacre, J.F., and Apt, J. (2010) "The economics of using plug-in hybrid electric vehicle battery packs for grid storage," *J. of Power Sources*, **195**(8), pp. 2377–2384.

Peterson, J. (2009) "Li-ion Batteries and How Cheap Beat Cool in the Chevy Volt," *Seeking Alpha*, March 23.

Pike Research Group (2011) "Cumulative Plug-in Electric Vehicle Sales to Reach 5.2 Million Worldwide by 2017," Press Release, August 22, 2011, www.pikeresearch.com.

PNGV Battery Test Manual Revision 3 (2001), DOE/ID-10597, February 2001.

Rodatz, P., Paganelli, G., Sciarretta, A., and Guzzella, L. (2005) "Optimal power management of an experimental fuel cell/supercapacitor-powered hybrid vehicle," *Control Engineering Practice*, **13**(1), pp. 41-53.

Ren, Y. (2011) "Solutions to the Deterministic Linear Micro-grid Scheduling Problem," Working Paper, Dept. of Mechanical Engineering, University of Michigan, Ann Arbor, MI.

Reyer, J. A. and Papalambros, P. Y. (2002) "Combined Optimal Design and Control with Application to an Electric DC Motor," *ASME J. of Mechanical Design*, **124**(2), pp. 183-191.

Rodriguez, J. F., Renaud, J. E., and Watson, L. T. (1998) "Convergence of Trust Region Augmented Lagrangian Methods Using Variable Fidelity Approximation Data," *Structural Optimization*, **15**(3–4), pp. 141–156.

Roy, R. (1990) *A Primer on the Taguchi Method*, Van Nostrand Reinhold Co., New York.

Shaffer, E.C., Massie, D.D., and Cross, J.B. (2006) "Power And Energy Architecture For Army Advanced Energy Initiative," *Army Research Laboratory Report*, Adelphi, Maryland.

Shiau, C.S., Peterson, S.B., and Michalek, J.J. (2010) "Optimal Plug-in Hybrid Vehicle Design and Allocation for minimum life cycle cost, petroleum consumption, and greenhouse gas emissions," *ASME International Design Engineering Technical Conference*, August 15-18, Montreal, Quebec, Canada, DETC2010-28198.

Shiau, C.S. and Michalek, J.J. (2010) "A MINLP Model for Global Optimization of Plug-In Hybrid Vehicle Designa dn Allocation to Minimize Life Cycle Greenhouse Gas Emissions," *ASME International Design Engineering Technical Conference*, August 15-18, Montreal, Quebec, Canada, DETC2010-28064.

Stadler, M., Marnay, C., Siddiqui, A., Lai, J., Coffey, B., and Aki, H. (2009) "Effect of Heat and Electricity Storage and Reliability on Microgrid Viability: A Study of Commercial Buildings in California and New York States," *Ernest Orlando Lawrence Berkeley National Laboratory*, Report LBNL-1334E-2009.

Stadler, M., Momber, I., Mégel, O., Gómez, T., Marnay, C., Beer, S., Lai, J. and Battaglia, V. (2010) "The added economic and environmental value of plug-in electric vehicles connected to commercial building microgrids," *Ernesto Orlando Lawrence Berkeley National Laboratory*, LBNL-3885E.

Tomić, J., and Kempton, W. (2007) "Using Fleets of electric-drive vehicles for grid support," *J. Power Sources*, **168**(2), pp. 459-468.

Tselepis, S. (2010) "Greek Experience with Microgrids: Results from the Gaidouromantra Site, Kythnos Island", *Vancouver 2010 Symposium on Microgrids*, 22 July, Vancouver, B.C., Canada.

Tu, J., Choi, K.K. and Park, Y.H. (1999) "New study on reliability-based design optimization," *J. of Mechanical Design*, **121**(4), pp. 557–564.

Tu, J., Choi, K.K. and Park, Y.H. (2001) "Design potential method for robust system parameter design," *AIAA Journal*, **39**(4), pp. 667–677.

United Nations (2010) *World Population Prospects (2010 Revision)*, http://www.un.org/esa/population/, accessed November 15, 2011.

Vallem, M.R., and Mitra, J. (2005) "Siting and Sizing of Distributed Generation for Optimal Microgrid Architecture," *Proceedings of the 27th Annual North American Power Symposium*, 23-25 October, Ames, IA.

Vyas, A.D., Ng, H.K., Santini, D.J. and Anderson, J.L. (1997) "Batteries for Electric Drive Vehicles: Evaluation of Future Characteristics and Costs through a Delphi Study," Argonne National Laboratory, *SAE International Spring Fuels and Lubricants Meeting*, May 5-7, Detroit, Michigan.

Wan, P. and Lemmon, M. (2010) "Optimal power flow in microgrids using event-triggered optimization," *Proceedings of the American Control Conference (ACC 2010)*, 30 June – 2 July, Baltimore, MD.

Waraich, R., Galus, M., Dobler, C. , Balmer, M. , and Andersson, G. (2009) "Plug-in Hybrid Electric Vehicles and Smart Grid: Investigations Based on a Micro-Simulation," *The 12th Intl.Conference of the International Association for Travel Behaviour* Research, 3-6 December, Jaipur, India.

Weather.com (2001) "Average Monthly Temperatures in Kabul, Afghanistan", http://www.weather.com/outlook/health/allergies/wxclimatology/monthly/graph/AFXX0003, accessed January 6, 2011.

Whitefoot, J.W., Ahn, K., and Papalambros, P.Y. (2010) "The Case for Urban Vehicles: Powertrain Optimization of a Power-Split Hybrid for Fuel Economy on Multiple Drive Cycles," *ASME International Design Engineering Technical Conferences*, Montreal, Quebec, Canada, August 15-18.

Whitefoot, J.W., Mechtenberg, A.R., Peters, D.L., and Papalambros, P.Y. (2011) "Optimal Component Sizing and Forward-Looking Dispatch of an Electrical Microgrid for Energy Storage Planning", *ASME International Design Engineering Technical Conferences*, Washington, DC, August 29 – 31.

Whitehead, J.W. (2001) *Design and Performance of Derivative-Free Optimization Algorithms Used With Hybrid-Electric Vehicle Simulations*, Master's Thesis, University of Michigan, Ann Arbor, MI.

Wipke, K., Markel, T. and Nelson, D. (2001) "Optimizing Energy Management Strategy and Degree of Hybridization for a Hydrogen Fuel Cell SUV," *Proceedings of 18th Electric Vehicle Symposium*, Berlin, Germany.

Wong, J. Y. (2001), *Theory of Ground Vehicles*, John Wiley and Sons, New York, NY.

World Bank (2011) *World Development Indicators*, http://wdr2011.worldbank.org/, accessed November 15, 2011.

Youn, B., Choi, K.K. and Park, Y.H. (2003) "Hybrid Analysis Method for Reliability-Based Design Optimization," *J. of Mechanical Design*, **125**(2), pp. 221–232.

Zoka, Y., Sugimoto, A., Yorino, N., Kawahara, K., Kubokawa, J. (2007) "An economic evaluation for an autonomous independent network of distributed energy resources," *J. Electric Power Systems Research*, **77**(7), pp. 831–838.